A STEP TOWARD RECYCLABLE SILICONE ELASTOMERS

AMIN NASRESFAHANI, B.Sc.(Eng.)

SUBMITTED IN PARTIAL FULFILLMENT
OF THE REQUIREMENTS FOR THE DEGREE

OF

MASTER OF SCIENCE

DEPARTMENT OF CHEMISTRY, BROCK UNIVERSITY
NIAGARA REGION, ONTARIO

SUPERVISOR:

DR. PAUL ZELISKO

COMMITTEE MEMBERS:

DR. MARTIN LEMAIRE

DR. TOMÁŠ HUDLICKÝ

EXTERNAL COMMITTEE MEMBER:

DR. SIMON RONDEAU-GAGNÉ

HEAD OF THE GRADUATE PROGRAM:

DR. GEORGII I. NIKONOV

When you see everything that happens in the world of science and in the working of the universe, you cannot deny that there is a 'Captain on the bridge'.

– Thomas Edison

Any intelligent fool can make things bigger and more complex. It takes a touch of genius and a lot of courage to move in the opposite direction.

– Albert Einstein

To My Parent

Who Made Me The Man I Am Today

&

To My Ancestors

Who Established The First Declaration of Human Rights, The Cyrus Cylinder

ACKNOWLEDGEMENTS

I would like to declare my sincere acknowledgment to my supervisor, Dr. Paul Zelisko who offered me the opportunity of working in his research group as an M.Sc. student. The strong supportive advice of him gave me a great extent of freedom to pursue my passions & objectives.

Special thanks to my committee members, Dr. Martin Lemaire, and Dr. Tomáš Hudlický for their guidance and suggestions. I owe my deepest gratitude to Dr. Travis Dudding and his postdoctoral fellow, Dr. Roya Mir, for their generous support and insightful comments. I would like to thank Dr. Thad Harroun, Dr. Anastasia Elias (University of Alberta), Marcia Reid (McMaster University), Liqun Qiu, Razvan Simionescu, and Dan Li (University of Alberta) for their precious help in collecting and providing technical services for differential scanning calorimetry, physical & mechanical tests, mass spectrometry, nuclear magnetic resonance, and infrared spectroscopy.

I would like to also extend my gratitude to my friends, and colleagues, all of whom created such a warm workplace and pleasant academic experience during the past couple of years.

ABSTRACT

This thesis introduces a new strategy for developing polysiloxane networks with the capacity of being recycled. The conventional methods of cross-linking polysiloxanes suffer from lack of self-repair and recyclability. Diels-Alder/retro-Diels-Alder (DA/RDA) equilibrium is a key to establish thermally reversible linkages among polysiloxane chains to enable the material's recyclability. The equilibrium is optimized to improve the extent of reversibility of the Diels-Alder adduct through functional groups such as carboxyphenyl, ester, and carbon spacers in the structures of maleimide and furan derivatives. The DA/RDA equilibrium is studied by various nuclear magnetic resonance (NMR) spectroscopy experiments and differential scanning calorimeter analyses. The DA reaction is found to be at its highest rate at 50˚C while the retro-Diels-Alder reaction is predominant at 110˚C. Comparison of the reaction rate constant of the optimized maleimide and furan derivatives at 50˚C with the literature suggests that the DA reaction is among those ones described as ultra fast kinetic. Accordingly, series of polysiloxanes are functionalized with the optimized maleimide and furan derivatives to obtain recyclable polysiloxane networks. Dynamic, variable-temperature solid-state ^{1}H NMR experiments are confirmed the rapid, reversible nature of the cross-links within the polysiloxanes. The injured networks are mended to the point that signs of defects were nearly imperceptible even by scanning electron microscopy. The binding strengths of the healed materials are quantified using stress-strain measurements. The healed networks displayed binding strengths that are equal or superior to the undamaged ones.

Contents

LIST OF FIGURES

Chapter 1

Chapter 2

Chapter 3

Chapter 4

Chapter 6

Chapter 1 Introduction

Recognizing the available tools for enhancing the properties of materials is the key point in designing advanced polymer systems. In fact, multi-component polymeric materials are widely used to increase durability and to impart a specific set of properties in a polymer for a given application. These materials have advantages that none of the individual components could offer in isolation. Thus, the purpose of this chapter is to provide a concise overview of the polymer design elements used in this thesis before discussing the main subject in the next chapters. Polymers in general, the unique properties of polysiloxanes, the hydrosilylation reactions, the characteristics of bimodal siloxane networks, and the opportunity for preparing truly dispersed silsesquioxane containing nanomaterials will be briefly discussed.

1.1 Silicon Atom

Silicon (^{28}Si) is among the six elements of periodic table known as the metalloids (i.e., boron, silicon, germanium, arsenic, antimony, and tellurium). Since silicon's electrons are more tightly bound to the nuclei compared to metals such as Cu, Al, and Au, it conducts electricity partially. The electron configuration of the valence shell is $3s^2 3p^2$. Commonly, it forms sp^3 hybridized tetrahedral structures with a oxidation state of 4+. The capacity of forming the most common bond in the nature (i.e., Si-O bond), is made silicon atom a leading element in the mineral world as oppose to carbon-carbon bonds which is the prime element in the living organisms world. **Table 1** briefly distinguishes the properties of silicon from carbon. The silicon atom is roughly twice larger than the carbon. Thus, the silicon bonds lengths are expected to be longer in comparison with the lengths of similar bonds to carbon. The longer distance exist between a silicon atom and the adjacent bonded element weakens the bonding and lowers the rotation barrier about the bonds. Due to the longer bond lengths, bulky adjacent groups cause less steric effects compared to the carbon analogues. Silicon's smaller electronegativity affects the bond polarity, which also provide a major effect on the bond lengths of the atom. Although the role of d orbitals in the bonding of silicon in has been controversial, a crucial differences between silicon and its analogous (i.e., carbon atom) is the

Property	Carbon	Silicon
Atomic radius (A°)	0.7	1.1
Covalent radius (A°)	0.77	1.16
van der Waals radius (A°)	1.7	2.17
Electron affinity (eV)	1.12	1.39
Electronegativity	2.74	2.13
Dipole polarizability (a.u.)	11.8	36.3

Table 1. A comparison between carbon and silicon properties.[1]

capacity of silicon to form stable hypervalent species such as 5- or 6-coordinate silicon derivates.[1]

Comparing to similar carbon-based compounds, the improved reactivity of silane derivatives can be attributed to the major characteristics of the silicon atom, including the availability of low-energy orbitals such as $\boldsymbol{\sigma}^*$ orbitals, ionic effects, the Si atomic size, and its lower electronegativity. The highest bond polarization occurs with Si-O and Si-X (X= halogens). The differences in electronegativity of bonding elements often can be used to predict the reactivity of a given covalent bond. In most cases, as opposed to carbon atom, silicon is positively polarized ($\boldsymbol{Si^{\delta+} - X^{\delta-}}$). However, the exceptional cases are known to be the silicon compounds bonded to highly electropositive elements (i.e., the alkali metals). As an example, the reaction of ($\boldsymbol{H_3C^{\delta-} - Li^{\delta+}}$) with the two similar compounds: ($\boldsymbol{Ph_3C^{\delta-} - H^{\delta+}}$) and ($\boldsymbol{Ph_3Si^{\delta+} - H^{\delta-}}$) can be considered. The first reaction yields ($\boldsymbol{Ph_3C - Li}$) & ($\boldsymbol{H_3C - H}$) whereas the analogous reaction produces ($\boldsymbol{Ph_3Si - Li}$) & ($\boldsymbol{Li - H}$). In fact, the nucleophile ($\boldsymbol{H_3C^{\delta-}}$) attacks $\boldsymbol{Si^{\delta+}}$ instead of the hydrogen. Generally, the bimolecular reactions that silicon participates in, are those the bond formation and breakage occurs simultaneously. Among any two elements within the periodic table, the covalent bond strengths between the halogens/oxygen and Si atom are of the strongest single bonds can be found. Compare to the silicon analogous bonds, the C-H bond is stronger while C-O and C-X bonds are weaker.[2,3]

Often, silicon atom uses $\boldsymbol{3s}$ and $\boldsymbol{3p}$ orbitals to form a bond. The $\boldsymbol{sp^3}$ hybridization or tetrahedral is known for most of synthetic or naturally produced silicon derivatives.[2] Although Si atom has access energetically to $\boldsymbol{d}$ orbitals, the bonding interactions which

involves $\boldsymbol{d}$ orbitals are generally described to be relatively negligible (i.e., modest contribution to the electronic delocalization) due to their high energies.[4–6] Thus, other orbitals are introduced in the literature to be responsible for the bonding interactions. In fact, silicon has low-lying $\boldsymbol{\sigma}^*$ orbitals participating in $\boldsymbol{\pi}$-type back-bonding interactions.[2,7] Often, back-donation happens via relocation of a lone pair that belongs to the adjacent heteroatom into a suitably oriented orbital of Si atom. This type of bonding interaction is utilized to explain observations such as the higher acidity of silanols in contrast to alcohols, low bending force constants of Si-O-Si, and the short bond lengths of Si-OR, Si-N, and Si-F bonds.[2,8]

Additionally, the quantum calculations suggest that $\boldsymbol{d}$ orbitals participation in hybridization does not have a significant role in the bonding. Instead, the qualitative notions such as the significantly polar bonds and the ionic contribution are utilized to explain these properties of Si atom.[6,9]

As an example of insignificant or unimportant contribution of $\boldsymbol{d}$ orbital, the interaction of $\boldsymbol{\pi(O) \rightarrow 3\sigma^*(SiO)}$ in $Si(OH)_4$ is 20 kcal/mol which is five times stronger than $\boldsymbol{\pi(O) \rightarrow 3d(Si)}$ interaction.[10] The $\boldsymbol{d}$ orbital on the central atom is described to have only a secondary role in $\boldsymbol{\pi}$-bonding.[9,11] In fact, it is shown the $\boldsymbol{d}$ functions of the second-row elements do not take a valence role and are polarization functions in nature.[6,12,13] However, a correct description of the bonding, structure, and energy in these cases relies on the $\boldsymbol{d}$ orbitals. In fact, they are additional central-atom acceptor functions, polarizing the available valence orbitals.[9]

Compared to the tetrahedral structure of $N(CH_3)_3$, $N(SiH_3)_3$ is planar. The nitrogen atom holds a higher partial negative charge in $N(SiH_3)_3$ rather than $N(CH_3)_3$. On the other hand, the silyl group in $N(SiH_3)_3$ possesses a partial charge significantly larger than the methyl group in $N(CH_3)_3$. It is, therefore, demonstrated that the $\boldsymbol{p_\pi \rightarrow d_\pi}$ bonding theory cannot directly explain the planarity of the $N(SiH_3)_3$. In fact, The planar geometry observed in trisilylamine is strongly attributed to the electrostatic repulsion among the silyl groups than the $\boldsymbol{\pi}$-type $\boldsymbol{p_\pi \rightarrow d_\pi}$ donation ($\boldsymbol{d}$-orbital participation) in the recent quantum mechanical calculations. In this regard, an effective long-range electrostatic repulsion between the silyl groups (where Si-N bond is more polar than the C-N bond) results in the planar structure of $N(SiH_3)_3$.[14,15]

Bond lengths and angles associated with silicon are influenced greatly by the nature of the central atom as well as the steric overcrowding. The relaxation of the stress resulted by sterically bulky silyl groups occurs via bond length stretch and an increase in the bond angle. Considering carbon as a central atom within two silicon atoms (Si-C-Si), the bond angle falls within ~104 to 123 degrees. However, depending on the central atom, the angle can be greatly altered even without existing bulky groups. For instance, the barrier to the linearization of Si-O-Si (i.e., dimethylsilicones) is known to be as low as 1.25 kJ/mole. The reason for such low energy barrier is attributed to the donation of a lone pair of the oxygen atom into silicon orbitals, shifting the hybridization of the central atom (i.e., oxygen) from $\boldsymbol{sp^3}$ to $\boldsymbol{sp}$. Therefore, $(Ph_3 - \boldsymbol{SiOSi} - Ph_3)$, $(Me_3 - \boldsymbol{SiOSi} - Me_3)$, $(-O(Me_2 - \boldsymbol{SiOSi} - Me_2)O-)$ are reported to be approximately 180°, 154°, and 145°, respectively.[2]

This large Si-O-Si angle is also attributed to Si-O bond's ionic contributions. Siloxanes have, on average, 1.63 Å Si-O bond length which is significantly less than the total covalent radii (1.84 Å) mostly due to the ionic contributions. The $\boldsymbol{d - p}$ bonding is relatively unimportant to explain the $\boldsymbol{\pi}$-acceptor properties of Si atom. In fact, electronegativity arguments are capable of explaining the bond lengths and angles in species based on silicon.[10,16]

Moreover, the electronegativity order is Si < H < C. Thus, it is proven computationally that $\boldsymbol{p}$-donation from lone pairs of oxygen to the $\boldsymbol{\sigma^*}$(SiH) bonds in SiH_3-OH is preferable compared to the analogous compounds based on carbon atom.[10]

As mentioned above, the bond lengths of Si-OR, Si-N, and Si-F bonds are shorter compared to the total summation of covalent radii. This phenomenon is also rationalized through the orbitals overlaps resulting in a stronger bond than a sigma bond. Bonding between silicon and heteroatoms can be also described through the ionic factors. It is shown that bond strength has a linear correlation with electronegativity. In fact, a more electronegative group bonded to Si atom leads to the formation of a stronger bond due to a higher contribution of the ionic factor $\boldsymbol{Si^{\delta+} - X^{\delta-}}$(X=heteroatom). As an example, because of having roughly the same values for electronegativities of sulfur and carbon, Si-C and Si-S bond strengths are

similar. Similarly, as disscussed above, the larger bond angles and the low bending force constants associated with Si-O-Si angles is due to the electronegativity differences.[2]

The S_N2-type reactions of carbon and silicon are a fundamentally different chemical phenomenon. This can be exemplified through the H-exchange. Compared to SiH_5^-, CH_5^- is reported to be only a transition state. However, SiH_5^- is a stable intermediate for certain reactions. Although the H-exchange reactions of Si and C are isoelectronic and isostructural regarding the valence electrons and the geometric types of the main species, the trigonal-bipyramidal CH_5^- is a high-energy transition while the trigonal-bipyramidal structure of SiH_5^- is an intermediate which has energy 13-20 kcal/mol lower than the reactants and products. Depending on the level of the quantum calculations, CH_5^- energy falls within 52-64 kcal/mol above the reactants and products. Under closed-shell ground-state condition, a bond can be formed provided that the fragment promotes itself to an excited open-shell configuration. The promotion energies must be low and the engaged orbitals are required to maintain large overlaps with the other fragments' orbitals. The computed energy promotion ($\boldsymbol{p} \rightarrow \boldsymbol{\sigma}^*$) is 55 kcal/mol less for SiH_3 compared to CH_3. In fact, the $\boldsymbol{\sigma}^* - \boldsymbol{H}$ overlap is described remarkable in the case of SiH_3 while the same overlap is roughly zero for CH_3. Thus, $\boldsymbol{\sigma}^*(SiH_3)$ has a strong bonding capacity in comparison with CH_3. Consequently, SiH_3 can bind to two more hydrogen atoms to form SiH_5^-. In contrast, the insignificant overlap capacity of $\boldsymbol{\sigma}^*(CH_3)$ reduces greatly the stabilization of CH_5^-, remaining a high-energy transition. Therefore, having high energy along with a poor overlap capability limits the bonding mechanism of CH_5^- to the $\boldsymbol{p}$-type bond. The $\boldsymbol{\sigma}^*$ bonding capacity is attributed to the atomic electronegativities of these two analogues elements (i.e., C and Si). In this respect, compared to CH_3, the $\boldsymbol{\sigma}^*(SiH_3)$ orbital is more concentrated on the Si atom, providing a long equatorial Si-H bonds which leads to the significant overlap described above. The sever crowding on CH_5^- can be also considered as another factor, lowering the stability of CH_5^-.[6,16,17]

Additionally, the spin-coupled computational approach, where each orbital is allowed to delocalize onto other centers to minimize the total energy, provides similar insights into the relatively high stability of SiH_5^-. Essentially, due to the lower electropositivity of carbon

(which is relatively the same as the electronegativity of the hydrogen) than Si atom, CH_5^- cannot achieve a high stability compared to SiH_5^- . Therefore, SiH_5^- is a stable intermediate whereas CH_5^- is reported to be only a high-energy transition state.[6]

1.2 ^{29}Si Nuclear Magnetic Resonance Spectroscopy

Nuclear magnetic resonance (NMR) spectroscopy is based on the magnetic properties of atomic nuclei. Rotation of nuclei around their axis creates a spin angular momentum ($\boldsymbol{L}$) which can be quantified via the spin angular momentum vector ($\boldsymbol{L} = \boldsymbol{I}\hbar$). In this correlation, $\boldsymbol{I}$ is the nuclear spin and $\hbar$ denotes Planck's constant divided by 2π. The movement of a spinning nucleus can be seen as a positive electric current flowing in a loop. The nucleus behaves as a magnetic dipole due to such movement, generating a magnetic moment with a magnitude of ($\boldsymbol{\mu} = \boldsymbol{\gamma L}$). The gyromagnetic ratio ($\boldsymbol{\gamma}$) is a unique nuclear constant for a given elemental nucleus. Nuclei with ($\boldsymbol{I} = 0$) do not generate a magnetic moment. Thus, those which hold ($\boldsymbol{I} \neq 0$) are utilized for NMR experiments. In fact, ($\boldsymbol{I} \neq 0$) occurs typically for those nuclei that have odd atomic numbers. Upon placing a magnetically active spinning nucleus in a magnetic field of $\boldsymbol{B_0}$, the magnetic moment ($\boldsymbol{\mu}$) aligns itself according to the magnetic field. $\boldsymbol{B_0}$ magnetic field also creates a torque on the rotation of a nucleus.[18,19]

According to the quantum mechanical rules, a nucleus with angular momentum ($\boldsymbol{L}$) has a discrete number of rotation (spin) states. The spin states and energy levels assigned to a nucleus are explained through the magnetic spin quantum number ($\boldsymbol{m_I} = [-\boldsymbol{I}, +\boldsymbol{I}]$). $\boldsymbol{m_I}$ contains $\boldsymbol{2I + 1}$ values, representing the total number of possible different energy levels ($\boldsymbol{E} = -\boldsymbol{\gamma}\hbar\boldsymbol{m_I}\boldsymbol{B_0}$). When nuclei with $\boldsymbol{I} = 1/2$ are exposed to a magnetic field, the nuclei with $\boldsymbol{m_I}$ = +1/2 and $\boldsymbol{m_I}$ = -1/2 orient their spin magnetic moment vectors parallel and antiparallel to the $\boldsymbol{B_0}$ field, respectively. Compared to those nuclei aligned parallel to $\boldsymbol{B_0}$, the ones that are antiparallel to $\boldsymbol{B_0}$ hold higher energy. The energy difference between these two types of nuclei is known as nuclear Zeeman splitting ($\Delta\boldsymbol{E} = -\boldsymbol{\gamma}\hbar\boldsymbol{B_0}\Delta\boldsymbol{m_I}$) where $\Delta\boldsymbol{m_I}$ is the difference between the lowest energy state (i.e., the ground state) and the excited one. With respect to the quantum mechanical rules, the transitions allowed to occur provided that $\Delta\boldsymbol{m}$

is equal to one. A transition from a higher energy to a lower energy level results in an emission of energy whereas absorption of energy takes place for a transition from a lower energy level to a higher energy. The NMR spectrum observes the net amounts of all transitions (i.e., absorption and emission) in a sample as a resonance signal. Pulses of a second oscillating electromagnetic field ($\boldsymbol{B_1}$) which holds a specific frequency ($\boldsymbol{\nu}$) induces series of transitions in a sample. The second magnetic field ($\boldsymbol{B_1}$) is adjusted to be perpendicular with respect to $\boldsymbol{B_0}$. If the pulse frequency ($\boldsymbol{\nu}$) imposes equal quantum energies ($\Delta \boldsymbol{E} = -\boldsymbol{\gamma}\hbar \boldsymbol{B_0} \Delta \boldsymbol{m_I}$), the nuclei absorb the energy, resulting in an excitation of the spins to higher energy levels. The magnetic field strength is directly correlated with the detected resonance frequency of the sample. In fact, a greater field strength ($\boldsymbol{B_0}$) provides a higher resonance signal from a sample. In the other words, utilizing a higher magnetic field increases the energy difference ($\Delta \boldsymbol{E}$), elevating the amount of absorbed energy. Consequently, a higher intensity and greater sensitivity of the resonance signal in the NMR experiment can be achieved. After exerting the pulse through the second oscillating electromagnetic field ($\boldsymbol{B_1}$), the nuclei start to relax via emitting energy at a particular frequency. The signal intensity represents the overall emitted energy and the number of excited nuclei. Accordingly, quantitative information about the numbers of nuclear spins excited to the higher energy is obtainable through the signal intensity.[18,19]

There are mainly two well-known methods for performing an NMR experiment. In continuous-wave NMR (CW-NMR), the detection frequency is fixed. However, the magnetic field is slowly increased during the experiment. A higher resolution requires a significantly higher experiment time. Often, repeated scans are necessary for low concentration samples. CW-NMR is rarely used as suffers significantly from the concentration constraints. In contrast, pulse Fourier Transform NMR (FT-NMR) spectroscopy is widely in used. Upon the application of frequent pulsing, a single NMR scan can be obtained in a few seconds for most cases. An intense $\boldsymbol{B_1}$ pulse, which contains a wide frequency range, excites all nuclei via a single scan. Consecutively pulsing a low concentration sample provides a significantly higher level of sensitivity compared to CW-NMR. After the pulse, the excited nuclei return (i.e., relax)

to their ground state. The free induction decay (FID) is the relaxation decay pattern associated with the excited nuclei. However, nuclei with different frequencies exhibit different decay rates. The length of time between pulses includes the longest portion of an FT-NMR experiment. Commonly, the pulse requires roughly 10 μs while acquiring the FID falls within milliseconds to a few seconds. In overall, the FT-NMR can be three orders of magnitude shorter than the CW-NMR.[18,19]

The surrounding environment of a nucleus alters the local magnetic field ($\boldsymbol{B_{loc}}$) of an individual nucleus. Thus, each individual nucleus may resonate differently due to the nucleus interactions with its surrounding environment in a given sample. Such alteration in a nucleus resonance provides quantitative information about the nucleus itself as well as the surrounding environment. Spin-spin (scalar), dipole-dipole, and quadrupole are among the possible effective interactions related to the surrounding environment. Therefore, the impact of the surrounding environment on the behavior of a nuclear spins gives valuable information on molecular structures. Electrons shield (i.e., surround) nuclei of a compound. The external magnetic field ($\boldsymbol{B_0}$) decrease the local magnetic field ($\boldsymbol{B_{loc}}$) of a nucleus as $\boldsymbol{B_0}$ interacts with the surrounding electrons. Thus, the magnetic field that a nucleus perceived ($\boldsymbol{B_{eff}}$) is a result of the external magnetic field ($\boldsymbol{B_0}$) as well as the electron density shielding the nucleus. Accordingly, the chemical shielding ($\boldsymbol{\sigma}$), which has a dimension of parts per million (ppm), can be used to define $\boldsymbol{B_{eff} = B_0(1 - \sigma)}$**.** The chemical shift ($\boldsymbol{\delta}$) is the difference of the resonance frequency with respect to a reference often tetramethylsilane. By considering the frequency of the examined substance ($\boldsymbol{\nu_s}$) and the reference frequency ($\boldsymbol{\nu_{ref}}$), the chemical shift can be defined as $\boldsymbol{\delta = [(\nu_s - \nu_{ref})/\nu_{ref}] \times 10^6}$.[18,19]

Due to the surrounding electrons, the nuclear spins are coupled. This phenomenon, also known as indirect or scalar coupling, results in the splitting of the nucleus energy states of the spin system. Therefore, the splitting of the signal appears as multiplets in an NMR spectrum. In this regard, the number of intervening bonds, and the nature of the bonds can be understood through the frequency differences between the multiplet peaks (the coupling constant) in the spectrum.[18,19]

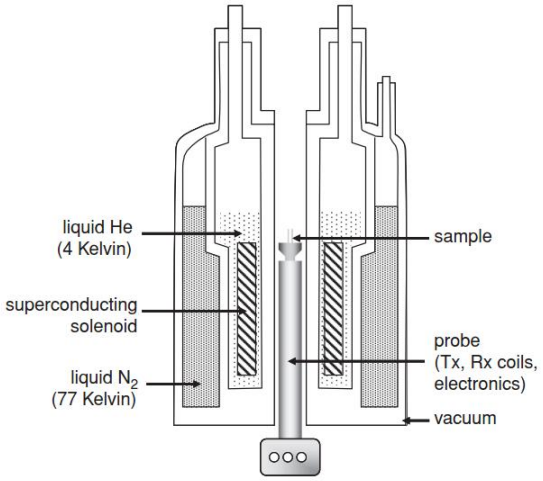

Figure 1. Schematic picture of a superconducting NMR electromagnet.[20] *(Adapted from the reference with permission)*

Practically, permanent magnets cannot be used for electromagnetic fields above 90 MHz. In fact, the previous generation of electromagnets required a high amount of electricity due to the coil resistance low and the necessity of cooling the magnet coils. The development of the superconducting wire made higher fields feasible. Below a critical temperature, superconducting wire exhibit approximately a zero resistance. Such critical temperature is known to be above the boiling point of liquid helium in most NMR magnets. Thus, the current continues to flow infinitely provided that the coil is maintained below the boiling point of liquid helium. As schematically shown in **Figure 1**, the liquid helium vessel is insulated through a vacuum layer as well as a liquid nitrogen Dewar to minimize the amount of liquid helium lost. The sample measurement area of the spectrometer insulated heavily from the magnet coils. The radiofrequency coils and the tuning circuits are located close to the sample in the middle part of the magnet. The probe consists of a series of electrical connectors housed in an aluminum cylinder. The sample placed in NMR tube is lowered into the center of the magnet through an airlift. The NMR tube, which often has a 5mm outside diameter, optimizes the filling of the receive coil in the probe. Based on typical sample requirements, the probes may have a variety of diameters. Commonly, the probe's outside diameter falls within 1 to 10 mm. A certain type of probe regards a specific nucleus or groups of nuclei such as proton and carbon. Moreover, a circuit designated within the probe is responsible for

monitoring deuterium to lock the spectrometer frequency, avoiding destructive drift by the magnet via the application of the deuterium resonance.[18–20]

Different environments of a nucleus impose different signal emission responses. As a result, the frequency absorbances captured by the spectrometer depends on locations of nuclei. This leading to a range of reproducible signals known as chemical shifts. In this regard, most structures are reported to be within 0-12ppm, 0-200ppm,-200-50ppm for ^{1}H, ^{13}C, and ^{29}Si, respectively. Also, ^{1}H can influence the signal of the adjacent hydrogens on neighboring carbon atoms, known as spin-spin coupling, resulting in reproducible splitting patterns in ^{1}H NMR. In fact, the original signal splits according to the number of hydrogens on neighboring carbon atoms plus one. However, the area underneath of the peaks represents the number of hydrogen atoms responsible for the signal.[20,21] **Table 2** illustrates the differences among ^{1}H, ^{13}C, and ^{29}Si. Due to the ^{1}H predominant natural abundance, ^{1}H nucleus gives a hundred times more sensitivity, providing better resolutions compared to ^{13}C.[21] Moreover, the natural abundance and gyromagnetic ratio of the ^{29}Si element is 4.7% (i.e., around one-fifth of a proton) and -5.314 ($10^{7}\ rad\ T^{-1}s^{-1}$), respectively. Among isotopes of silicon atoms (i.e., ^{28}Si (92.21%), ^{29}Si (4.70%), and ^{30}Si (3.09%)), only ^{29}Si has a nuclear spin of 1/2 to establish a magnetic moment. Moreover, ^{29}Si has a magnetic moment of -0.961 with a sensitivity of 3.69×10^{-4}. Although ^{29}Si has a higher proportion in the isotopic mixture, the magnetic moment's absolute value is lower than of ^{13}C, leading to a poor resonance frequency. Therefore, the low sensitivity of ^{29}Si NMR needs to be compensated through expanding the NMR experiment time, enriching the concentration of the NMR sample, increasing the number of scans, or utilizing a higher NMR magnetic fields.[20–22]

	Abundance	$\boldsymbol{\gamma\ (10^{8}\ rad\ s^{-1}T^{-1})}$
^{1}H	99.98	2.674
^{13}C	1.108	0.672
^{29}Si	0.047	-0.531

Table 2. Natural abundance and gyromagnetic ratio of different nuclei.[22]

In terms of silicon NMR, a known difficulty is the relaxation time which most often is greater than 20 second, causing the experiment to become highly time-consuming. The interpretation of silicon chemical shifts is described based on the charge on the silicon atom. In this regard, a parabola curve behavior can be observed by comparing the total electronegativities of the substituents on silicon atoms versus the silicon chemical shifts. It is assumed that the paramagnetic factor is responsible for such behavior. Thus, the magnetic shielding $\boldsymbol{\sigma}$ includes three components which are the diamagnetic component ($\boldsymbol{\sigma_d}$), the paramagnetic factor ($\boldsymbol{\sigma_p}$), and the neighboring atoms influence ($\boldsymbol{\sigma_n}$). The chemical shift is mostly affected through elements bonded to the Si atom. However, common parameters such as ring strain, solvent effects, and silicon atom coordination number have impacts on the chemical shifts. Interaction of the magnetic nuclei in a sample imposes the splitting patterns. With respect to ^{29}Si NMR, there are two distinguished occasions. In the first case, the isotopes such as ^{1}H, ^{19}F, or ^{31}P couples with ^{29}Si, resulting splitting patterns in ^{29}Si spectra. On the other hand, small satellite lines on each side of the main line are a result of coupling with rare spins such as ^{29}Si itself or ^{13}C. ^{29}Si, which has a spin quantum number of $\boldsymbol{I}$ = -1/2, is the only NMR-active isotope for silicon found naturally. The relatively insensitivity of the nucleus as well as the low a natural abundance (4.7%) constrained severely the application of silicon NMR for many years. However, the silicon NMR is become a routine experiment owing to the development of NMR spectrometers based on Fourier transform and pulse sequences.[23–25]

Application of a paramagnetic relaxation agent is among many techniques that are introduced to enhance the sensitivity of the ^{29}Si NMR experiment. Commonly, an addition of 0.1% solution of the agent (e.g., chromium complex) in the NMR solvent lowers the total acquisition time by a factor of ten. Appropriate non-glass NMR tubes, which are mainly based on Teflon@ or fluorinated ethylene/polypropylene, and silicon-free probes are utilized to minimize/remove the background signals. Moreover, a number of techniques are developed based on the coupled nearby protons such as Si-H or Si-CH_3 to improve the slow acquisition rate of silicon NMR. In fact, these advanced techniques aim to exploit the relaxation time and sensitivity of protons nuclei coupled to the silicon atoms. In these techniques, however,

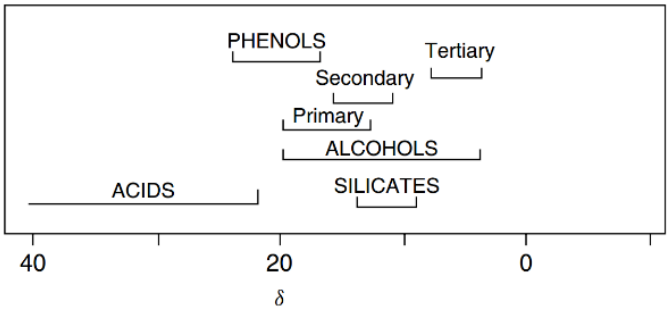

Figure 2. The chemical shift ranges for the trimethylsilyloxy derivatives.[25]*(Adapted from the reference with permission)*

noncoupled structures are not observable. Thus, remarkable improvement is achievable when Si atom is directly bonded to the hydrogen atom.[23–25]

In [29]Si NMR, the tetramethylsilane chemical shift is widely used as a reference. Trimethylsilyl (TMS), $(\boldsymbol{CH_3})_3\boldsymbol{Si}-$, is among the most common group in silicon NMR. The chemical shifts of $(CH_3)_3Si-\boldsymbol{C}$ occurs mostly near 0 ppm. More precisely, the upper and lower chemical shifts of TMS derivatives bonded to $-\boldsymbol{C}$, $-\boldsymbol{O}$, and $-\boldsymbol{N}$ are [-25,+30], [-1,+59], and [-29,+40] ppm, respectively. In terms of trimethylsiloxy category, the chemical shifts are related to the

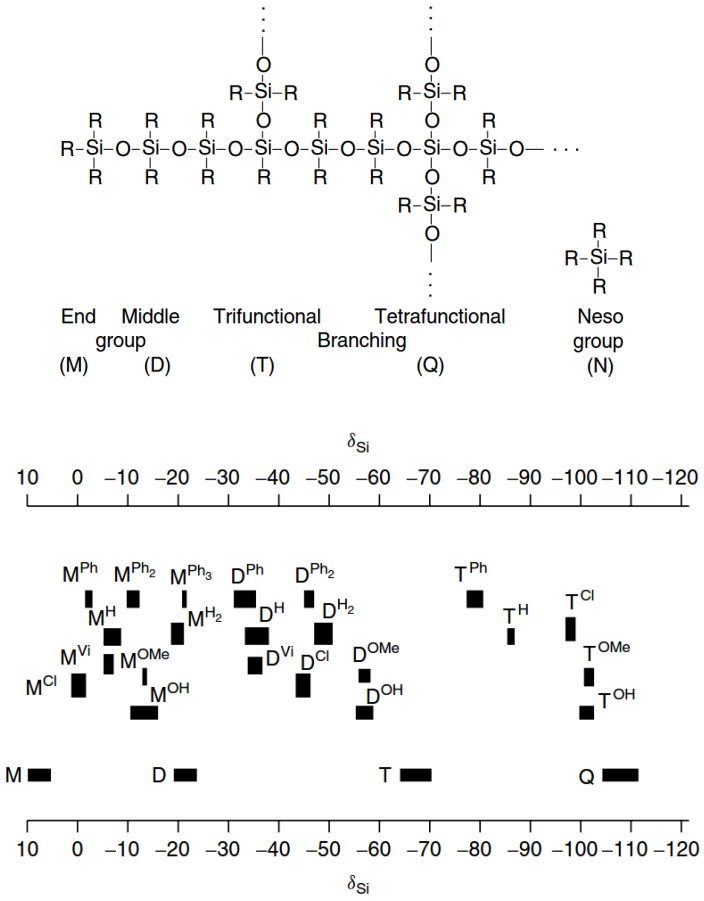

Figure 3. Structural representation of the polysiloxanes and the chemical shift regions attributed to the units.[25]*(Adapted from the reference with permission)*

oxygen atoms charges and the polar substituent effect. The chemical shift ranges for the trimethylsilyloxy derivatives are shown in **Figure 2** for a variety of substituents.[25]

^{29}Si NMR widely has been utilized to characterize oligomeric and polymeric siloxanes. In fact, the characterization of oligomeric and polymeric siloxanes is among the primary applications of the silicon NMR. In this regard, the main aim is to assess the building units of the silicone-based macromolecules (**Figure 3**). Often a superscript notation is used to distinguish a type of repeating unit with respect to the substituent bonded the silicon atom. The number of oxygen bonded silicon atom is the main difference between the building units shown in **Figure 3**. With exception of the **M** group, the substitution of an **R** group with an oxygen atom results in a shift toward lower frequencies. As discussed above, the chemical shifts are sensitive to the neighboring effect of the adjacent group. Thus, in the polysiloxane chain structure, such effect is widely used to understand the microstructure of the polymers.[23–25]

1.3 Esterification

Carboxylic acids are known as weak acids. However, their acidity is higher than alcohols or phenols. For instance, the $\boldsymbol{K_a}$(i.e., acid ionization constant) of acetic acid is significantly ($\sim 10^{11}$ times) higher than ethanol. Such higher acidity is attributed to the resonance stabilization of the negative charge in the conjugate base, where the negative charge is placed on the oxygen atom. Inductive effect is another factor affecting the carboxylic acids acidity. In fact, the O—H bond is polarized by the carbonyl group via attracting electron density through the sigma bonds, weakening the H—O bond. Consequently, the acidity of the ionizable hydrogen atom increases due to the reduced electron density of the H—O. On the other hand, an alkyl or aryl group attached to the carbonyl carbon atom has another inductive impact on $\boldsymbol{K_a}$. Alkyl groups are electron-donating compared to hydrogen atom. The acid is stabilized by the alkyl through an electron density release to the carboxyl group. In contrast, this effect destabilizes the conjugate base. For instance, the $\boldsymbol{pK_a}$ of acetic acid (~4.74) is higher than acid than formic acid (~3.75). Since an aryl group, which possess an $\boldsymbol{sp^2}$-hybridized carbon atom, is relatively electron-withdrawing compared to the alkyl group, the

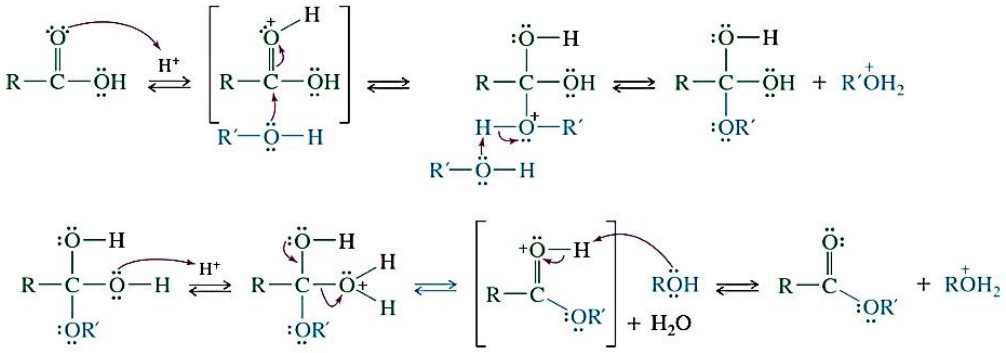

Figure 4. Fischer esterification mechanism.[27]*(Adapted from the reference with permission)*

pK_a of benzoic acid (~4.19) is lower than that of acetic acid. Thus, the adjacent of an electron-withdrawing group to carboxylic acids lowers the pK_a, resulting in more acidic structures.[26] The esterification of a carboxylic acid is not feasible under base-catalyzed mechanism as the basic catalyst deprotonates the carboxyl group to generate the carboxylate conjugate base, which is unreactive as a result of the resonance stabilization of the negative charge.[27]

Fischer esterification is an acid-catalyzed reaction of a carboxylic acid with an alcohol to form an ester. Since the Fischer esterification is an equilibrium, the reaction has to be pushed forward to obtain high yields. An excess amount of reactants (i.e., the alcohol or acid), the addition of dehydrating agents to reduce the amount of water produced can help to force the equilibrium toward the esterification. The reaction consists two main steps (**Figure 4**). In the first step, the protonation renders the carbonyl group more electrophilic, the addition of the alcohol, and deprotonation completes the reaction to yield the ester hydrate. Through the second step, acid-catalyzed dehydration occurs to produce the ester.[27]

Novozym-435® (N435) as a catalyst lowers the energy barrier of the esterification reaction while the equilibrium of the reaction is not influenced. Similar to the Fischer esterification, the equilibrium constant of the ester formation/hydrolysis relies on the substrate reactivity, and a complete conversion is often feasible with either excess amounts of reagents or the removal of water molecules. The unique functions of N435 as a catalytically active protein is due to its complex three-dimensional structure. Compared to the Fischer esterification, an enzymatic esterification has distinguishable characteristics such as accelerated reaction rates, high selectivity toward the substrates (i.e., the enzyme may favor significantly a specific

set of substrates), and the resulted product of an enzymatic reaction often follows a specific regulation (rule). More precisely, N435 is highly enantioselective towards chiral secondary alcohols. This is attributed to the structure of the active site of the enzyme where the secondary alcohols must adopt specific spatial conformations to coordinate or fit into the N435 pocket (i.e., active site). Thus, the enzymatic esterification is enantioselective with respect to chiral secondary alcohols. According to Kazlauskas' rule[28], the N435 pocket favors the (***R***)-enantiomer of bulky substituents compared to the (***S***)-enantiomer. Therefore, N435 enables the esterification to be highly selective (e.g., stereoselective, and enantioselective) toward substrates.[29]

The reaction of a carboxylic acid with an alcohol can be catalyzed by enzymes based on the same principle as the Fischer esterification (e.g., the protonation renders the carbonyl group more electrophilic). In fact, commercially available N435 is widely used in transesterification or esterification reactions due to its high stability and activity. It is a non-toxic, renewable

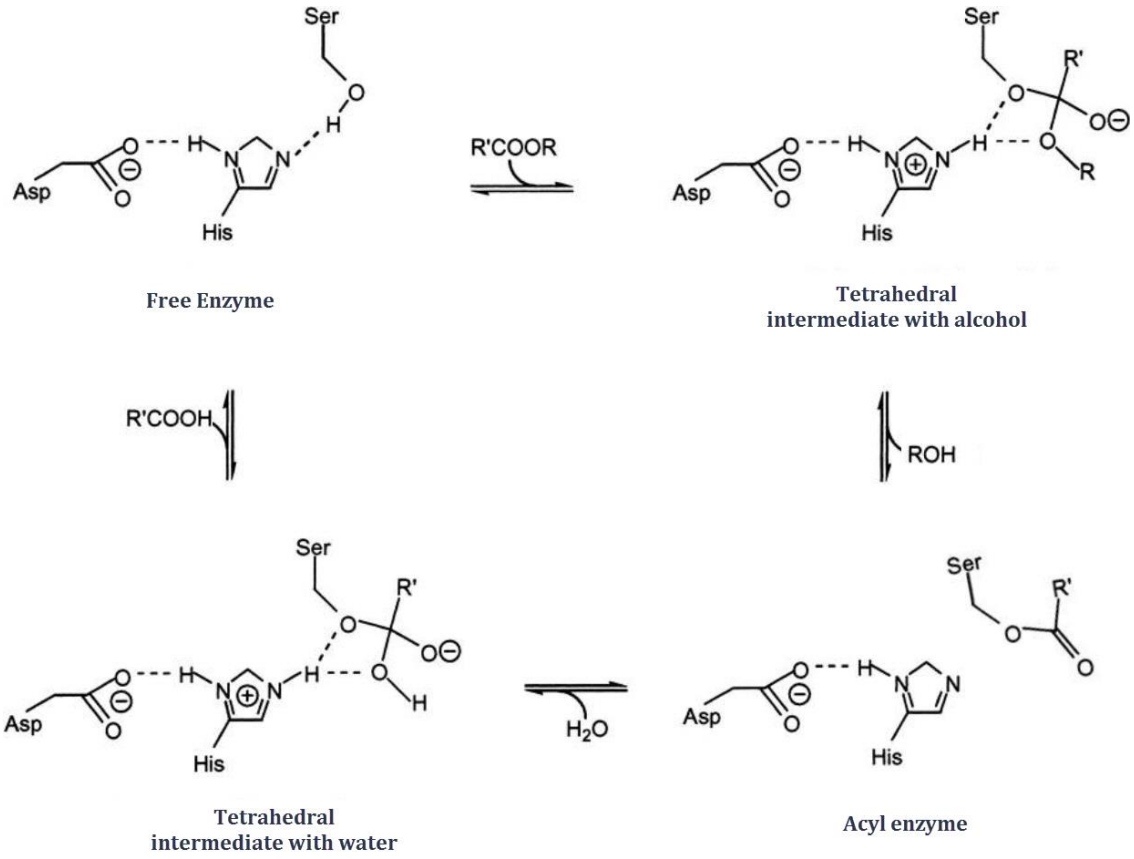

Figure 5. Novozym-435® can be used as a transesterification/esterification catalyst.[30]*(Adapted from the reference with permission)*

catalyst. N435 is an immobilized lipase which can be readily separated, recovered, and recycled for repeated usages. The catalytic triad of N435 is consist of histidine (base), serine (nucleophile), and aspartate which are located inside the active site (**Figure5**). Three hydrogen bond donors stabilize the transition states and the tetrahedral intermediates. A nucleophilic attack via serine on the carbonyl carbon leads to the acyl-enzyme intermediate. As shown in **Figure 5**, the interaction of an alcohol with the acyl-enzyme intermediate in the active site forms the second intermidiate (i.e., tetrahedral intermidiate with alcohol), leading to the desired ester. Similar to Fischer esterification, the mechanism's reactions are all reversible. Therefore, reducing the amount of water as a product or using excess amounts of reactants improves the reaction yield.[30–33]

1.4 Polymeric Materials

Polymers are consist of long molecular chains made by the chemical bonding of repeating units (monomers). While a homopolymer has only one type of monomer along its backbones, a copolymer has more than one repeating unit. The building blocks of the copolymers chains, however, can be aligned at more or less regular intervals within the chains. On the other hand, graft copolymers are a special type of branched polymers in which the chain backbone include more than one distinct repeating unit where pendant groups are tethered, **Figure6**.[34] Although many people probably do not realize it, modern life without polymeric materials would not be feasible. Even though plastics and rubbers are all around us in everyday use, polymers are almost anonymous for a majority of consumers. Polymers are a versatile class

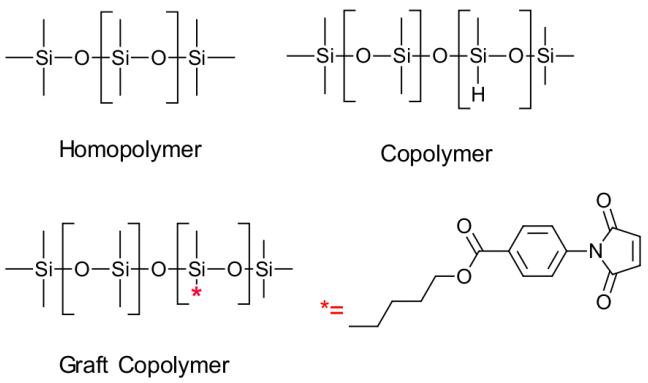

Figure 6. Structures of a homopolymer, a copolymer, and a graft copolymer.

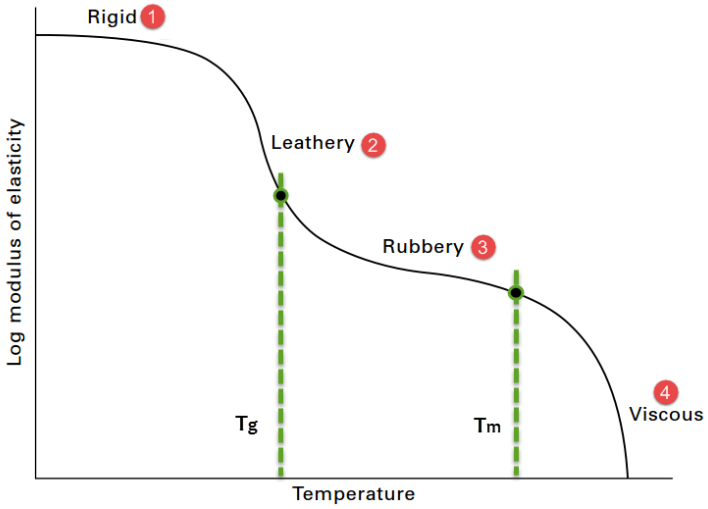

Figure 7. Different possible physical states for polymers.[36] *(Adapted from the reference with permission)*

of materials covering a wide range of properties. For example, a typical elastic modulus for a rubber can be as low as 10 KPa, whereas for a fiber of a liquid-crystalline polymer this value could be as high as 350 GPa or 35,000 times stronger. Another example is the electrical conductivity of polymers. The best insulating polymer could have a conductivity as low as $10^{-18}\ \Omega^{-1}\ m^{-1}$ while polyacetylene may have a conductivity value of $10^{4}\ \Omega^{-1}\ m^{-1}$, which is 10^{22} times higher.[35]

The elastic modulus, also known as Young's modulus, is a measure of the stiffness of solid materials. Polymers experience different physical states as the temperature changes (**Figure7**), which can result in a significant change in the elastic modulus. At low temperatures, as a result of low internal energies, polymer chains hardly move under an applied force (i.e., large deformations are suppressed). In this condition, polymers are described as being glassy or brittle. The glass transition temperature (T_g) is a reversible change in the physical state where polymers undergo a transition from a hard and glassy (crystalline) state to a soft and rubbery state. Such significant alterations in the materials' properties have made the T_g an important factor in designating a reliable operating temperature for polymers. At the melting temperature (T_m) chains can flow as a highly viscous liquid as a result of the increased amount of energy available. However, depending on the type of polymers, one or more physical states can be observed.[36]

Thermoplastics, thermosetting polymers (or thermosets), and elastomers are the three main groups of polymeric materials. A polymer's bulk properties are a reflection of its microstructures. That is why the thermoplastics, thermosets, and elastomers exhibit distinct physical and mechanical properties. The term "plastics" comprises the two first groups of polymers, namely thermoplastics and thermosets. Thermoplastics can be distinguished from the other types of polymers by their unique responses or behaviors in a stress-strain test or through the effect of temperature on the elastic modulus (**Figure 8**) which originates from their linear or branched chains that are entangled or intertwined with each other. Such structures can be enhanced to provide useful physical properties, including high ductility, toughness, and impact resistance. In fact, the recyclability or remoldability of thermoplastics

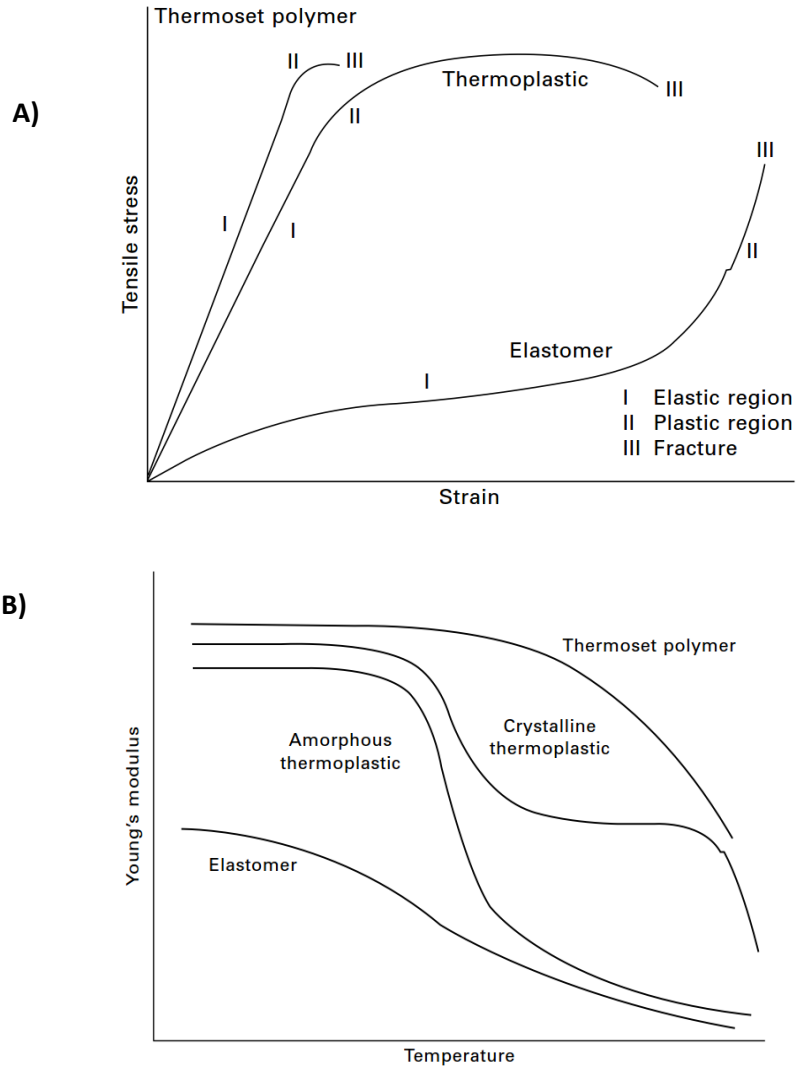

Figure 8. Sketch of A) tensile test B) temperature sensitivity of the elastic modulus for thermoplastics, thermosets, and elastomers.[36] *(Adapted from the reference with permission)*

arises from their capacity to soften and melt upon heating. However, in thermosetting polymers, chains are covalently linked together, resulting in a rigid three-dimensional molecular structure/network. Polymers may achieve a higher elasticity and tensile strength through these irreversible cross-links, but they become brittle as the rigidity of the network increases. Since these networks do not flow, thermosets do not have a T_m. Moreover, rubbers, or elastomers, contain chains with a lower cross-link density than the thermosets. Elastomeric chains structures are typically random coils with a T_g well below room temperature. The chains can be stretched reversibly without being permanently deformed as a result of their highly flexible backbones.[36]

1.5 Polysiloxanes

The unique properties of polysiloxanes [−Si(RR')O −] have resulted in this type of polymer being one of the most studied polymers about commercial applications.[37–39] Over a wide range of temperatures, polysiloxanes exhibit extraordinarily high flexibility, low viscosities, excellent thermo-oxidative stability, and high moisture resistance. These fascinating criteria come from the chains structural characteristics, which can be summarized as follows:[37–39]

- In comparison to C-C bonds (1.53 Å), the significantly longer Si–O skeletal bond (1.64 Å) reduces steric interference and intramolecular congestion.
- As disscussed earlier in **section 1.1**, the molecular orbital calculations suggests that ~144° is the intertetrahedral, Si–O–Si bridging bond angle which minimizes the bond energy. However, there is a small variation in the bond energy from 120° to 180°. As a result, Si–O–Si can obtain a wide range of angles.[40–42] Thus, the Si–O–Si bond angle (~143°) is much more open than the common tetrahedral bonding (~110°).

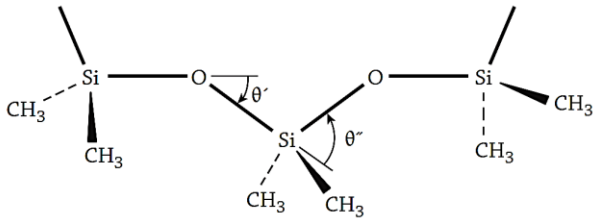

Figure 9. Sketch of a portion of polydimethylsiloxane chain, bonds angles θ' = 37°, θ'' = 70°. [37] *(Adapted from the reference with permission)*

- Unlike carbon-based polymer chains, the substituted silicon atom followed by the oxygen atom are greatly different in size, establishing a non-uniform cross-section along the chain. As a result, polysiloxane chains pack differently in the bulk or amorphous state compared to polyolefins. The polysiloxane's unusual compressibility[43,44] and the equation-of-state are attributed to this behavior.[37,43,45]

Therefore, polysiloxane chains are in elastic, random coil structures. Due to the high flexibility and mobility of the chains, polysiloxanes entangle or intertwine with each other at higher molecular weights compared to polyethylene chains. In fact, The chains entanglement's onset reported for polydimethylsiloxanes (PDMS) begins with 404 siloxane repeat units corresponding to a molecular weight higher than 30,000 g/mol.[46,47] This value represents one of the largest critical numbers of chain atoms for the onset of entanglement couplings.[48,49] Therefore, as a reflection of this microstructure, some of the lowest T_g values observed (i.e., below -100°C) among polymers belongs to PDMS chains.[38]

The application of polysiloxanes can be categorized into two main groups: medical and non-medical applications. Typical non-medical applications include high-performance rubbers, membranes, electrical insulators, water repellents, antifoaming agents, adhesives, mould-release agents, protective coatings, release control agents for agricultural chemicals, encapsulation media, mould-making materials, coatings, and hydraulic or heat transfer fluids.[37,50] These applications are based on the mentioned structural properties along with the ease of modifying the material surface. Silicones have also been developed for numerous

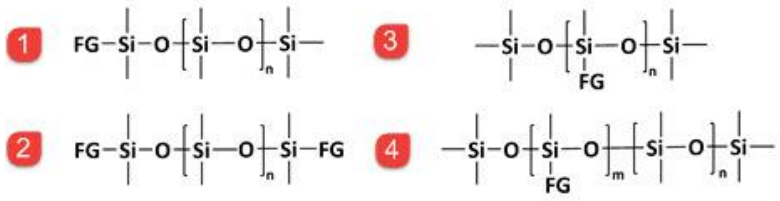

Figure 10. Different types of modified silicones. Functional groups (FG) can be at one end (1), at both ends of a siloxane chain (2), wthin of siloxane chains as a grafted homopolymer (3), or copolymer (4) with adjustable numbers of repeat units.

medical applications as a result of their inert nature, stability, and flexibility. Artificial organs, facial reconstruction motifs, vitreous substitutes, tubing and catheters, contact lenses, and drug delivery vehicles are medical usage of polymers based on siloxane repeat units.[37,51]

Often it is necessary to augment the properties of pure siloxane polymers for a specific target application. Aside from the addition of common ingredients such as fillers, processing aids, heat-aging additives, and pigments, the addition of pendant groups attached to the polymer backbone is a typical method for imparting unique properties to silicones (**Figure 10**). For instance, fluorinated polysiloxanes have been a popular type of modified silicone as they are preferred for applications that require the polymer to come into contact with fuels, lubricants, hydraulic fluids, and solvents due to their high fuel-resistance, wide operating service temperature range, and hardness.[52]

Cross-linking of polymer chains is a common approach for enhancing the physical and mechanical properties of a polymer system. Often, cross-linked polymers have superior properties such as higher durability, solvent resistance, dimension stability, and extended lifetimes. However, cross-linking may also result in polymers that are brittle and less toughened. The amount of energy required to break a material in a tensile test (the area under the stress-strain curve) is a practical way to measure the toughness of a cross-linked

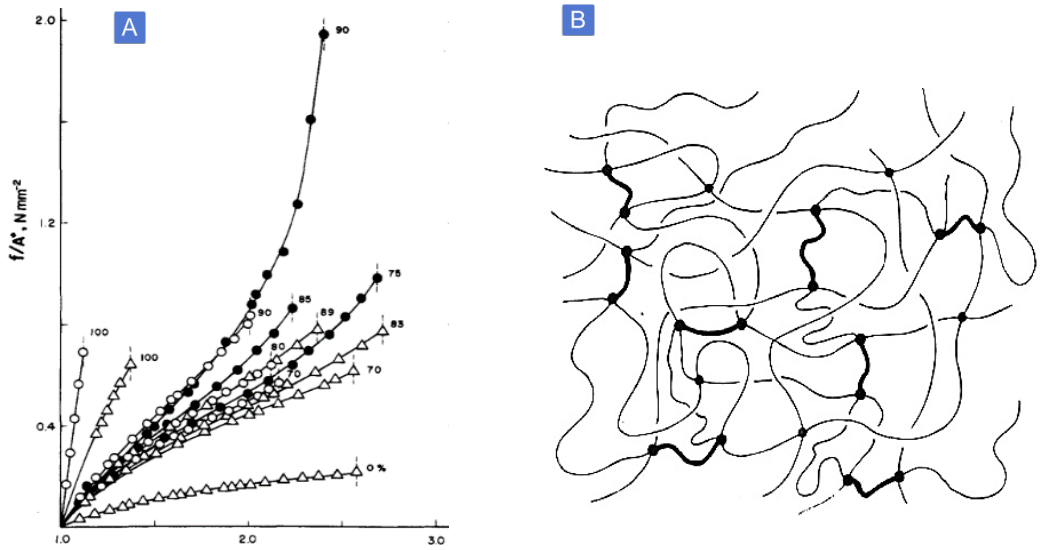

Figure 11. A) Stress-elongation plot for bimodal PDMS networks consisting of chains having relatively large molecular weight, $\bar{M}_c$ =18,500 g/mol, blended with short chains [$\bar{M}_c$ =1100 (△), 660 (○), and 220 (●) g/mol]. Each curve is labeled with the mol percentage of the short chain. B) Sketch of a bimodal network. Short chains are drawn thicker than long chains, dots represent the cross-links.[53] *(Adapted from the reference with permission)*

polymer system. In terms of PDMS networks, incorporating short chains (about a few hundred g/mol) along with relatively long chains (around 18,000 g/mol) led to increase not only in stiffness but also toughness of the material. Often, these two criteria are inversely correlated, meaning the higher the stiffness, the lower the impact resistance. The short chains increase the overall stiffness while the long chains are responsible for retarding the rupture process through their stretchability. Thus, such siloxane networks, commonly referred to as bimodal networks, exhibit an unusually high elastic modulus at large extensibilities, resulting in a higher toughness (**Figure 11**).[53] Therefore, utilizing different chain lengths in siloxane networks preparation is a valuable strategy to gain and avoid the beneficial properties of cross-linked polymers and its disadvantages, respectively.

1.5.1 Hydrosilylation, A Well-known Route to Functional Silicones

In silicone chemistry, cross-linked network structures can be prepared by hydrosilylation[14-16], cross-linking with free radicals[57,58], radiation[59,60], and more recently through "Click Chemistry"[61–63]. Additionally, silicones grafted with acryl, epoxy, vinyl, and styrene functional groups are also capable of cross-linking under the influence of light.

Hydrosilylation establishes a convenient route to polycarbosilanes through an addition reaction of Si-H bond to unsaturated bonds. Generally, the catalyst can be based on precious metals such as platinum, rhodium, and iridium or non-precious metals such as iron, and nickel. The relative catalytic activities of these metals are found to be in the order platinum, rhodium, iridium at ambient temperature.[55,64,65] The hydrosilylation catalysts based on aluminum, boron, alkaline-earth metals, copper, and titanium are **not** appealing to the industry due to their common poor reactivities and yields.[65] Among various catalysts, hexachloroplatinic acid $H_2PtCl_6/iPrOH$ (Speier's catalyst)[66] and $Pt_2[(CH_2 = CHSiMe_2)_2]_3$ (Karstedt's catalyst) have been the most commonly used hydrosilylation catalysts. Often, hexachloroplatinic acid, $H_2PtCl_6 \cdot 6H_2O$, is dissolved in an organic solvent such as isopropyl alcohol (1-10%) to obtain Speier's catalyst.[65,66] Karstedt's catalyst exhibits an improved in

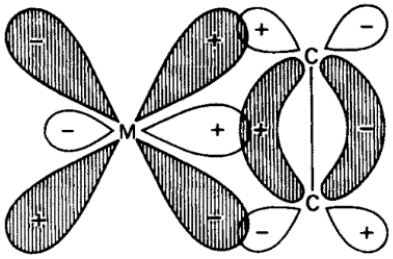

Figure 12. Metal-olefin bonding of catalysts based on transition metals. [65] *(Adapted from the reference with permission)*

activity, selectivity, and solubility in polysiloxane compounds compared to Speier's catalyst, widening the applications of hydrosilylation reactions. That is why $Pt_2(dvs)_3$ has been used mostly as a benchmark for the reactivity comparion of the other hydrosilylation catalysts even though platinum element is one of the most expensive, precious metals.[22,55,64,65,67–69] Similar to the other transition metals, platinum can form complexes with unsaturated organic compounds through donor-acceptor interactions (**Figure 12**). Based on the Dewar-Chatt explanation[70], the formation of bond includes two independent steps. In the first step, lone-pair donation of the ligand results in an overlap of the π-electron density of the olefin with σ-electron density of the metal. In the second one, the flow of high electron density from filled metal d_x^2 or other $d_\pi - p_\pi$ hybrid orbitals into antibonding, low-lying empty p orbitals of the olefin leads to the back-bonding.[22,55,65,70] After coordinative addition of the substrate to

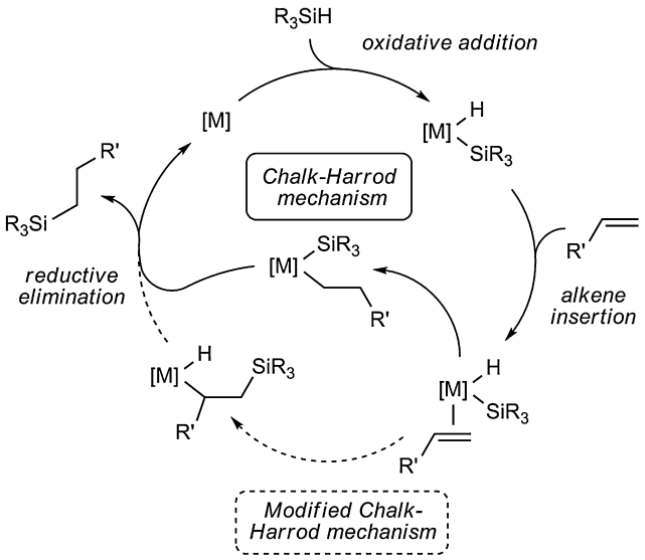

Figure 13. Explanation of the transition metal catalyzed hydrosilylation of alkenes via Chalk–Harrod mechanism and its modified version. [64] *(Adapted from the reference with permission)*

the metal, a hydrogen atom transfers intramolecularly from the olefin substrate to the metal atom. Subsequently, a nucleophilic attack on the coordinated ligands occurs which is followed by the insertion of the substrate.[65,67,70] More specifically, the Chalk–Harrod mechanism[71] is widely used to describe the platinum-catalyzed hydrosilylations (**Figure13**).[22,69,71,72] The reaction is consist of the oxidative addition of silanes ($HSiR_3$) to a metal alkene complex followed by an insertion of the alkene into the $M-H$ bond, prior to the final step (i.e., reductive elimination) which leads to $Si-C$ bond formation. A modified version of the mechanism is also described in the litrature to rationalize the other phenomena such as the induction period and the formation of vinylsilanes (**Figure 13**).[72,73] In fact, in the develeoped Chalk–Harrod mechanism, the alkene insertion to the $M-Si$ bond is followed by reductive elimination of the $C-H$. However, computational studies indicated the Chalk–Harrod mechanism in Pt-catalyzed hydrosilylation reactions is favorable energetically compared to the modified Chalk–Harrod mechanism.[74,75] Although platinum-based catalysts are extensively used in industry as a result of having enhanced catalytic activities, and a higher stability towards heat, oxygen and moisture compared to other hydrosilylation catalysts, they impose side reactions such as dehydrogenative silylation, hydrogenation, isomerization, oligomerization, and redistribution of hydrosilanes shown in **Figure 14**.[64,69,72]

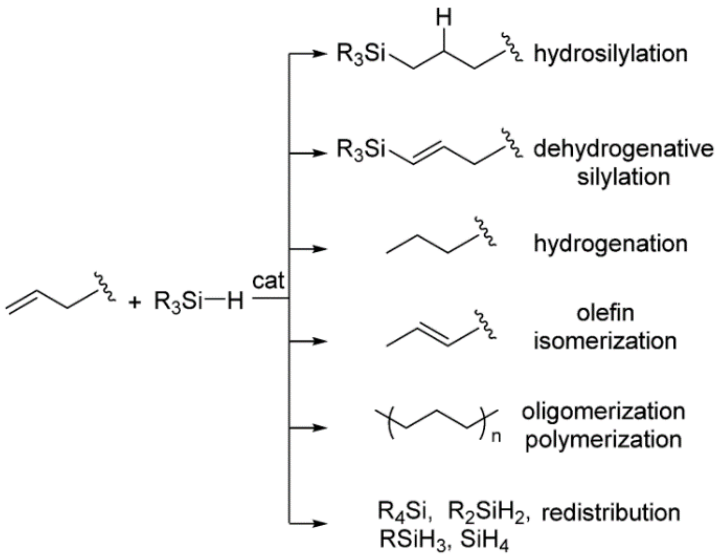

Figure 14. Hydrosilylation and side reactions of platinum-based catalysts.[69] *(Adapted from the reference with permission)*

In platinum-catalyzed hydrosilylation of 1-alkenes, the reaction follows the anti-Markovnikov rule, producing β-hydrosilylated 1-silylalkanes as the major product.[22,65,67,70] As shown in the catalytic pathway of the Karstedt's catalyst (**Figure 15**), O_2 is found to serve as a crucial cocatalyst for Pt-based hydrosilylation reactions to generate the active Pt-colloid, $Pt_x^0(O-O)$, turning the reaction mixture a yellow color. The active colloid reacts with a hydrosilane to form the Pt-hydrosilane complex (**2**). Through preventing irreversible colloid agglomeration, molecular oxygen not only influences the catalyst to be more susceptible to the nucleophilic attack of the olefin but reduce the darkening effect on the reaction mixture's color.[22,67]

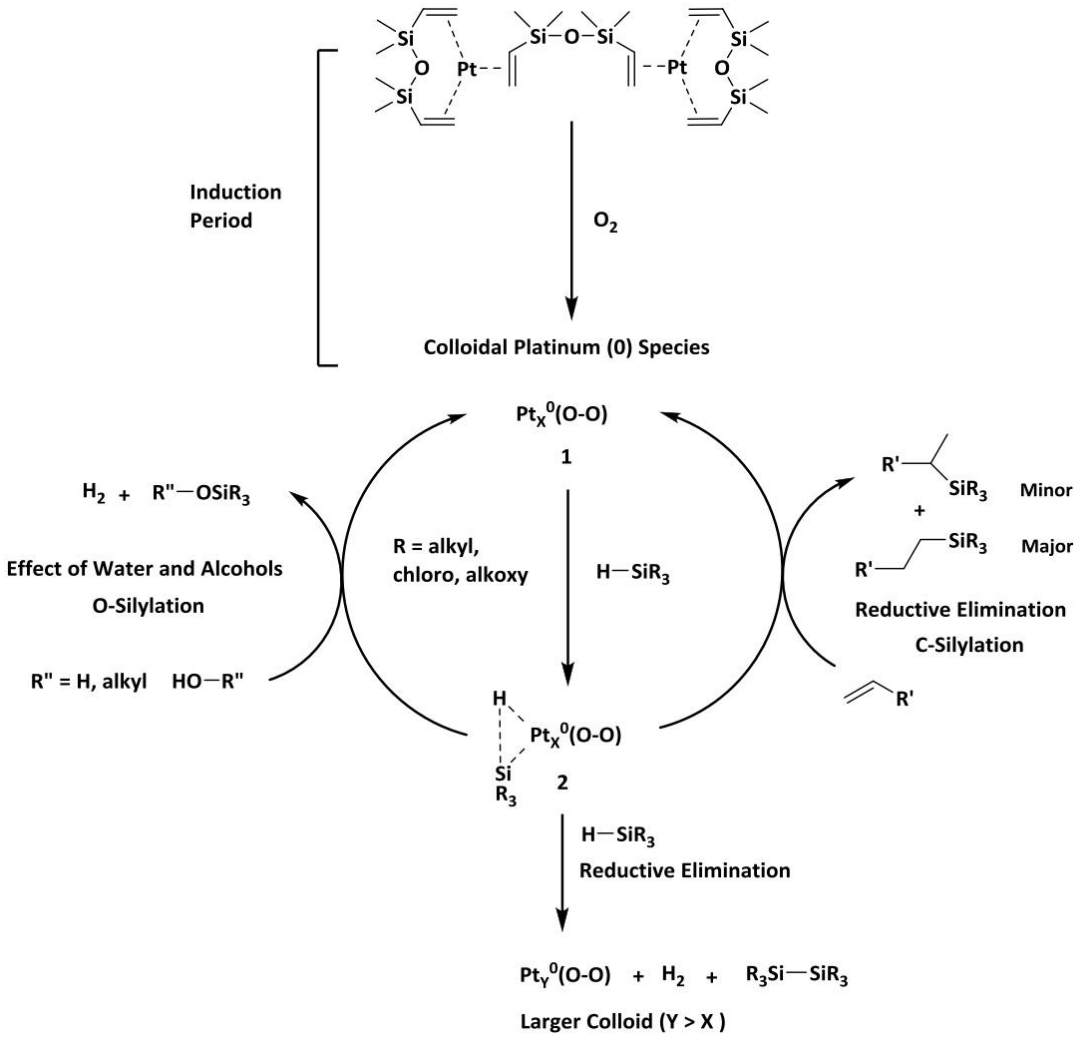

Figure 15. Hydrosilylation reaction pathway for Karstedt's catalyst.[54] *(Adapted from the reference with permission)*

In the presence of a catalytic amount of Pt(II), vinyl groups efficiently react with silanes (Si–H). As a result of this reaction, a variety of functional groups can be grafted onto polysiloxanes, often without the formation of a negligible amount of side products. The addition of polyfunctional silicon hydrides to polyvinylsiloxanes along with Pt(II) complexes leads to well-defined networks.[76] As discussed earlier, Karstedt's catalyst undergoes an induction period (**Figure 15**). The trace amount of oxygen is necessary to form the colloidal platinum complex **1,** which acts as a hydrosilylation promoter. Subsequently, intermediate **2** is generated via the oxidative addition of the silane group to the complex. Through the nucleophilic attack of a vinyl group, the hydrosilylation product and platinum catalyst **1** are obtained. Commonly, the hydrosilylation reaction yields two adducts known as α and β (major product) along with some minor compounds resulted from the side reactions shown in **Figure 15**. Regarding side reactions, trace amounts of water or alcohols, and a slow further attack of H−SiR_3 on complex **2** may deviate the hydrosilylation from its main route to generate alkoxysilanes and deactivate the hydrosilylation catalyst by producing species containing Si-Si bonds, respectively.[54] Si-H bonds can react with alcohols, amines, and carboxylic acids.[77] These functional groups, in the presence of alkenes or alkynes, may result in competition with O- or N-, and C-silylation. Therefore, protection of reactive groups is of vital importance to avoid O- or N-silylation during the preparation of oligosiloxanes with such substituents.[78–82] In contrast, allyl alcohol, 2-allyloxyethanol, and 4-penten-1-ol can predominantly result in C-silylation without protecting hydroxyl groups (**Figure 16**).[81,83–85] High catalyst concentration, excess amounts of hydroxyl groups, and solvent are the major factors eliminating almost all O-silylation reactions.[81]Also, platinum oxide is known as an O-

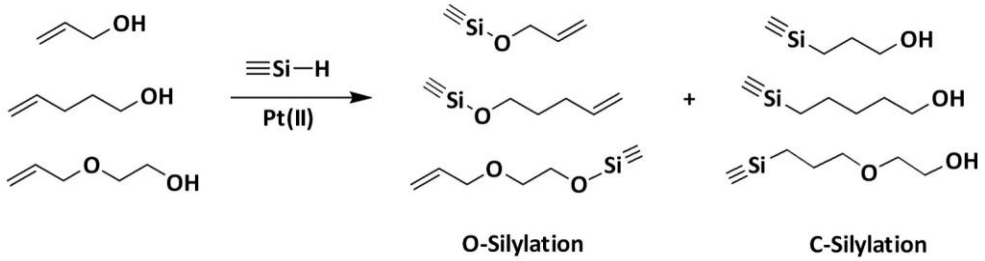

Figure 16. O-silylation versus C-silylation. Depending on hydrosilylation condition, C-silylation may exclusively occur.

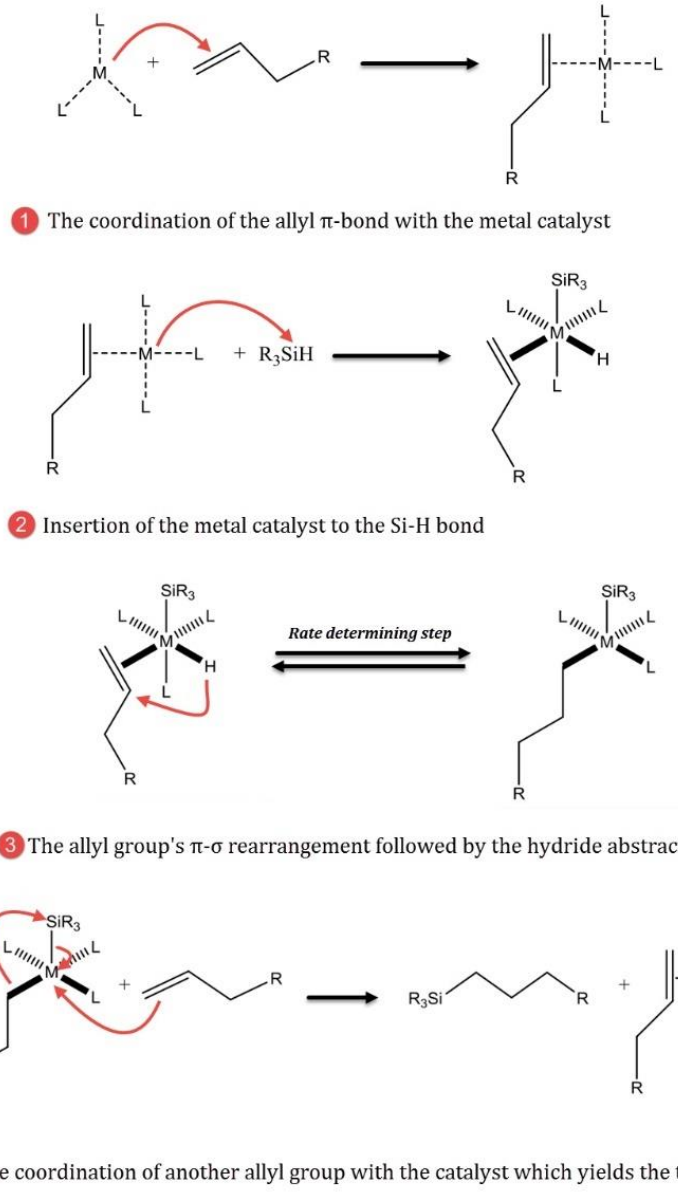

Figure 17. The Chalk-Harrod mechanism of a metal-catalyzed hydrosilylation with the assigned mechanism's arrows.[87]

silylation tolerant catalyst.[55,86] According to the Chalk-Harrod mechanism of a metal-catalyzed hydrosilylation, the mechanism's arrows are drawn as **Figure 17**.[87]

Rhodium, iridium, and ruthenium are the most industrially known alternatives to platinum based hydrosilylation catalysts.[64,69] Based on recent reports, an improved temperature resistance, prevented discolorations, and extended reactivity time are the of the advantages described for newly introduced rhodium-based catalysts.[64] However, as rhodium is even more expensive than platinum, there has been little interests to develop hydrosilylation

catalysts based on this element. Although iridium has a price substantially lower than Pt or Rh, the lack of high reactivity and low lifetime impose using high catalyst concentrations. Thus, iridium-catalyzed hydrosilylation is more industrially preferred as an alternative to prevent Pt-based catalysts selectivity issues.[64,65,69] As an advantage of rhodium-based catalysts, they are known to provide improved regioselective because of following preferentially the modified Chalk–Harrod mechanism as opposes to the platinum complexes. For instance, the reaction of trichlorosilane with olefinic nitriles (such as acrylnitrile) reported to produce selectively the desired β-cyanoalkylsilanes.[64,69] Similar to the other metal complexes, chloroplatinic acid, Pt/C, and Ru-based catalysts (e.g., Wilkinson's catalyst) are unable to hydrosilylate predominantly the $C = C$ bond of alcohols or carboxylic acids. In most cases, not only the c-silylation but also the competitive reactions (e,g., O-silylation or dehydrocondensation) occur, causing the production of alkenoxysilane and acyloxysilane compounds. Although, the reaction conditions, polarity of the solvent, usage of cocatalyst, and strcuture of the catalyst are reported to be effective on the products ratios, it is essential to protect the hydroxy groups to avoid all O-silylation products. In terms of unsaturated esters, Pt/C and Speier's catalyst are known to exhibit a higher cpacity of C-silylation.[22,64,65,67,69,71–75] Due to the poisoning impact of the amino functionality, Speier's catalyst and Karstedt's catalyst are reported to have low to moderate (20%-50%) yields for the hydrosilylation of aminated alkenes. However, at the same conditions, Pt/C and PtO_2 provided 95% reaction yields. More recently, PtO_2 is introduced as a compatible hydrosilylation catalyst which tolerates many functional groups such as amine, acid, nitrile, ester, ketone, and ether to yield highly C-silylation products.[68] In contrast to Karstedt's catalyst, platinum(0)-carbene complexes are shown to be highly active and selective catalyst having compatibility with wide a range of functional group including hydroxy, and epoxy.[88] Additionally, platinum(IV) dioxide (i.e., PtO_2) is reported to be highly tolerant toward carboxylic acids.[88,89]

Complexes based on Fe (iron) are another low-cost hydrosilylation catalysts, where the aim is to replace the precious metals with iron while preserving a cost-efficient catalytic activity

comparable to the widely used Pt catalysts. Perhaps, iron pentacarbonyl $Fe(CO)_n$ is one of the well-known hydrosilylation catalysts in this category. However, the reaction associated with $Fe(CO)_5$ is prone to the dehydrogenative silylation of alkenes where vinylsilane may become the main product. Compared to Speier and Karstedt's catalysts, iron-based catalysts are known to be less general or practical. In fact, their occasionally comparable activities to the Pt catalysts is mainly acknowledged industrially for tertiary silanes. Commonly, Fe complexes are efficient and regioselectivities compared to the platinum-based catalysts with respect to the hydrosilylation of terminal olefins with tertiary silanes. The catalysts in this category are typically described to be well-compatible toward a variety of functional groups such as halide, primary amine, ester, ketone, and nitrile for yielding the anti-Markovnikov products. In fact, the iron-based catalysts are often capable of undergoing a chemoselective reaction where the terminal alkene's double bonds are targeted as opposed to the carbonyl groups. The iron centers in these complexes are electron-rich. Thus, the catalysts favor the alkene's double bond over the C–O double bond.[90,91]

1.6 Molecular Weight Determination of Polymers

Generally, polymers are composed of carbon and hydrogen atoms in quite simple configurations. However, they can be used in a variety of applications, including human bone prosthetic implants, gas pipelines, car bumpers, synthetic fibers, and plastic films. The reason for this outstanding versatility is that microstructural characteristics, such as distributions of molecular weight, polydispersity index or heterogeneity index, chemical composition (short-chain or long-chain branching), have an enormous impact on the macroscopic criteria and applications of a given polymer.[34,35] Polymers are consist of repeat units (monomers) chemically bonded into long chains. Understanding the physical properties of a polymer such as mechanical strength, solubility, and brittleness, requires knowledge of the length of the polymer chains. Chain length is often expressed in terms of the molecular weight of the polymer chain, related to the relative molecular mass of the monomers and the number of monomers connected in the chain. However, all synthetic polymers are polydisperse,

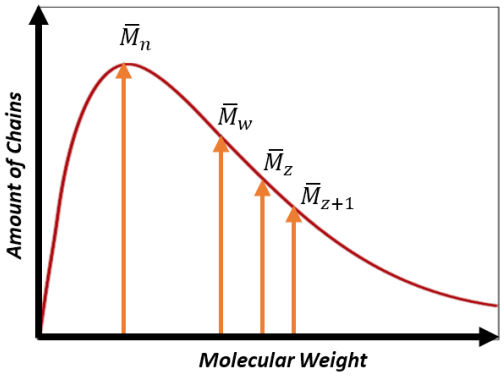

$$\overline{M_n} = M\frac{\sum nP_n}{\sum P_n}$$

$$\overline{M_w} = M\frac{\sum n^2P_n}{\sum nP_n}$$

$n = number\ of\ repeat\ units$

$P_n = chains\ frequency\ of\ chain - length\ n$

$M = average\ moleculare\ weight\ of\ repeat\ units$

Figure 18. Distribution of molecular weights for a typical polymer.[294]*(Adapted from the reference with permission)*

meaning that they contain unequal chains lengths, and therefore the molecular weight is not a single value. Thus, polymer chains exist as a distribution of chain lengths and molecular weights, **Figure 18**.[92,93] The molecular weight of a polymer must be described as an average molecular weight calculated from molecular weights of all chains in a given sample.[35] In gel permeation chromatography (GPC), also known as size exclusion chromatography (SEC), a dilute polymer solution passes through a column which is packed with porous beads. The stationary phase is the small, porous particles. Depending on the size of polymer chain (i.e., hydrodynamic radius), the molecule can or cannot pass through small pores of the column. The larger molecules pass by and continue to stay in the mobile phase of the column without diffusing inside the beads. However, low molecular weight oligomer chains diffuse in and out of the pores via Brownian motion, remaining inside of the column for extended amounts of times. Therefore, the GPC experiment's result is a reflection of molecular weights. The molecular weight distributions can be determined through comparison of a sample with monodisperse standards or a reference polymer such as polystyrene. Furthermore, Matrix-assisted laser desorption/ionization (MALDI) is another method to obtain the molecular weight distribution (MWD) of polymer chains. Compared to GPC which is a relative method to derive the MWD, mass spectrometry is a direct technique. Laser irradiation of a thin layer made by a given polymer's sample results in desorbing the polymer into the gas phase. Subsequently, the ions are guided toward the mass spectrometer's channels to be analyzed. Typically, the laser pulse is followed by a delay in time prior to application of the voltage.

This enables the ions to move out of the ion source. Afterwards, these ions are accelerated via an electric potential. Due to the differences in mass-to-charge ratios (i.e., m/z), ions' velocities vary which produces a series of signals representing MWD.[94]

Number-average molecular weights can be obtained through values of boiling point elevation, melting point depression, vapor pressure lowering, and osmotic pressure. Placing these parameters inside mathematical equations gives an estimate of $\overline{Mn}$. More sophisticated methods are based on dynamic light-scattering and neutron-scattering applied to polymer solutions. Also, the ratios of repeating units can be found by comparing the integral values of the repeating units in proton NMR. The heterogenity index, previously known as polydispersity index, is used as a measure of the broadness of a molecular weight distribution of a polymer sample defined by the ratio of $\overline{Mw}/\overline{Mn}$. The larger the value, the broader the molecular weight. In a mono-disperse sample ($\overline{Mw}/\overline{Mn}$=1), all chains have an equal length. However, the best controlled synthetic polymers which are using for calibrations, have a dispersity index of 1.02 to 1.10.[34,35,92,93]

1.7 The Cubic Silsesquioxanes

The empirical formula $RSiO_{1.5}$, represents $Q_8M_8^R$ Silsesquioxane structures where R can be a wide range of functional groups. Interest in utilizing polyhedral oligomeric silsesquioxanes (POSS) in polymer structures is based on the unique opportunity available for preparing truly dispersed hybrid (inorganic–organic) materials. The POSS's unusual structure is formed by the connection of siloxane rings in a finite molecular skeleton. It is the smallest silica particle with a diameter between 1 and 3 nm when the side groups are included. This dimension is large enough to be comparable to polymeric segments. Unlike silica particles or other traditional fillers for polymers, POSS can be compatible with a variety of polymers, biological systems, or surfaces by modifying the substituents attached to the vertices.[95–97] Functional groups, such as methacrylate, acrylate, styrene, norbornene, amine, epoxy, alcohol, and phenol, provide routes for obtaining a diverse library of POSS-containing polymeric materials.[98,99] A prime example of such compatibility is the amphiphilic POSS designed for

encapsulating bioactive molecules.[100] Thus, POSS molecules offer a unique opportunity to embed inorganic nanosized structures in polymeric materials.

Regarding incorporating POSS into polymers, several strategies are described in the literature. Blending POSS particles into a polymer matrix, covalently bonding mono-functional POS molecules into polymer chains as pendant groups or building blocks, and cross-linking polymers via tri- or higher functional POSS structures have led to a variety of POSS-containing polymers.[98,99] Phase separation and aggregation of the POSS cages are problematic aspects of introducing conventional reinforcing fillers such as carbon black, and silica to polymeric media. As a significant advantage over traditional filler technologies, a true

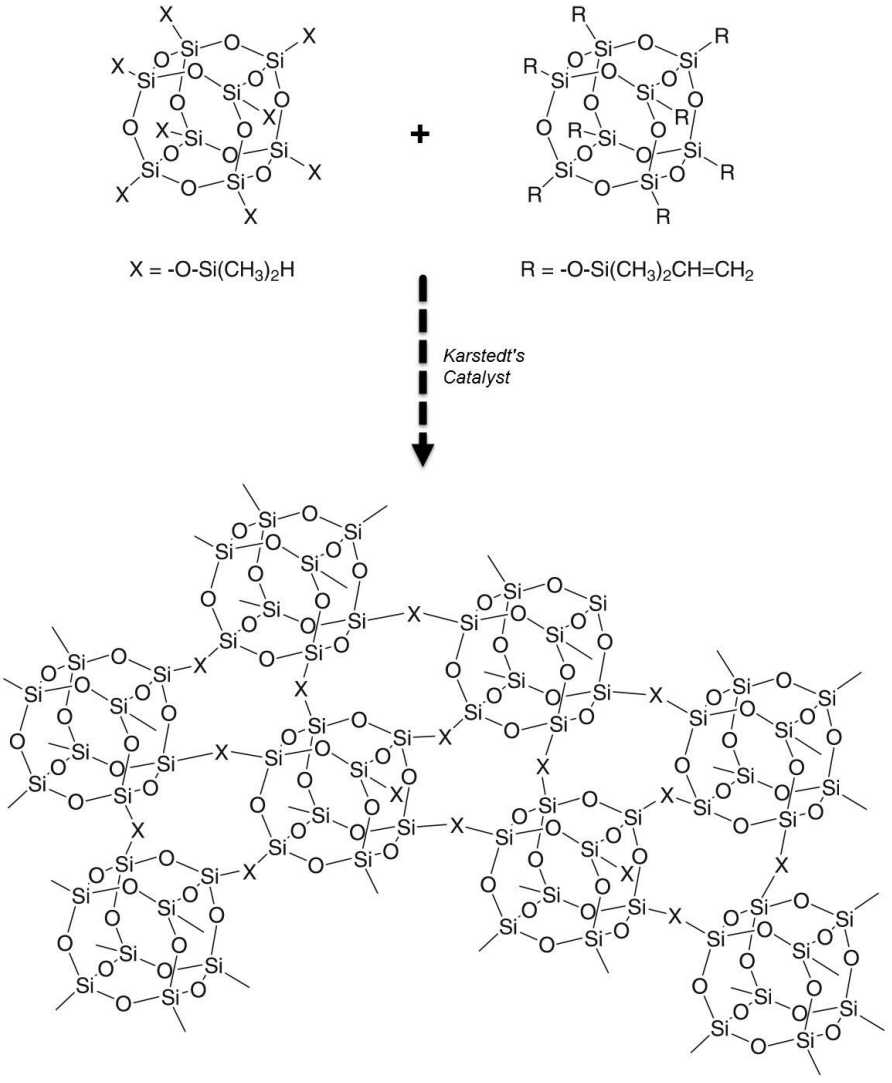

Figure 19. Hydrosilylation of multifunctional vinyl POSS and $Q_8M_8^H$ macromonomers using Karstedt's catalyst.[96,101] *(Adapted from the reference with permission)*

molecular dispersion is achievable as long as the POSS cages are soluble in the reaction media.[97,98]

Hydrosilylation is an efficient route for developing POSS micro- (<2nm) or mesoporous (2nm-50nm) hybrid materials. Based on the gelation times, POSS with higher flexible bridging groups can be more reactive due to steric effects and accessibility of the R groups (**Figure 19**). Lengthy, flexible functional groups provide more conformational freedom than regid bridging groups. Thus, the time required to reach the gelation point (i.e., the onset of having all POSS groups connected to each other as a whole network) may decrease noticeably. Consequently, the degree of cross-linking at a given period of the reaction may significantly experience an increase in the length of the intercube units increases.[96,97,101]

Employing POSS as a component of elastomeric systems can improve thermal stability, oxidation resistance, resistance to fire, surface hardening, mechanical strength, and viscoelastic properties. Polyimide-POSS polymers are an outstanding example of the potential thermal stability that POSS can offer. The mass loss of polyimide-POSS is reported to be less than 5% at temperatures below 500°C. Such thermal stability is crucial to achieve the protection needed for spacecraft and satelites.[97–99] POSS molecules are generally described as hard blocks or reinforcing particles in high-performance polymer materials.[95–97] Typically, the incorporation of POSS into polymeric materials not only increases the T_g, but also broaden its range.[96] The large mass, and steric structure of the POSS unit restrict its displacement, and the segmental motion nearby polymer chains. In fact, segmental motion is greatly hindered due to the interactions between polymer chains and POSS molecules. Therefore, chains mobilities and segmental motions are more difficult in the presence of POSS units. As a result, higher temperatures are required to alter the physical state of POSS-containing polymers from a glassy to a rubbery state. This mechanism is analogous to the ''sticky reptation'' model[102] described for hydrogen-bonded elastomers.[97,103] Additionally, this steric impact can be amplified or even diminished by the type of bridging groups connecting POSS structures to polymers chains. Therefore, the rigid bridging via arylic,

acrylic, or acetylenic groups amplifies the influence of POSS on glass transition temperatures while flexible alkyl groups helps to decrease the effect.[96,104]

1.8 Summary

Polymers are capable of being used in a variety of applications. Adjusting the physical properties of polymers can be achieved through a combination of different factors. In fact, multi-component hybrid materials can offer not only the thermal stability of POSS but also the flexibility and toughness of siloxane bimodal networks. The material's higher durability and performance may beneficially impact the environment as it opens possibilities to minimize exploiting natural recourses and the hazards associated with production & processing of polymeric materials, as well. Moreover, utilizing the available, efficient & less toxic reactions such as hydrosilylation provides materials that potentially can be categorized as highly demanded commercial polymers. Therefore, the ultimate aim of this thesis is to embed the self-healing criteria discussed in next chapters, into POSS-containing bimodal siloxane networks via efficient reactions.

Chapter 2 Self-Healing

Welding, gluing, and patching are the traditional methods used to repair materials that have been mechanically damaged. The ultimate goal of the self-healing strategies is to minimize manual interventions during the repair process of damaged materials. Self-healing polymers are a class of smart materials capable of responding to a specific stimulus, commonly thermal and mechanical energies, to heal the damaged areas through a chemical reaction or physical interaction.[105]

Polymeric materials are susceptible to damage over the course of their lifetime. As a result, engineered materials have been developed with the aim of damage suppression/management to extend the lifetime and reliability of synthetic polymers. Cross-linking is often employed as a means of enhancing the physical and mechanical properties of polymers. Compared to thermoplastics, which are not chemically cross-linked, thermoset materials can have higher durability, extended lifetimes, greater solvent resistance, and dimensional stability. However, a great challenge in designing such materials is how to incorporate self-healing features into polymers architectures to integrate the required physical and mechanical properties with the self-repairing capabilities.[106,*]

This chapter deals with the important parameters involved in designing self-healing polymers. It reminds readers that the essence of the self-healing phenomena is originated from the many biological examples surrounding us.[107,108] In fact, studying these biological examples helps us to apply a simple version of their self-healing mechanisms to polymeric networks, leading us toward chemical reactions and physical interactions suitable for self-healing. Different types of self-healing mechanisms will be compared and contrasted in this chapter. The use of nanoparticles such as POSS and carbon nanotubes is discussed as another pathway to develop self-healing materials.

---

[*] *This paragraph is taken from the author's recent paper.*

2.1 Origin of Self-Healing Materials

Perhaps, a fascinating feature of many living organisms is the capacity for self-repair. In these systems, the damage itself activates a series of biological mechanisms to heal the defects that are formed. To apply the self-healing features to synthetic materials, scientists have monitored many living organisms. "*Weeping Fig"* and "*Delosperma cooperi"* are among those biological systems observed (**Figure 1**). Often self-repairing mechanisms can be categorized into two distinct processes.[107,108] Upon the damage, the organism tries to rapidly seal the injured site to retard any further propagation of the damage through the release of a sticky liquid called latex. Subsequently, the color of the latex gradually changes from a white, opaque material to a colorless liquid as a result of a series of chemical reactions through which the organism regenerates the lost tissues. These two subprocesses are known as rapid sealing and latex coagulation, respectively. The self-healing process was analyzed by infrared spectroscopy with attenuated total reflection (ATR-IR) (**Figure 2A**) where the reflected beams from a certain depth of the material were measured. As a result of interacting with the covalent bonds, the reflected beams are attenuated and weakened. Water loss caused by evaporation and the formation of amide bonds between latex particles at the damaged zone is described as the main factor changing the beam's absorbance (**Figure 2A**).[107] Moreover, the stress-strain tests shown in **Figure 2B**, clearly illustrate the immediate recovery of the material's elastic modulus (Young's modulus) in less than 5 minutes. Therefore, the functions

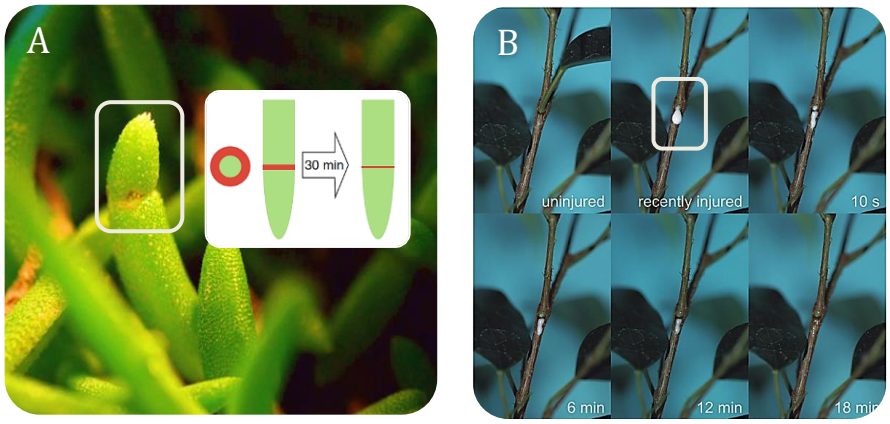

Figure 1. A) a leaf of "Delosperma cooperi" plant was partial cut using a razor blade. The damaged area, specified by the red colour, significantly healed after 30 minutes. B) an injured branch of the "Weeping Fig" tree. Macroscopic observation shows that after the damage, a latex droplet seeps out to immediately seal and heal the wound. [107,108] ***(Adapted from the reference with permission)***

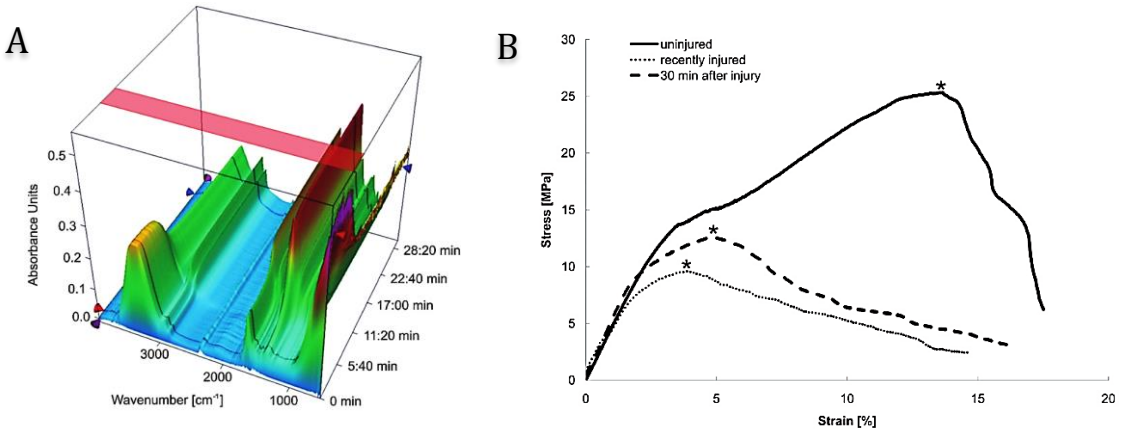

Figure 2. A) ATR-IR spectra of an injured "Weeping fig" tree, covering the whole self-repairing process. B) a comparison of "Weeping fig" tree tensile strengths among uninjured, recently injured, and 30 minutes after injury.[107] *(Adapted from the reference with permission)*

and mechanical properties of the injured tissues quickly can be restored during the self-healing process. Regardless of the type of self-healing mechanisms, the ultimate goal is to restore the initial properties so that the system functions nominally again.

Inspired by living organisms, several approaches have been introduced to equip synthetic materials with simplified versions of biological self-healing systems. In polymeric materials, these approaches can be divided into two major groups known as extrinsic and intrinsic self-healing methodologies. As each method brings its own advantages and limitations, it is necessary to realize which one would be suitable for a given application. Understanding the physical aspects is a requisite for designing self-healing polymers.[109]

2.2 Physical Principles of Self-Healing

Self-healing approaches in polymeric materials are commonly based on the formation of new networks that reconnect the loose chains ends in the damaged zones.[110] Depending on the approach selected, the healed network can be the result of covalent bonds, physical interactions, or the chains' entanglements. Although Wool and O'Connor's crack-healing theory[111,112] is focused on thermoplastic polymers, this theory can be considered as a universal model for self-healing concepts. In this theory, chains segmental motions are a primary factor in designing efficient self-healing systems. As depicted in **Figure 3**, segmental

surface rearrangement, surface approach, wetting, diffusion, and randomization are the processes that led the injured site to ultimately restore its physical and mechanical properties.[110–112] At, or above, the glass transition temperature, polymer chains have sufficient energies to accomplish the five steps of the healing process outlined above. Although polymer chains with low glass transitions enable fast molecular motions, long chains not only promote material strength but also provide a higher strength recovery at the interface as a result of having more reliable physical cross-links formed upon the diffusion and randomization steps. Damage causes the cleavage of polymer chains, which is often followed by conformational changes in the macromolecules at the surface of the polymer matrix. Chains migrate to the surfaces to fill the areas that have experienced mass loss. During the wetting step, the distance between the damaged surfaces begins to decrease as the loose ends of the polymer chains reach the opposite surface. Subsequently, chain diffusion completely eliminates the gap between the surfaces. During the final step of the process, known as randomization, further molecular diffusion and conformational changes increase interactions between adjacent polymer chains at the damage site. Thus, the polymer chains easily can entangle, physically interact, and/or react with each other.[113]

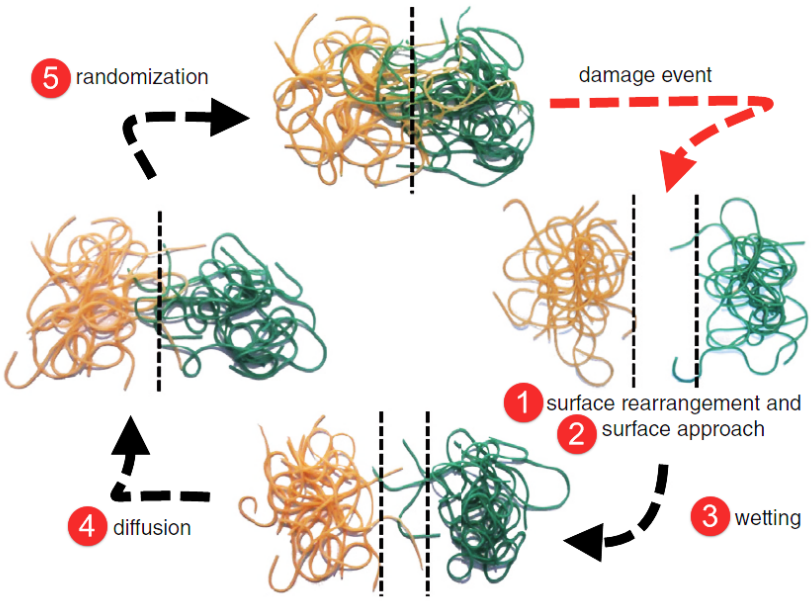

Figure 3. Polymers self-healing mechanism occurs in five steps based on the Wool and O'Connor explanation.[110] *(Adapted from the reference with permission)*

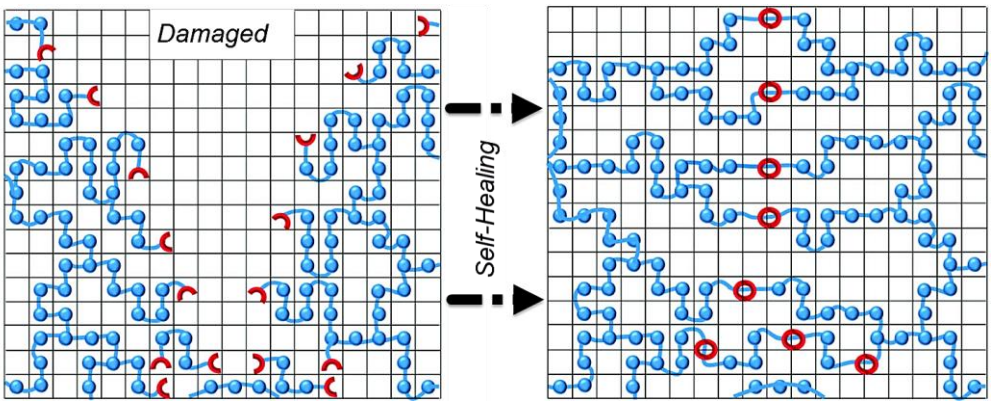

Figure 4. Demonstration of self-healing through the lattice model. The red half-circles and the red complete-circles represent interactive/reactive species and chains ends before and after healing, respectively. [116] ***(Adapted from the reference with permission)***

Welding in polymeric materials is a long-established method of healing that relies on the same mechanism discussed above.[113–115] Formation of chain entanglements between the two contacting polymer interfaces restores the original mechanical properties of the ruptured area during the randomization step. Swelling and patching can be considered as the two separate subdivisions of welding where the manual usage of solvents and cross-linking agents, commonly known as adhesives[115], improves the healing capacity. The temperature and the roughness of the contacting surfaces, as well as the type of the adhesive used at the damaged area, can significantly affect the efficiency of the welding method.[49,50] However, as the mobility of thermoset polymers is strictly hindered by permanent cross-links, patching has been the only traditional way to heal these polymeric networks. For the sake of clarity, self-healing in the context of this thesis only refers to the methods that aim to minimize or eliminate the manual intervention during the healing process of polymeric networks. In this regard, the lattice model[113,116] shown in **Figure 4** more specifically describes those self-healing approaches that mainly rely on interactive or reactive species in polymeric networks. In this model, a series of infinitesimal equilibration steps have to occur to eventually heal the polymeric matrix considered as a lattice. Upon the reconnection of the interactive or reactive functional groups, the crack closes and the lattice subsequently recovers its initial physical and mechanical properties. Similar to the explanation developed by Wool and O'Connor, the

lattice model regards the glass transition temperature as an important factor reflecting chains mobility at the molecular level.[113]

2.3 Chemical Principles of Self-Healing

Based on the type of the networks designed to heal the damaged area, the chemistry of self-healing has been commonly classified into two main divisions: covalent and supramolecular approaches. While the former, often categorized in the extrinsic and intrinsic methodologies, utilizes covalently bonded networks at the damaged site which it may or may not be reversible, the latter aims to heal the material through reversible physical interactions, including hydrogen bonding, metal–ligand coordination, π-π stacking, and ionic interactions. However, the self-healing chemistry may also be categorized by considering whether the bonds formed are reversible or not. Therefore, irreversible strategies only comprise extrinsic methods whereas reversible ones include the intrinsic and supramolecular approaches.[117,118]

2.3.1 Irreversible (Extrinsic) Strategies

Similar to biological systems, the self-healing process in extrinsic systems is designed to be activated autonomously upon physical damage. In these approaches, reactive species, known as self-healing agents, are stored within the polymer matrix. Depending on the number of reagents involved in the self-healing process, often the non-reactive components are homogeneously blended with the material's matrix whereas the flowable components such as catalysts, initiators, or monomers are encapsulated inside hollow fibers or protective shells that are embedded throughout the polymer matrix. Damage ruptures the protective shell of the reactive components triggering the reaction designed to heal the injured site (**Figure 5**).[119]

The self-healing methods based on irreversible network formations were initially developed by embedding dicyclopentadiene microcapsules in an epoxy matrix containing ruthenium-based catalysts.[120] Rupture of the microcapsules upon damage of the polymer matrix results in the dicyclopentadiene migrating towards the injured zone to react with the catalyst. A rigid network obtained by ring opening polymerization of dicyclopentadiene efficiently healed the

crack. Since then many other systems have been studied not only to reduce the cost and toxicity of the catalyst but to also develop efficient self-healing systems with negligible air and water sensitivity that can be applied under ambient temperatures. These extrinsic systems often utilize ring-opening metathesis[120–124], cationic polymerizations[125,126], radical polymerizations[127,128], hydrosilylation reactions[129], and Michael additions as the irreversible reactions necessary for the self-healing process.[110,130]

Accurate calculation of the mechanical energy required for rupturing the protective layer of capsules has been a crucial factor. The protective layer has to guarantee the protection of the reactive species during the material's normal operating conditions. On the other hand, the energy obtained from a damage must result in the release of the encapsulated components to trigger the healing process.[119] It is noteworthy to consider that embedding microcapsule or hollow fibres within a network may lower the material's structural integrity.[105,117] In fact, although materials can be equipped with excellent self-healing features, it might be necessary to sacrifice a portion of the polymer's physical and mechanical properties in favour of self-

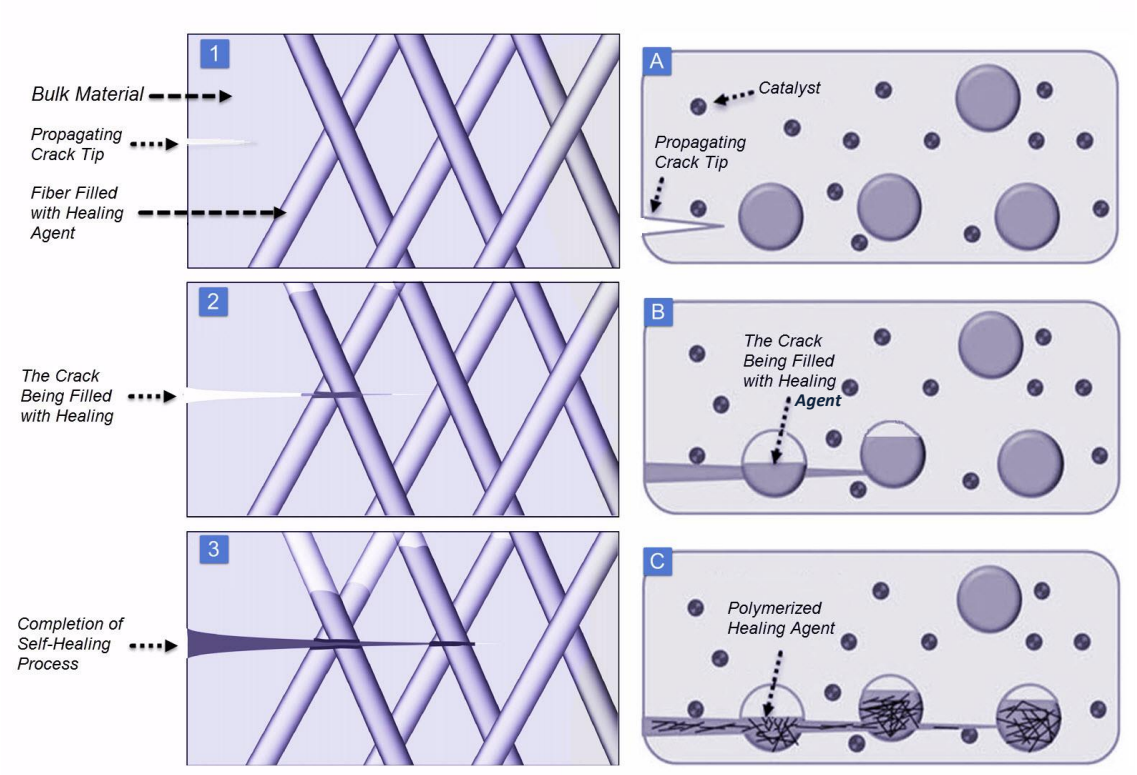

Figure 5. The self-healing process of the extrinsic approaches based on hallow fibres (the images on the left side numbered as 1,2,3) and spherical particles (the images on the right side named as A,B,C).[120,131]
(Adapted from the reference with permission)

healing. Thus, the extrinsic self-healing procedure (i.e., the type of self-healing components considered for a given material) has to be compatible with the polymer matrix to minimize the loss of mechanical strength. Likewise, the size of the capsules, homogeneous distribution, mechanical strength, and miscibility of the protective shell within the polymer matrix can significantly affect the self-healing efficiency.[119,131,132]

Microvascular networks are a more recent approach for self-healing that relies on the same concepts as the hollow glass fibers and the spherical particles. However, the interconnection of the hollow fibers filled with self-healing components establishes a mesh within the polymers matrix, enabling injured sites to be healed again upon subsequent damage (**Figure6**). The mesh not only functions as a protective layer similar to the previous generation of capsules but also as a carrier of self-healing agents through the capillary effect. Therefore, extrinsic self-healing approaches based on microvascular networks eliminate the conventional limitations of traditional encapsulating systems where the healing process could not be repeated at previously healed areas.[132,133]

Self-healing methods based on the irreversible formation of networks is extremely beneficial in sensitive applications where propagation of a microscopic crack may result in the failing of the entire system. Most often in these cases, it is not only impractical or challenging to

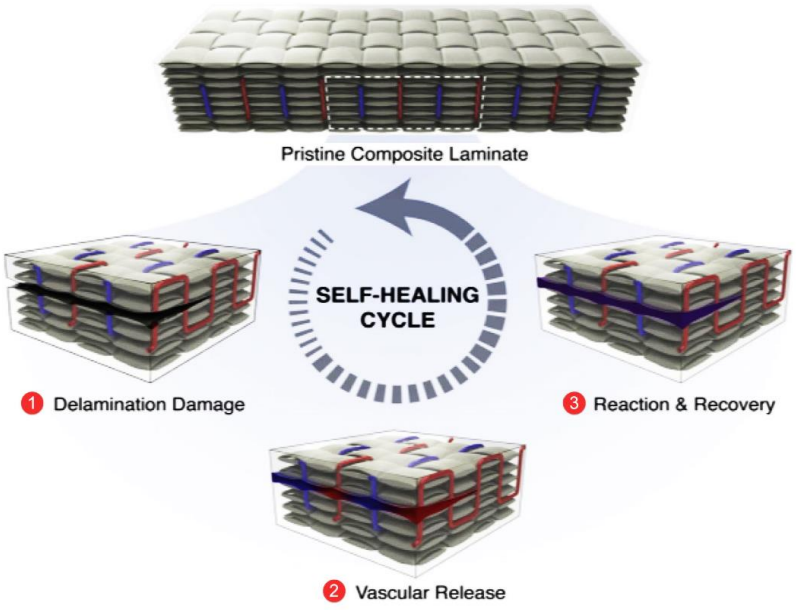

Figure 6. The three phases of the microvascular self-healing cycle including delamination, vascular release, and reaction and recovery.[132] *(Adapted from the reference with permission)*

manually repair the damaged material but also difficult to detect the defect at its early stage. Examples of such polymer matrices include those being used in aerospace applications, high-rise buildings, marine equipment, underground piping, turbines, and nuclear waste vessels where the long-term reliability on consistent physical and mechanical properties is vital. Therefore, the immediate self-healing response upon the application of a damaging event helps maintaining the optimal properties of the material.[105,133–135]

2.3.2 Reversible (Intrinsic) Strategies

Intrinsic, reversible, or occasionally non-autonomous approaches are the names of categories of self-healing materials where polymeric networks are cross-linked by physical interaction or a chemical equilibrium. Perhaps, accessibility to efficient damage-healing cycles and the single-component nature of these networks make reversible strategies appealing. Applying an external stimulus such as heat, light, or mechanical force alters the state of the equilibrium from a cross-linked polymer phase towards a linear one. In fact, the self-healing methods based on reversible strategies aim to disassemble the damaged part of the material's network by returning its components into linear chains to facilitate rebuilding the network. Thus, the healing process can be described as two consecutive phases where first the polymer chains are decoupled, which allows the chains to be mobile at or near the damaged area, and the second stage involves, re-coupling of the polymer chains, which, reforms the network. Therefore, the physical or chemical equilibrium originated from supramolecular (non-covalent) interactions or dynamic covalent bonds is an important element in this context.[110]

2.3.2.1 Supramolecular Interactions

The molecular architectures of supramolecules rely on physical intermolecular interactions dragging polymer chains toward each other.[136,137] Examples of supramolecular structures include the double-helix structure of deoxyribonucleic acid (DNA) molecules or various metalloproteins in living organisms.[138] Self-healing supramolecular networks are mainly assembled via hydrogen bonding, π-π stacking, metal–ligand coordination, and ionic

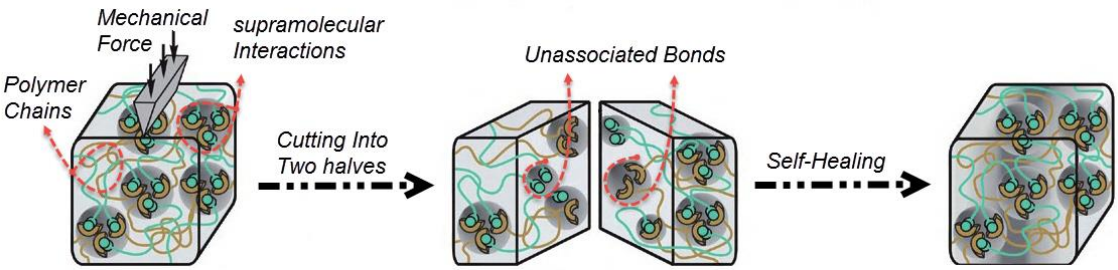

Figure 7. Self-healing mechanism of supramolecular networks at ambient temperature.[142,143] *(Adapted from the reference with permission)*

interactions of low-molecular-weight polymers called oligomers.[110,139–142] Although the strength of the network is often ranked as amongst the lowest in self-healing approaches, the high extent of thermal reversibility of these cross-links and the rapid response to stimuli are the two appealing features. In fact, these features enable the material to effectively change its physical state from solid to fluid through altering the equilibrium in favor of the decoupling reaction. Similar to the extrinsic approaches for self-healing, the external mechanical force originated from a damage, triggers the self-healing process in intrinsic self-healing systems. Since the physical intermolecular interactions are extremely weak in comparison with the covalent bonds along the chains, the damage disturbs the equilibrium by perturbing the supramolecular bonds at the fractured surface. Timely contact of the surfaces re-establishes the equilibrium by reconnecting the broken bonds at ambient temperature (**Figure 7**). However, the unassociated bonds may diffuse back from the surface into the bulk of the material or even be neutralized with moisture, providing a new equilibrium on the damaged surface of the material. That is why, in these systems, as time passes, the self-healing efficiency at ambient temperature may decrease significantly. Nevertheless, even though the material may lose its self-healability at ambient temperature on the damaged surface over time, increasing the material's temperature commonly re-enables the self-healability. In overall, networks based on supramolecular interactions have a capacity for self-healing at ambient temperature along with recyclability.[109,142,143]

Supramolecular interactions are relatively weak (e.g., 0.2–40 kJ/mol for a hydrogen bond, in comparison with covalent bonds; 345 kJ/mol per C-C bond).[80,144] Thus, the number of bonds

between polymer chains becomes an important factor in providing the strength required in designing a polymeric network.

Hydrogen bonding is one of the leading interactions in the chemistry of supramolecules. In fact, an additional hydrogen bond provides a 7.4 kJ/mol increase in the overall strength of the interaction between adjacent polymer molecules.[144] Thus, utilizing structures with multiple hydrogen bonds promotes intermolecular bonds to the point where they become comparable to covalent bonds regarding their overall strength. Examples of these structures are the quadruple H-bonds of ureidopyrimidinone[145] (**Figure 8A**), the sextuple H-bonding based on the Hamilton wedge and barbituric acid[146] (**Figure 8B**), the triple H-bonds between thymine and 2,6-diaminotriaine[147] (**Figure 8C**), and the diamidonaphthyridine and guanosine's quadruple H-bonds interactions[148] (**Figure 8D**). Although this strategy increases the thermal stability of the self-healing material based on the supramolecular interactions, having physical interactions that rival the strength of covalent bonds imposes the physical interactions to become less likely to be broken under mechanical stress. Thus, as the interactions become stronger, the proportion of covalent bonds cleaved at the damaged zone

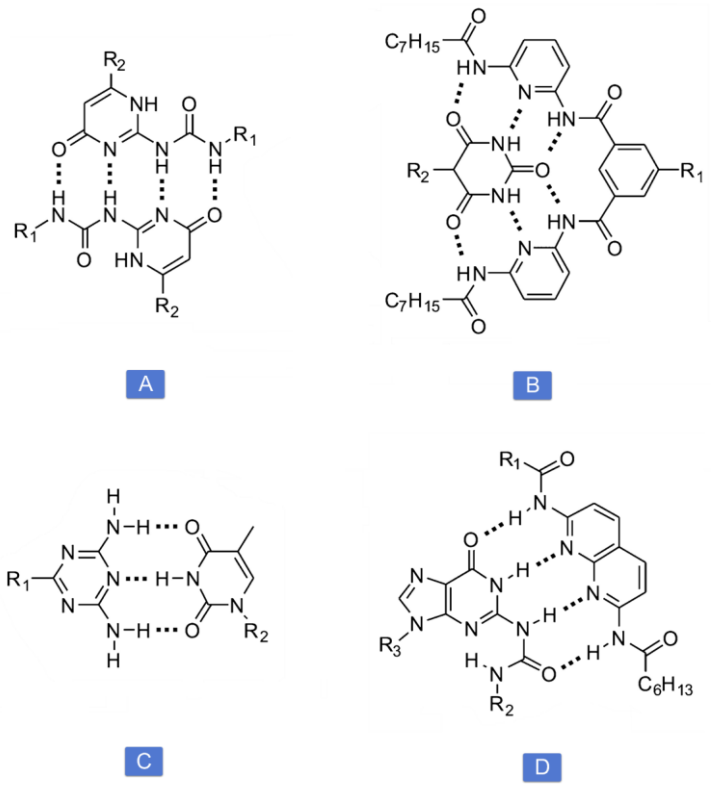

Figure 8. The multiple-hydrogen-bond structures used in self-healing supramolecules. R1 and R2 are the oligomeric part of the structures.[82,84] *(Adapted from the reference with permission)*

gradually increases, which subsequently diminishes the occurrence of efficient self-healing processes at ambient temperatures. Although single complementary structures such as ureidopyrimidinone may seem to be a promising strategy in the preparation of the supramolecular based self-healing materials, the poor solubility in most organic solvents originating from their strong intermolecular interactions often hinders the synthesis of the networks on the basis of the single complementary units.[149,150]

In addition to hydrogen bonds, the interaction between π-electron-rich and π-electron-poor moieties, known as aromatic π-π-stacking interactions, is employed to physically cross-link polymer chains (**Figure 9**).[151–153] Spectroscopic and crystallographic methods indicated that the formation of a network relies on the physical interactions of folding "tweezer-type" structures.[153] As a result of these repetitive folded structures, the physical and mechanical properties of self-healing materials based on the interaction between the low-molecular-weight polymers end-capped with pyrene groups and naphthalenediimide functionalized oligomers, was found to be quite similar to the common properties of reversible covalent approaches (i.e., an ultimate tensile strength of up to 6.7 MPa with an enhanced thermal

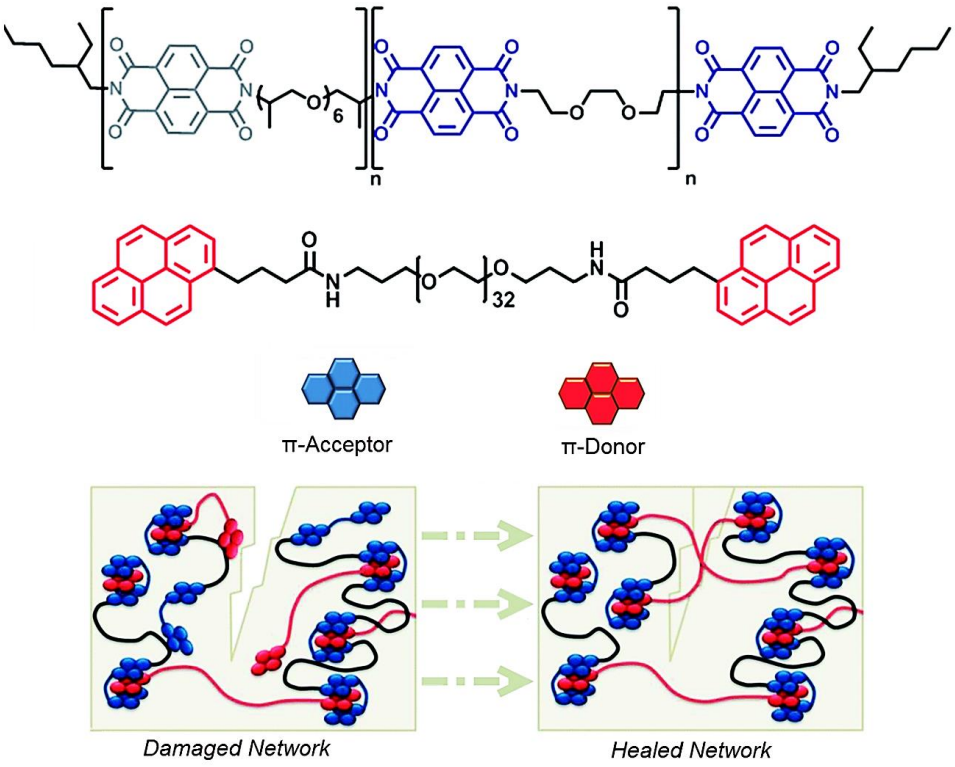

Figure 9. Illustration of the self-healing concept based on π-stacking interactions. The folding "tweezer-type" structures are a result of polydiimide and pyrenyl end-capped chains interactions.[151] *(Adapted from the reference with permission)*

stability).[152] Depending on the network's structure, efficient self-healing requires elevated temperatures, above 50°C, which is also common in the intrinsic self-healing materials based on thermally reversible covalent bonds.[151,154]

The application of metal–ligand systems in self-healing was first observed in living organisms such as mussel species where inflicted damage could be repaired through reversible interactions between iron(III) ions and 3,4-dihydroxyphenylalanine moieties.[155] Self-healing materials based on metal–ligand interactions are among the most recent approaches in the research field where metal ions are recognized as cross-linking agents. Establishing metal–ligand interactions by employing polymeric ligands designed to interact with metal ions such as Zn, Fe, Co, or Ni, is the basis of metallo-supramolecular polymers. The capacity of the metal ions to obtain several interactions with corresponding ligands maintains the structure of these networks (**Figure 10**). While pH, heat, and UV-irradiation have been reported as the stimuli for efficiently activating the self-healing process, self-healing at ambient conditions has also been found in some cases. In fact, mechanical force can be designed to profoundly disconnect the physical bonds. Structural flexibility and mobility ease the chain rearrangements and interpenetrations necessary for a successful ambient temperature self-healing process. Moreover, metal–ligand cross-links have the capacity to convert absorbed energy from UV-irradiation into heat, resulting in physical bonds that are temporarily disconnected. As a result, the material can restructure the damaged areas. The availability of

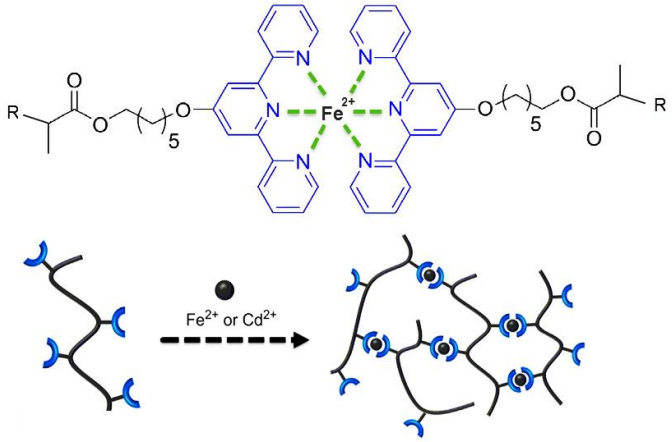

Figure 10. Thermally self-healing terpy-containing metallo-supramolecular polymer. The R group represents an oligomeric chain connected to the structure.[141,295] ***The oligomer was synthesized based on copolymerization of methacrylate monomers (methyl methacrylate, n-butyl methacrylate, and lauryl methacrylate) with a terpyridine (terpy) containing methacrylate monomer.*** *(Adapted from the reference with permission)*

a wide range of different metal ion and ligand combinations permits a great deal of flexibility in designing self-healing networks based on this strategy.[140,156]

Polymeric networks based on ionic cross-links, known as ionomers, can also be employed for the purpose of self-healing. Commonly, carboxylates and sulfonates are used in this approach where the aggregation of ionic groups effectively cross-link the polymer chains and maintain the structure of the network (**Figure 11**).[157] The reported self-healing ionomers are mainly based on equivalent amounts of Na^+ and $R-COO^-$ groups in which the sodium counter-ions are coordinated by several carboxylate groups.[158–161] However, the $R-COO^-$ groups can occasionally weakly correlate with (be neutralized by) less water sensitive metal ions such as Zn^{2+}, and Fe^{3+}.[162,163] In contrast to hydrogen bonds, metal complexes, and ionic structures are employed less frequently in self-healing materials. Compared to conventional copolymers, ionomers generally exhibit improved physical and mechanical properties such as tensile strength, toughness and flexibility. The nature of the ionic groups and counter-ions, the bond association strength of the ionic groups, the extent of neutralization, the flexibility of polymer chains, and the matrix's dielectric constant are among those factors affecting the self-healing properties. For instance, the number of available acid groups within the network and the ion:counter-ion ratio are directly correlated to polymeric chains features such as stiffness, melt viscosity, and segmental relaxation time. Similar to other supramolecular approaches, the ionomer's Young's modulus rapidly drops at elevated temperatures as a consequence of the physical cross-links dissociation. Increasing the temperature above the glass transition for the cluster allows the material to be processible as a viscous fluid. In addition, the thermal sensitivity of the ionomer's properties can be lowered by extending the

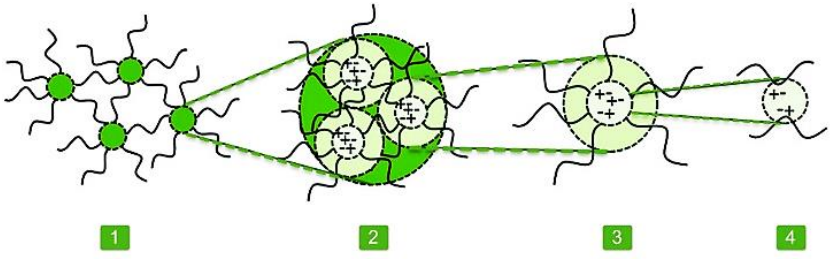

Figure 11. A graphical view of the networks based on ionic interactions. The encircled regions highlight the areas where chain mobility is greatly restricted.[157,161] *(Adapted from the reference with permission)*

rubbery plateau of the material by the addition of plasticizers. The most noticeable application of the ionomeric structures is in packaging films for consumable products where the stiffness and transparency of ionomers is required.[164,165]

Overall, aromatic π–π stacking, hydrogen bonding, metal–ligand interactions, and ionic clusters result in self-healing materials based on dynamic, non-covalent bonds. Physical and mechanical properties strongly depend on temperature. These self-healing systems are often sensitive or reactive to solvents and residual reagents. Ideally, materials whose cross-links are not only fully reversible in response to heat, but that can be autonomously reconnected at ambient temperature. However, an effective ambient healing process is only possible when the strength of the physical interactions in the material is lower than that of the covalent bonds within the material's matrix to minimize the breakages of irreversible covalent bonds along the chains upon the damage event. Thus, the material's strength needs to be compensated to a great extent if an efficient self-healing is desired at ambient temperature.[110,164,166]

2.3.2.2 Dynamic Covalent Bonds

Although numerous dynamic covalent bonds have been introduced[167–169], the concept of self-healing networks based on the formation of reversible covalent bonds mostly relies on a limited number of reversible linkages that are either cycloaddition reactions[62], exchange reactions[170–172], or reversible radical-based reactions.[173–176,110,177] In fact, only these classes of reversible reactions are suitable candidates for obtaining an efficient selective self-healing process. Heat, light, pH, and mechanical forces are among the common self-healing stimuli reported in this category of self-healing systems. Unlike supramolecular self-healing materials, a higher mechanical strength, dimensional stability, and solvent resistance can be achieved as a direct consequence of the reversible covalent bond used in these systems. Depending on the target application, such properties can be considered as an advantage in the design of self-healing materials. Often, two main ultimate aims can be satisfied in the design of the materials falling into this category of self-healing polymers. While the first aim

is to provide high-strength recyclable networks known as remendable polymers, obtaining intrinsic autonomous self-healable materials is the second aim.

Cycloaddition reactions, in particular, a [4+2] cycloaddition called Diels-Alder (DA) reaction, have been extensively investigated to obtain mendable polymers.[62,110,118,178] Although the DA bonds require a high activation energy to undergo the reverse reaction, mechanical force has been shown to facilitate the [4+2] cycloreversion reaction is known as retro-Diels-Alder (RDA) reaction (**Figure 12**).[179–181] Moreover, self-healing networks based on [4+2] cycloaddition reactions are not only recyclable and insensitive to air, but also potentially can exhibit mechanical properties similar to epoxy resins.[182–186] In fact, the strength and reliability of the DA linkages reach to the level that they have been considered as suitable candidates for the preparation of recyclable tires.[187,188] Generally, the self-healing process requires a local heating/cooling cycle at the damaged zone. At elevated temperatures, commonly higher than 50°C, the equilibrium starts to gradually shift toward the starting materials. Decoupling the cross-links enhances the mobility and flexibility of the polymer chains so that they can migrate into the physical defect. By giving an adequate amount of time, chains fill the crack and diffuse to the bulk. Subsequent cooling eventually cross-links the decoupled linkages and consequently mends the injured site.[189] Although the sole usage of thermal energy cannot activate the self-healing process in [2+2] or [4+4] cycloaddition reactions of cinnamate, coumarin, or anthracene derivatives due to the mismatch between the frontier molecular orbitals (**for the detailed disscussion see section 3.2**), the simultaneous application of UV-irradiation (>280nm) and heat improves the self-healing efficiency.[62,190–192] In fact, [4+2] cycloaddition is known as thermally allowed reaction whereas [2+2] or [4+4] cycloaddition both occurs under excitation of the molecular orbitals and are thermally forbidden (**for the detailed disscussion see section 3.2**).[193] Light-induced self-healing materials are mostly suitable in self-healable coating applications as the limited penetrating power of light hinders the self-healing process to be efficiently triggered within the bulk of materials. Interestingly, the self-healing process of polyperfluorocyclobutanes is reported to be thermally triggered at temperatures above

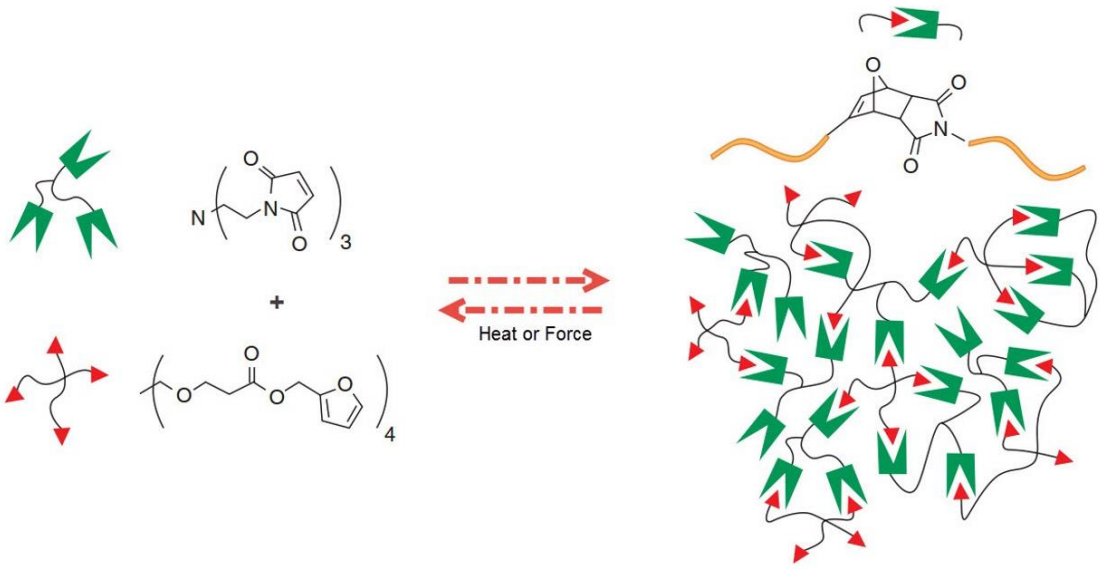

Diene	Dienophile	Condition	Adduct
Furan	Maleimide	$RT \leq T_{DA} \leq 120\ ^{\circ}C$ $120\ ^{\circ}C \leq T_{rDA}$ Several Hours≤Time	
Cyclopentadiene	Cyclopentadiene	$80\ ^{\circ}C \leq T_{DA} \leq 120\ ^{\circ}C$ $180\ ^{\circ}C$ or $120\ ^{\circ}C \leq T_{rDA}$ Several Hours ≤Time	
Cyclopentadiene	Dithioester	$RT \leq T_{DA} \leq 80\ ^{\circ}C$ $80\ ^{\circ}C \leq T_{rDA}$ Several Minates ≤Time Catalyst:Trifluoroacetic acid	

Figure 12. Representative examples of self-healing networks based on a thermally and mechano-chemically reversible Diels-Alder linkage. The table indicates the reaction condition of several common [4+2] cycloaddition cross-links. R^1 and R^2 represent aliphatic chains.[176,189,296] *(Adapted from the reference with permission)*

150˚C. Occurrence of the thermally forbidden [2+2] cycloaddition in perfluorocyclobutane cross-links is attributed to the weakness of the π-bond in fluorinated alkenes. Thus, the application of thermal treatment ultimately heals the damaged area by converting the mechanically formed trifluorovinylethers into perfluorocyclobutanes (**Figure 13**).[176,194] It is noteworthy to mention that when mechanical forces are evenly distributed within the network, bond rupture typically occurs at positions exhibiting the lowest bond strengths. However, the presence of entanglements or irreversibly cross-linked points within long intertwined chains may lead to uneven redistribution of external forces. Accordingly, not

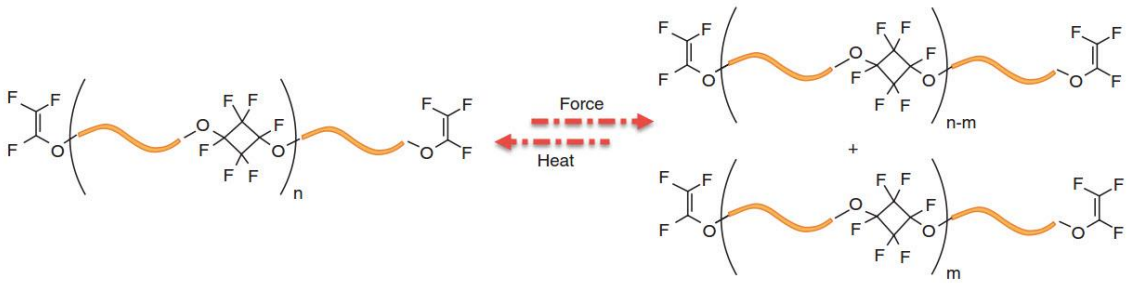

Figure 13. Thermomechanically self-healable polyperfluorocyclobutanes based on reversible [2+2] cycloaddition reactions of trifluorovinyl groups.[176] *(Adapted from the reference with permission)*

only the weakest bonds, but also the other available bonds may break depending on the magnitude of the force.[195] Thus, careful selection of chains lengths is of vital importance if mechanochemical self-healing is desired.

One of the pioneering observations of the mechanochemical reactions was the self-healing phenomenon in vulcanized rubbers. Cleavage of S–S bonds through mechanical damage results in long-lived reactive sulfur radicals that are capable of self-healing in the absence of oxygen.[176] In fact, disulfide bonds are susceptible to metathesis exchange reactions in which the neighboring S-S bonds disrupted by light, heat, or mechanical stress can reform through

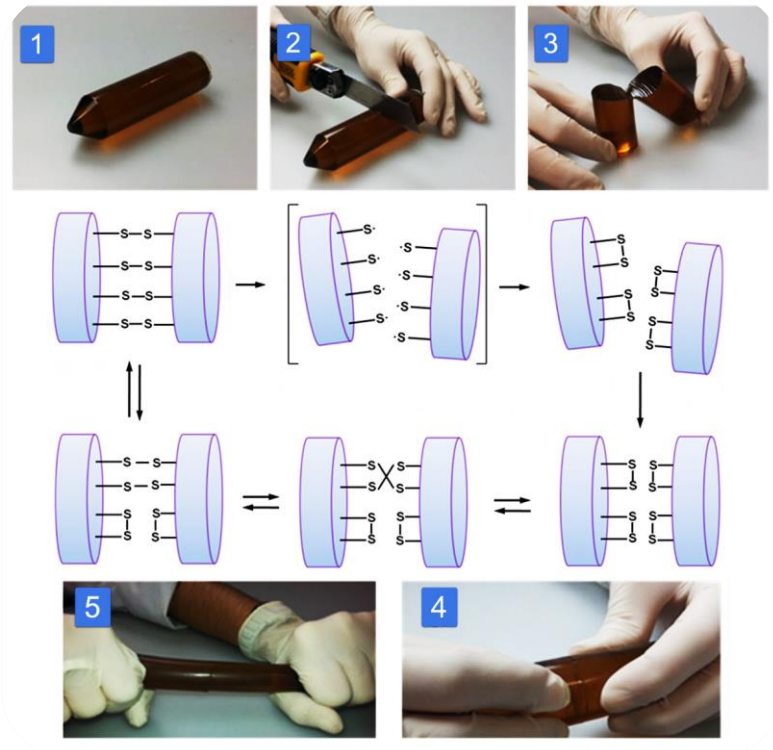

Figure 14. Self-healing process of a polymeric network based on disulfide exchange reactions. The healing process was accomplished by contacting the damaged surfaces for 2h at room temperature.[198] *(Adapted from the reference with permission)*

free radical or ionic intermediates (**Figure 14**).[196–198] The generation of free radicals is the result of covalent bond cleavage caused by mechanical damage in polymeric materials. Thus, the injured area can regain its integrity by reconnecting with free radicals located at the damaged surfaces. Commonly, these free radical lifetimes are less than that is necessary for such reconnections. In fact, the oxidation process heavily hinders their reactivity, and thus terminates the self-healing process. However, the free radicals lifetimes generated from mechanical stress, photolysis, or thermolysis of trithiocarbonate[199], thiuram disulfide derivatives[175], or alkoxyamines[200–202] can exceed the time required for the self-healing steps (i.e., the rearrangement, diffusion, and randomization steps discussed earlier in this chapter). The dissociation of alkoxyamines is another opportunity for obtaining thermally reversible cross-links where the cleavage of the NO-C bonds is responsible for the self-healing (**Figure15**). The cleavage of the alkoxyamine bonds at temperatures above 60°C results in complementary stable radicals of styrene and tetramethylpiperidinyloxy (TEMPO). Subsequent cooling to lower temperatures enables the material to reform the broken chemical cross-links through a radical exchange reaction. As the mobility of the free radicals connected to the backbones is limited to the chains' segmental motions in the solid-state, their reactivity is reduced compared to that of the liquid or gas phase. In this case, self-healing requires the complementary radicals to relocate themselves to positions where they are accessible to each other. However, with side reactions such as oxidation, the efficiency of the self-healing process can be hindered to the point where the material loses its self-healing

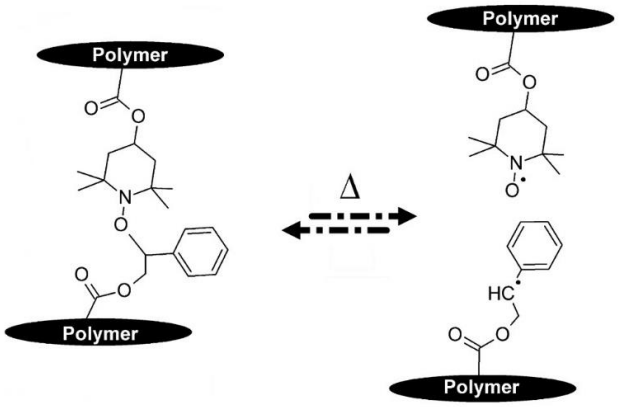

Figure 15. Dissociation/association of the alkoxyamine cross-links used to graft aliphatic polymer chains.[189] *(Adapted from the reference with permission)*

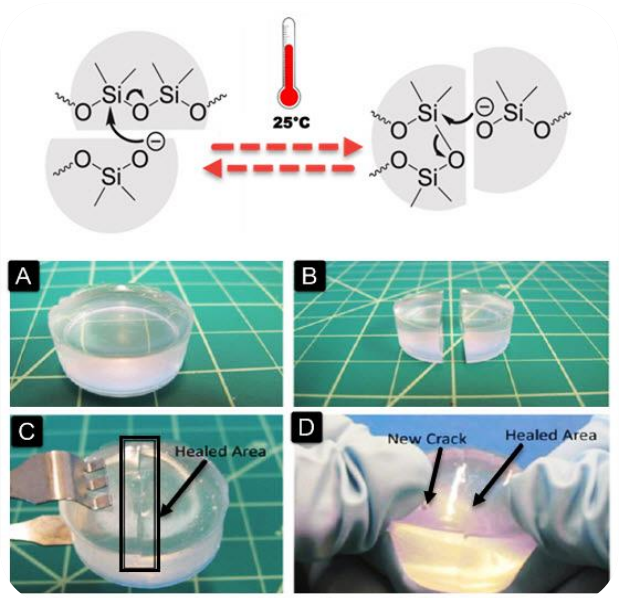

Figure 16. An intrinsic self-healing material based on siloxane exchange reactions. A, B, C, and D illustrate the original, the damaged, and the healed version of a siloxane-exchange self-healing material, respectively.[170,171] ***(Adapted from the reference with permission)***

properties. Additionally, as these free radicals are the consequences of broken covalent bonds, the mechanical energy required for the bond scission may reach a comparable level to C-C bonds. Accordingly, the damage breaks also C-C bonds and thus the material may not fully self-repair itself. Operating conditions (e.g., temperature, or presence of water or oxygen) may cause a major barrier for the stability of these free radicals.[133,201,203,204]

Self-healing mechanisms based on tetramethylammonium dimethylsilanolate anionic end groups are quite similar to those discussed for supramolecules. Damage locally disrupts the equilibrium between cross-linkers and cyclic oligomers by dissociation of covalent bonds (**Figure 16**). Subsequently, the system aims to restore it. However, unlike supramolecules, the formation of covalent bonds at the injured area is responsible for the recovery of the physical and mechanical properties. An advantage of using siloxane groups is their stability toward air and water.[170,171] However, the cyclic oligomers are volatile, which limits their applications to isolated or enclosed systems. Although applying heat increases the rate of healing, materials based on the disulfide or siloxane exchange reactions are reported to be also capable of self-healing at 25°C (**Figure 14** and **Figure 16**).[170,171,205,206] The acid catalyzed acylhydrazone/acylhydrazine equilibrium,[169] reversible urea bonds with bulky

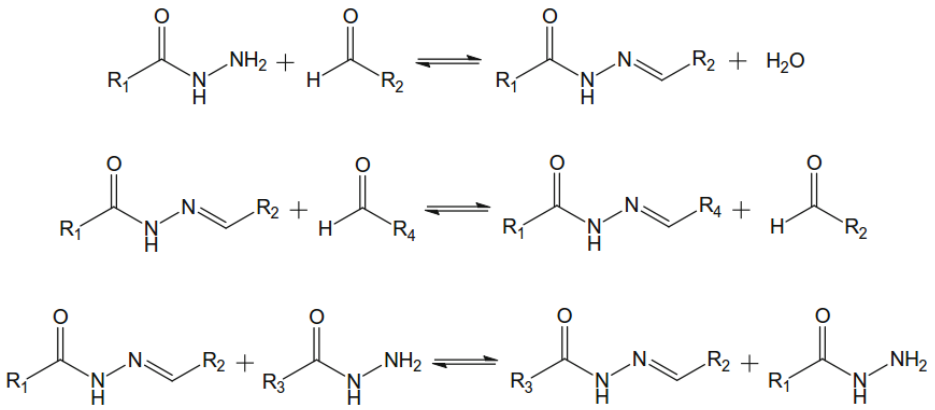

Figure 17. The equilibrium based on an aldehyde and a hydrazide derivative.[207]*(Adapted from the reference with permission)*

substituent,[168] and boronic ester exchange reactions[172] are other valuable strategies employed to obtain autonomous self-healable networks at moderate temperatures. However, the main challenges for these two concepts are improving the solid-state reaction rates and reducing the moisture sensitivity or the toxicity of the functional groups, particularly free-NCO groups.[118]

Condensation reactions of aldehydes with acylhydrazines establishes a valuable approach in self-healing materials based on dynamic covalent bonds. In fact, the acylhydrazone functional groups exhibit a dynamic character based on the reversibility of the imino bond (**Figure 17**). In the acidic environment (pH<4) the equilibrium goes toward predominantly the starting materials, enabling the material to heal damaged areas. Thus, the alteration of pH in the system triggers the self-healing process. As an example, swelling of poly(ethylene oxide) end-capped acylhydrazines and tris[(4-formylphenoxy)methyl]ethane in a solvent at a pH above 4 resulted in a cross-linked network. Due to sol–gel phase transition ability of the system in

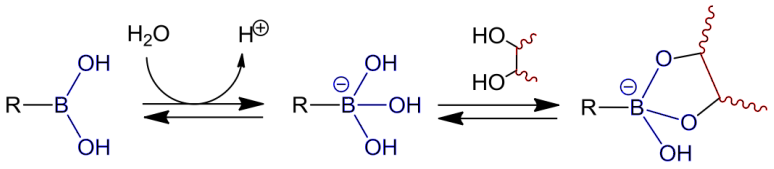

Figure 18. Self-healing hydrogel based boronate ester equilibrium.[210]*(Adapted from the reference with permission)*

response to the alteration of pH, the damaged gel plate were healed in 7h autonomously at ambient temperature.[165,207,208]

Additionally, dynamic boronic esters are known as pH-responsive dynamic covalent bonds (**Figure 18**). The combination of a salicylhydroxamic acid and a boronic acid is reported to provide cross-linked hydrogels at neutral pH (7.5).[209] Under acidic condition (i.e., pH=4.5), the cross-links can be decoupled to enable the healing process by pushing the reaction toward the starting materials. As an advantage of dynamic bonds based on boronic esters over the acylhydrozone/acylhydrazine equilibrium, the pH values which regulate the cross-linking and decross-linking reactions can be tuned via utilizing various substituents. Therefore, self-healing materials based on the dynamic boronic esters can be designed to function over a wide range of pH. For instance, the self-healing hydrogels based on boronate ester crosslinks are obtained by mixing four-arm oligomers end-functionalized with catechol with 1,3-benzenediboronic acid at pH=9. Neutral to acid pH values resulted in a gel-to-sol transition to trigger the healing process.[209–211] Boronic acid-containing polymers can be potentially used for medical applications such as drug delivery systems, nucleotide adsorbents, and sensors for sugars.[210]

More recently, urea bonds bearing a bulky group on the nitrogen is shown to exhibit dynamic covalent bond characteristics. Reversible formation of the urea bonds which can dissociate into the corresponding isocyanate and amine allows the damaged areas of the network to be healed. The healing process of a severely damaged specimen resulted in 12h to heal at 37 ˚C autonomously. According to **Figure 19**, in both cases (**A** & **B**) the bulky groups appended to

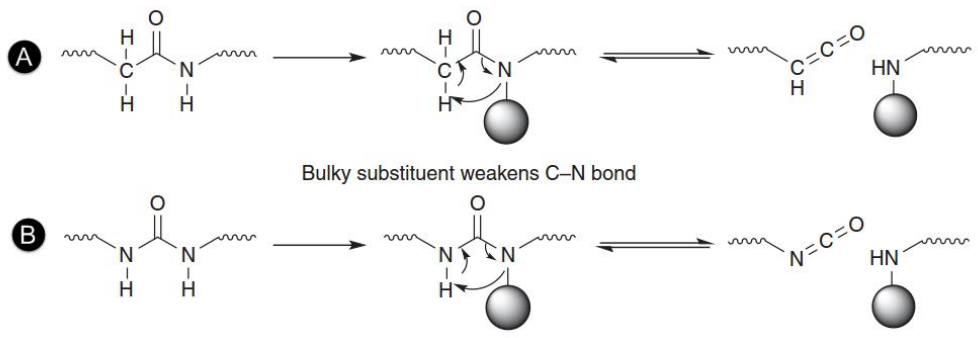

Figure 19. The equilibrium of carboxylate-amine bonds bearing bulky N-substituent.[212] *(Adapted from the reference with permission)*

the nitrogen atom improves the reversibility of the ketene intermediate through weakening the C-N bond at ambient temperature.[212,213] However, water is reported to distrurb the equlibrium and reduce substantially the self-repairing capacity of the material.[213]

Analogous to supramolecular-based self-healing networks, self-healable materials based on reversible covalent bonds do not require the external embedment of healing agents within the matrix. Likewise, the capability of having several self-healing cycles at the same damaged site is an inherent feature of the self-healing networks based on reversible bonds. Although the intrinsic healing process of the reversible covalent bonds often requires applying heat, a careful selection of the network's components yields materials capable of autonomous self-healing at moderate temperatures. Compared to networks relying on physical cross-links, incorporation of dynamic covalent bonds commonly promotes mechanical strength, dimensional stability, and extends the operating temperature ranges of self-healable materials.[214]

2.4 Design Factors

Depending on the operating condition, an ideal self-healing approaches can be recognized in the design of self-healing materials. Whether the suitable strategy is intrinsic or extrinsic, the architecture of the polymer chains, the average molecular weight of the polymer chains, the average intercross-link molecular weight, the cross-linking density, and the heterogeneity index affect the majority of properties ultimately found in the material.[106,117]

As earlier discussed through the physical principles of the self-healing in this chapter, the mobility and flexibility of chains affect the self-healing process substantially. In other words, facilitating the segmental motion leads to a higher self-heling efficiency. As glass transition is a reflection of the mobility and flexibility of chains, it can be used to rationalize the impact of manipulating the structure of polymers on self-healing. For instance, increasing molecular weight, lowering the average intercross-link molecular weight, or increasing the cross-linking density are known to increase the glass transition temperature. Thus, the efficiency of self-healing reduces, accordingly. Regarding molecular weight distribution, if the reason

of broadening (i.e., increment in the heterogeneity index) is the addition of low molecular weight chains then as a result of lowering T_g, the self-healing efficiency can be improved. In contrast, the addition of high molecular weight chains imposes a possible reduction in the efficiency of healing process.[34,35,93,106]

Generally, materials based on the extrinsic self-healing methods recognize the matrix and self-healing approach as two different compatible systems. The matrix is where the material gains its mechanical properties whereas the embedded fibers or capsules containing self-healing agents are the origin of the autonomous self-healing efficiency.[106] However, embedding hollow fibers, microcapsules, or microvascular networks into the matrix drastically may alter the mechanical properties of the material. On the other hand, the intrinsic concepts require direct modifications of the matrix.[57] Thus, the material obtains both its mechanical properties and self-healing efficiency from the matrix itself. The mechanical strength of the matrix is often inversely correlated with the intrinsic self-repairing efficiency.[46] For instance, the rigidity of chain backbones results in higher physical and mechanical properties, yet lowers the flexibility and mobility of chains within the matrix hindering the self-healing process under mild conditions.[148] Therefore, the polymer chains not only need to be adequate for the physical and mechanical properties required for the target operating condition, but also for achieving the desired self-healing process. To overcome such destructive relationships in intrinsic strategies, one question has to be answered: is it possible to facilitate segmental motions and simultaneously strengthen the networks mechanical properties? One answer is to bring heterogeneity into self-healing materials. The usage of copolymer backbones comprising soft and hard blocks, as well as functionalized nanostructures such as SiO_2 nanocage, nanoparticles, nanofibers, carbon nanotubes, and graphene creates microphase-separated systems.[57] In this regard, the matrix is divided into soft and hard domains. While the former is responsible for the flexibility and mobility, which is necessary for the self-healing process, the latter increases the mechanical strength of the matrix. Furthermore, by incorporating hybrid structures or allocating a portion of the cross-links to irreversible bonds, materials can retain their integrity during the

intrinsic healing process.[117] However, the dynamic bonds should respond significantly faster to stimuli than the chain rearrangement and diffusion processes if deformation or shape loss of the material is to be avoided during the self-repairing process.[148] As discussed in the previous chapter, bimodal networks[38,215] might be another solution for to the question mentioned above where the application of short and long cross-links throughout the network enhances Young's modulus and the elongation ratio, simultaneously.[106,177,216]

2.5 Summary

The traditional idea behind developing polymeric networks has been strengthening the matrix to avoid mechanical damage. In fact, the conventional approaches aim to provide damage resistant/tolerant polymers instead of dealing with the damage itself. In this regard, the network architecture can be enhanced by optimizing the cross-linking density, the rigidity of polymer chains, the crystallinity or by applying external reinforcing agents such as exfoliated clays, graphene plates, carbon black, and silica. On the other hand, self-healing concepts inspired by living organisms offer alternative strategies based on damage repair. Incorporating stimuli-responsive elements such as encapsulated healing agents, dynamic covalent bonds, and supramolecular interactions into polymers has provided a reliable insight in designing advanced materials. Aside from the constraining factors imposed by self-healing approaches, the preparation of self-healing materials should be effortless and cost effective to be industrialized. In this case, starting materials need to be relatively inexpensive, stable, and environment-friendly. Overall, perhaps one of the most appealing on-going investigations has been high strength recyclable networks where the notion is to find a promising substituent for irreversible elastic networks.

Chapter 3 Diels-Alder Reactions

The focus of this chapter is to provide insight into reversible Diels-Alder (DA) reactions. Besides briefly reviewing the fundamental knowledge regarding [4+2] cycloaddition reactions, the parameters substantially affecting the reversibility of the adducts are discussed. The chapter can mainly be divided into two categories of macromolecular structural design, and the factors necessary to optimize the adducts. The chapter indicates that various macromolecular structures can be integrated with the intrinsic self-healing features via DA chemistry. Optimization factor, on the other hand, is considered as a precious tool in achieving thermally-controlled reversible adducts for a variety of applications. Further along in the chapter, the superior features of using furan/maleimide derivatives as the diene/dienophile, the theories involved in the DA adducts' self-healing process, the impact of the adjacent functional groups, and the strategy of using carbon spacers with siloxane linear chains are also reviewed.

3.1 Introduction

The development of the [4+2] cycloaddition reaction by Otto Diels and Kurt Alder[217] in 1928 provided a powerful synthetic tool for synthesizing various polymeric architectures from structurally different copolymers to a series of dendrimers and star polymers.[218] The Diels-Alder (DA) reaction, is a thermally allowed, concerted, suprafacial [4+2] cycloaddition in which the new sigma bonds are formed simultaneously on the same face of the reactants.[193] The term [4+2] indicates that the reaction occurs between a 4-electron rich conjugated system, known as a diene, and a 2-electron deficient system named as the dienophile. The reaction is thermally feasible provided that the highest occupied molecular orbital of the diene reacts suprafacially with the lowest unoccupied molecular orbital of the dienophile while conserves the orbital symmetry (**for the detailed disscussion see section 3.2**).[193] DA reaction can occur readily between a *cis*-form of an electron-rich diene and an electron-deficient dienophile to yield conjugated six-membered rings called adducts. The [4+2] cycloaddition of a 1,4-substituted diene and a dienophile may yield different stereoisomers

(i.e., *endo* and *exo* adducts). The *endo*- and *exo*-adduct are kinetically and thermodynamically stable, respectively. Accordingly, the DA reaction profoundly produces the *endo*-adduct at low temperatures (e.g., room temperature) whereas as the *exo*-isomer becomes profoundly favorable at high temperatures.[219] Although the reaction of a 1,4-substituted diene and a dienophile may form different stereoisomers (i.e., *endo* and *exo* adducts), polymer chemistry recognizes them as one adduct due to their negligible influence on polymers' physical and mechanical properties.[187] Commonly, cyclic dienes are more reactive than linear ones as only *cis*-dienes participate in [4+2] cycloaddition reactions. The adduct can be decomposed into the starting materials through a thermal [4+2] cycloreversion named retro-Diels–Alder (RDA) reaction. The DA cycloaddition and RDA cycloreversion are tunable reactions by the frontier molecular orbital theory, meaning that the reactivity of the starting substrates depends on the energy gap between the highest occupied molecular orbital (HOMO) of the diene and the lowest unoccupied molecular orbital (LUMO) of the dienophile.[189] Electron withdrawing groups lower the energy of a molecular orbital whereas electron donating ones raise the energy (**for the detailed disscussion see section 3.2**). Therefore, the DA reactions can be accelerated by electron-donating and electron-withdrawing substituents in the structure of the dienes and dienophiles, respectively. The equilibrium between the starting materials and the adduct strongly depends on the diene–dienophile combination (**Figure 1**)**.** As a prime example, while furandicarboxylic acid is not very reactive in [4+2] cycloaddition reactions with maleimide due to the electron-withdrawing effect of the carbonyl groups directly connected to the furan, the [4+2] cycloreversions of the anthracene-maleimide-based adducts often are practically impossible as they occur near the polymers' degradation temperatures.[62,178,218,220]

Due to high efficiency, versatility, and selectivity of most dienes and dienophiles, as well as the capacity of the DA cycloaddition reaction to occur under mild and metal-free conditions, it is eligible to be classified as a "click-unclick" reaction.[62,178] A reaction involving polymeric reagent(s) can be named as a polymer "click" reaction in which equimolar amounts of reagents are converted into the product(s) efficiently, in a short-timescale under

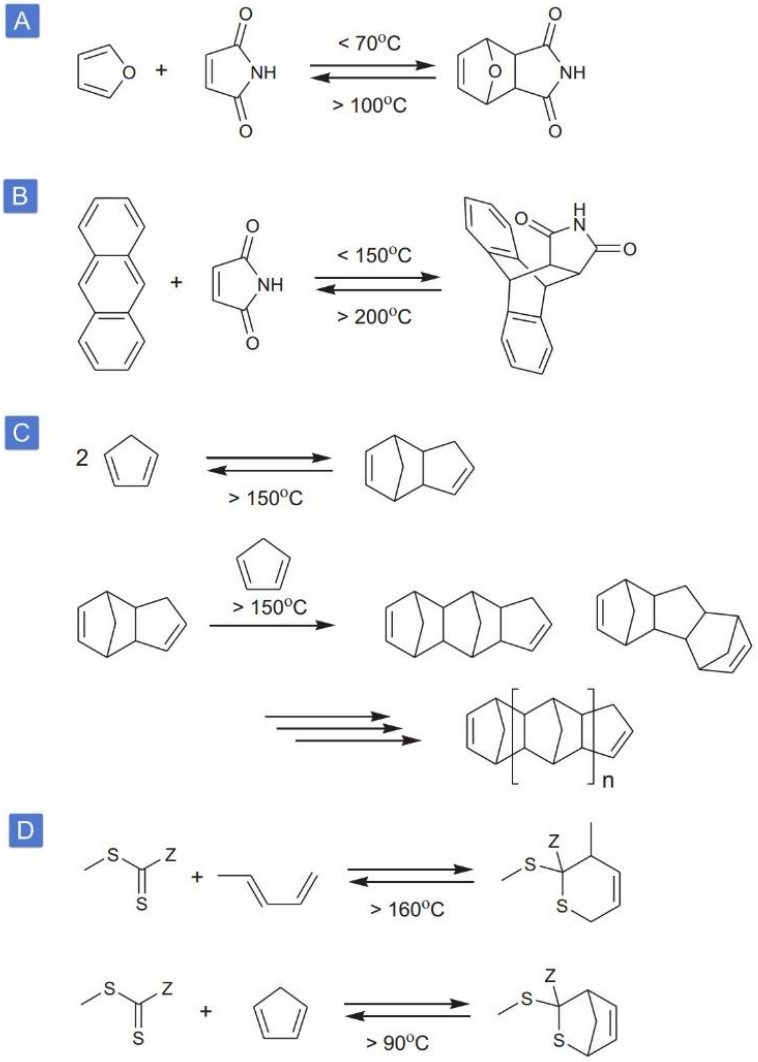

Figure 1. Common diene and dienophile used in polymer chemistry. In D, Z represents an electron withdrawing group such as pyridyl.[220] *(Adapted from the reference with permission)*

atmospheric air or oxygen-free atmosphere, and is amenable to a facile large-scale purification.[221] In terms of macromolecules chemistry, the environmental sustainability protocols attempt to provide renewable alternatives from biomass for synthetic polymers or monomers.[222] In this regard, furan derivatives such as furfural, bishydroxymethylfuran, and hydroxymethylfurfural are readily available from fructose, glucose, sucrose, cellulose, and inulin.[222–225] Thus, the [4+2] cycloaddition reaction is not only a powerful synthetic tool but also a sustainable one in designing functionalized polymers.

3.2 The frontier Molecular Orbital Theory

The frontier molecular orbital (FMO) theory is a powerful model to describe a chemical reactivity which was developed initially by Kenichi Fukui.[226] The reactivity of conjugated reactant molecules (e.g., diene and dienophile) can be rationalized through the highest occupied molecular orbital (HOMO) and the lowest unoccupied molecular orbital (LUMO). In this concept, the orbital phase and symmetry determine the outcome of the reaction. In Diels-Alder reaction, the bond formation requires the electrons located at the HOMO of the diene to move into the LUMO of the dienophile. In fact, upon proper positioning of the reactants, the charge transfer between the diene and the dienophile occurs rapidly without intermediates, making the Diels-Alder a concerted reaction. Thus, the two bonding molecular orbitals form the new sigma bonds in the adduct. The molecular orbital energies depend on the adjacent groups in the structures of the diene and dienophile. Electron-withdrawing groups, such as carbonyl or carboxyphenyl, in the dienophile, significantly reduces the LUMO energy to alleviate the energy gap exists toward the HOMO of the diene. The Diels-Alder (DA) reaction, is a thermally allowed, concerted, suprafacial [4+2] cycloaddition in which the new sigma bonds are formed simultaneously. In this context, suprafacial means that the formation of the new sigma bonds occurs on the same face of the diene & the dienophile. The term [4+2] indicates that the reaction occurs between a 4-electron rich conjugated system, known as a diene, and a 2-electron deficient system named as the dienophile. The reaction is thermally feasible provided that the highest occupied molecular orbital of the diene react suprafacially with the lowest unoccupied molecular orbital of the dienophile while conserves the orbital symmetry. DA reaction can occur readily between a cis-form of an electron-rich diene and an electron-deficient dienophile to yield conjugated six-membered rings called adducts. As an example, the FMOs of the butadiene and ethylene along with their relative energies are shown in **Figure 2A**. There are two possibilities for the cycloaddition to occur. The **SS** and the **AA** pathways shown in **Figure 2A**, both of which react suprafacially and conserve the orbitals symmetry. Addition of an electron withdrawing group appended to the ethylene, however, reduces the energy gap allowing the reaction to occur readily (**Figure 2B**).

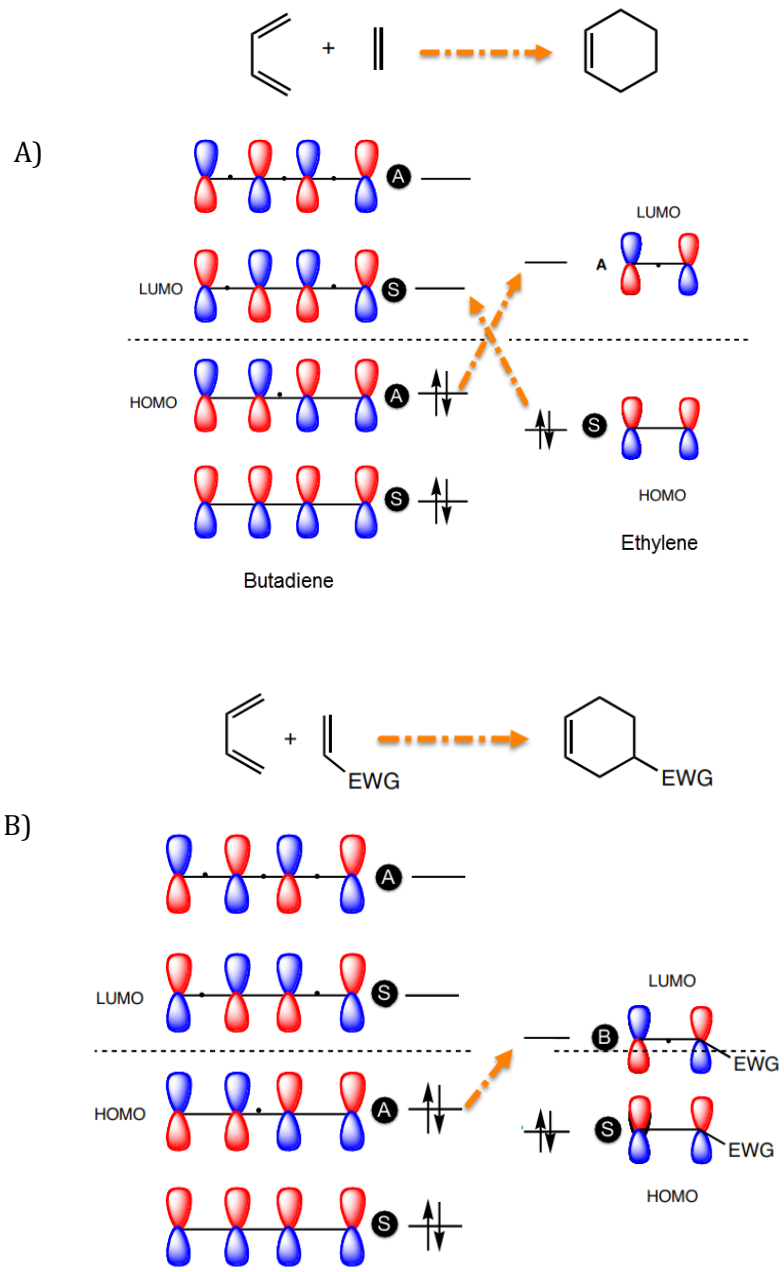

Figure 2. Effect of the electron withdrawing group appended dienophile on [4+2] cycloaddition ethylene and butadiene. The red and blue color of the p orbitals signify the difference between the orbitals wave functions. S and A stand for symmetrical and antisymmetric, respectively.[227,193]

Regarding [2+2] Cycloaddition, as shown in **Figure 3,** the symmetry elements mismatch between the HOMO and LUMO of ethylene to undergo the cycloaddition via a concerted suprafacial mode. As a result, the cycloaddition of two ethylenes is thermally forbidden. However, radiation of light can promote an electron from the bonding HOMO to the non-bonding LUMO. Therefore, it can provide the symmetry necessary for the cycloaddition

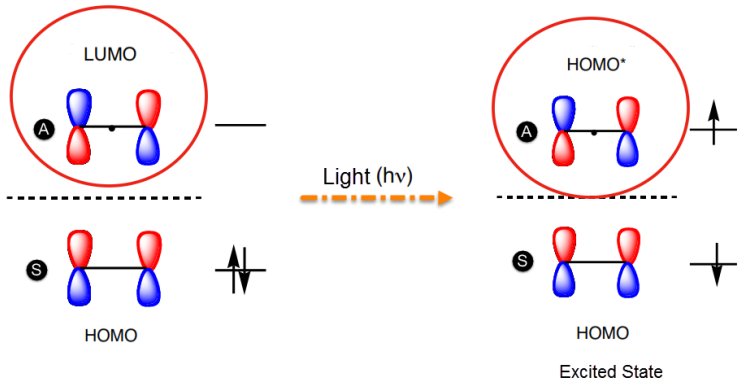

Figure 3. Excitation enables the [2+2] cycloaddition of two ethylenes.[227,193]

reaction. Since the HOMO* has the same symmetry of the ground state LUMO, the [2+2] reaction is feasible photochemically.[193,226,227]

Electron-withdrawing groups lower the energy of a molecular orbital whereas electron-donating ones increase the energy. The reason relies on the electronegative perturbation molecular orbitals theory where the electron-density of a given structure redistributes due to the adjacent groups. In fact, the additional electron-density resulted by attaching electron-rich groups to a molecule raises the molecular orbitals energy. In contrary, attaching an electron-withdrawing moiety to a structure reduces the molecular orbitals energy due to the removed electron-density.[16,228]

3.3 Diels-Alder Macromolecular Structures

Diels-Alder-based polymers can be categorized by "furan and maleimide derivatives", "anthracene and maleimide derivatives", "cyclopentadiene derivatives", or "a diene and a dithioester derivative bearing an electron-withdrawing group", which are the most common reversible DA reactions widely used in synthesizing polymers (**Figure 1**).[62,178,218,220,229,230] The structures of Diels-Alder-based polymers or monomers commonly vary among the ones illustrated in **Figure 4**. X and Y are different groups from maleimide, furan, anthracene, cyclopentadiene, dithioester, and hexadiene derivatives while 'Z' represents an electron-withdrawing group such as pyridyl. Linear structures can be obtained by the reaction of "$\mathbf{X_2}$ & $\mathbf{Y_2}$" or "**XY**" monomers. Telechelic reactions of end-capped "$\mathbf{PX_2}$" polymers with "$\mathbf{Y_2}$"

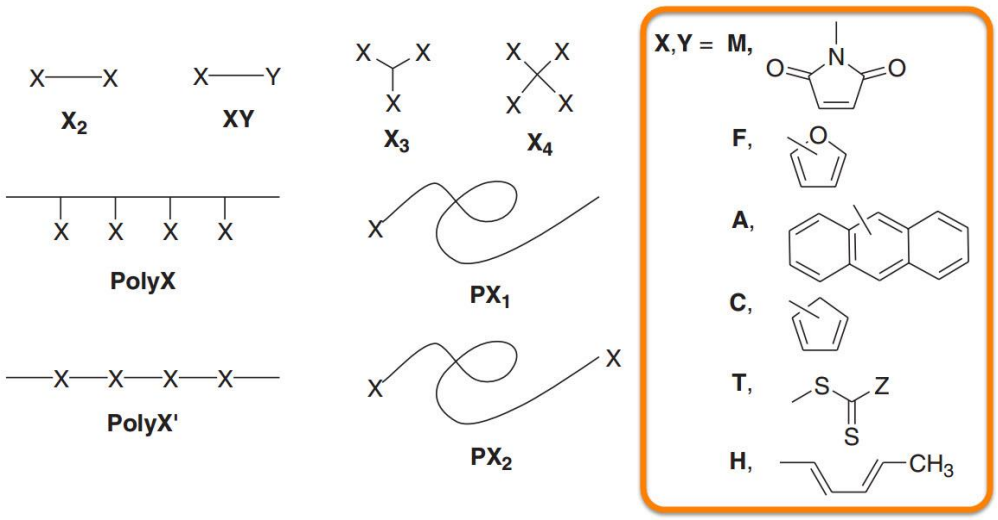

Figure 4. The structures of polymers or monomers based on the DA substrates. X and Y are different groups from the family of M, F, A, C, T, and H. 'Z' represents electron- withdrawing group such as pyridyl.[220] *(Adapted from the reference with permission)*

monomers extend the linear chains. Employing at least one monomer with functionality (F) above 2 ($\mathbf{X_{2<F}}$) with other structures except "$\mathbf{PY_1}$" yields polymeric networks. Moreover, grafted polymers (**PolyX**) or **X**-containing backbones (**PolyX'**) can be cross-linked via "$\mathbf{Y_{1<F}}$" or **PolyY**.[220,231] An outstanding example is the self-healing networks obtained from the [4+2] cycloaddition of polyfurandimethylene succinate (**PolyF'**) and bismaleimides ($\mathbf{M_2}$).[232] Since the cyclopentadiene functions as both the diene and the dienophile, **X** and **Y** are the same in this context.

3.4 The Main Categories of DA Reactions

Depending on the moieties adjacent to the furan and maleimide groups, the formation of the DA adduct occurs from room temperature to ~70°C (**Figure 1A**). However, anthracene and maleimide functional groups undergo the DA reaction at even higher temperatures. While 110°C-150°C is commonly known for the RDA reaction of the furan-maleimide (FM) adducts, the DA reaction of anthracene and maleimide generally occurs at such high temperatures. The cycloreversion of anthracene–maleimide adducts often falls into temperature ranges above 200°C where most polymer chains decompose (**Figure 1B**). Therefore, furan–maleimide-based DA reactions are the best candidate when a feasible RDA reaction is necessary.[231]

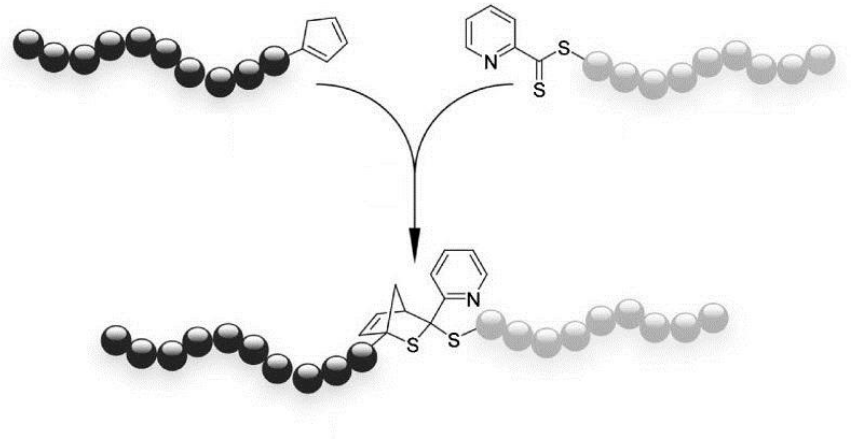

Figure 5. TFA catalyzed hetero-DA click reaction of cyclopentadienyl end-functionalized polystyrene and electron-deficient dithioester capped polyisobornylacrylate. The reaction was completed in less than 10 min at ambient conditions.[239] *(Adapted from the reference with permission)*

In addition to furan-anthracene DA adducts, the single-component DA reaction of cyclopentadienes at room temperature provides thermally stable adducts often up to 150°C (**Figure 1C**).[220] Although the common RDA reaction temperature is well below the degradation temperatures of polymer chains, the irreversible side reactions may hinder the reversibility of the adduct after several self-healing cycles. However, a limited number of successful strategies are reported.[233–235] These approaches aim to modify the already coupled cyclopentadiene dimers in order to use them as a monomer.

Dithioesters, which behave as dienophiles, undergo [4+2] hetero-DA reactions with hexadienes or cyclic dienes (**Figure 1D**). Trifluoroacetic acid (TFA) and catalytic copper systems are known for catalyzing the hetero-DA reaction of dithioesters (**Figure 5**). Quite similar to the other DA categories, using a cyclic diene such as cyclopentadiene instead of an open-chain diene effectively facilitates the DA reaction at ambient temperatures. For instance, the reaction of end-capped hexadiene chains with dithioester functionalized polymers has been reported to occur in just a few minutes even without the use of a catalyst.[236–239] While the RDA reaction of dithioester-hexadiene-based adducts occurs above 160°C,[240] the reversibility of the DA product of dithioester and cyclopentadiene was observed above 90°C.[241,242]

3.5 Self-Healing FM-DA Polymers

Functionalizing polymers with the reversible FM adducts opens a valuable door toward stimuli-responsive materials where repeatable DA/RDA reactions are responsible for the self-healing and recyclability of thermosets[186], adhesives[243], foams[185], etc.[178,229] In addition to the thermoreversible nature of the FM adducts, mechanical stress preferentially cleave the weak covalent bonds formed by the DA reaction. Therefore, due to the availability of the disconnected adducts induced by mechanical force at damaged surfaces, the reconnection of diene and dienophile does not require the temperatures at which the RDA reaction predominates. Depending on the flexibility, mobility, and reactivity of the DA functional groups, the healing process can be achieved by contacting the ruptured surfaces at mild temperatures such as 60°C.[179–181] However, chain entanglements and/or exchange reactions contribute to self-healing at low temperatures (**Figure 6**). Since the DA reaction between furan and maleimide is an equilibrium between the starting materials and the adduct, an exchange reaction between nearby adducts is possible at mild temperatures. In fact, the furan or maleimide group of an adduct can be exchanged with a furan or maleimide from an adduct which belongs to the opposite side of the damaged surface. Thus, the material can recover its mechanical and physical properties at fairly low temperatures. In the case of lengthy flexible

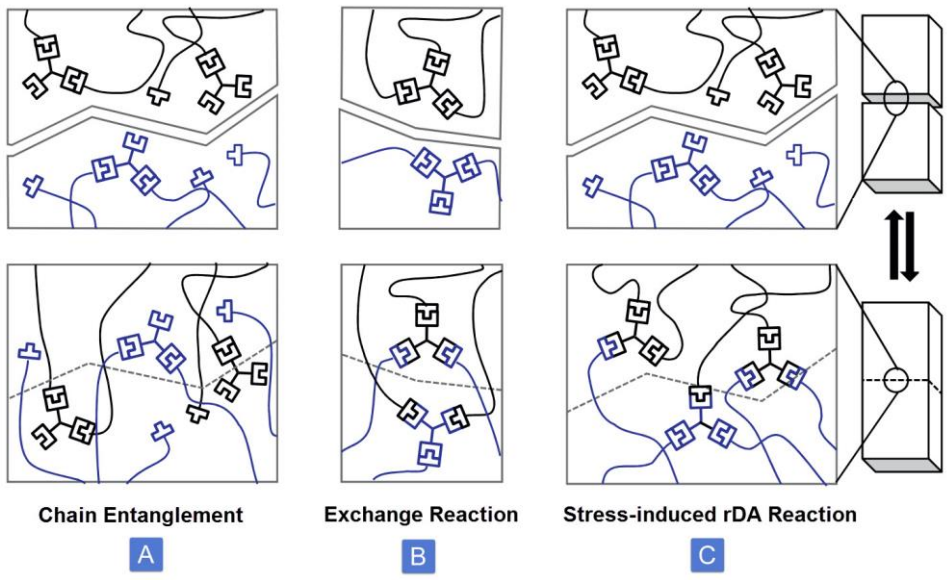

Figure 2. Schematic representations of the possible self-healing mechanisms for FM-DA cross-linked networks at mild temperatures.[179] *(Adapted from the reference with permission)*

chains or solvent-containing networks (gels), the entanglement of dangling chains is another probable mechanism in the healing process.[179,220]

3.5.1 Tuning FM-DA Cross-Links

Aside from temperature, solvent, and concentration affecting the DA equilibrium, the design of a thermally reversible DA cross-link based on furan and maleimide units requires careful consideration of the electronic and regiochemical effects surrounding the diene and dienophile substituents. In fact, the adjacent groups greatly affect the DA equilibrium, altering the adduct's stability from being practically irreversible (large exergonic DA reactions, $0>>\triangle G$) to reversible (slightly exergonic DA reactions, $0\geq\triangle G$). Thus, dynamic covalent bonds can be achieved based on the electron withdrawing (EW) or donating (ED) substituents. As shown previously[219,244,245], ED and EW substituents increase the reactivity of furan and maleimide toward DA reactions, respectively. Therefore, the furan derivatives (**1-4**) & maleimide (**5**) illustrated in **Figure 7** can be sorted based on the $\triangle G$ of the DA reaction or the stability of the resulting adducts from the lowest $\triangle G$ (the highest stability) to the highest $\triangle G$ (the lowest stability): **2, 3, 1,** and **4**. Similarly, sorting the reaction of furan (**1**) and maleimide derivatives (**5-8**) concerning $\triangle G$, ranks the reactions in the order of **6, 8, 7,** and **5** from the lowest to the highest $\triangle G$. Additionally, placing the substituents at the 3rd position of furan instead of the 2nd one was found to amplify the reactivity of the dienes by lowering the $\triangle G$.[244]

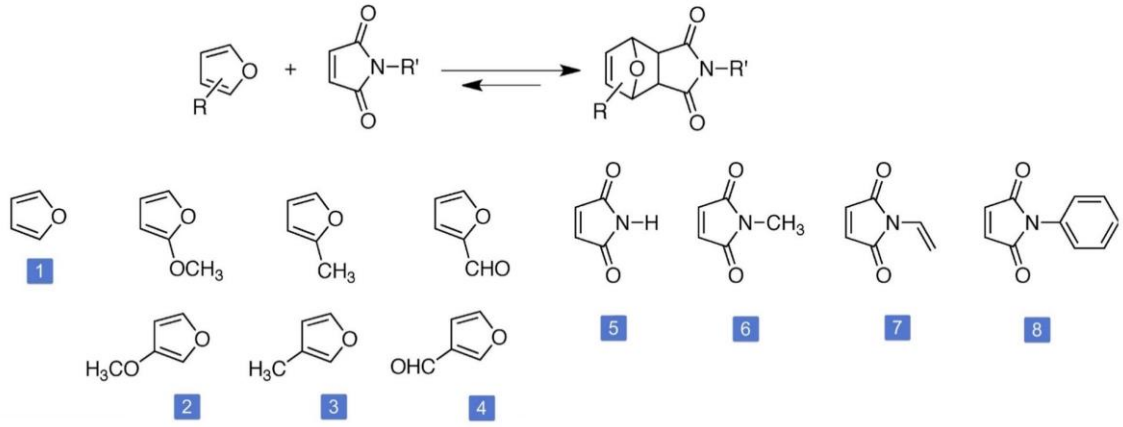

Figure 7. Different adjacent groups next to the maleimide and furan.[244]

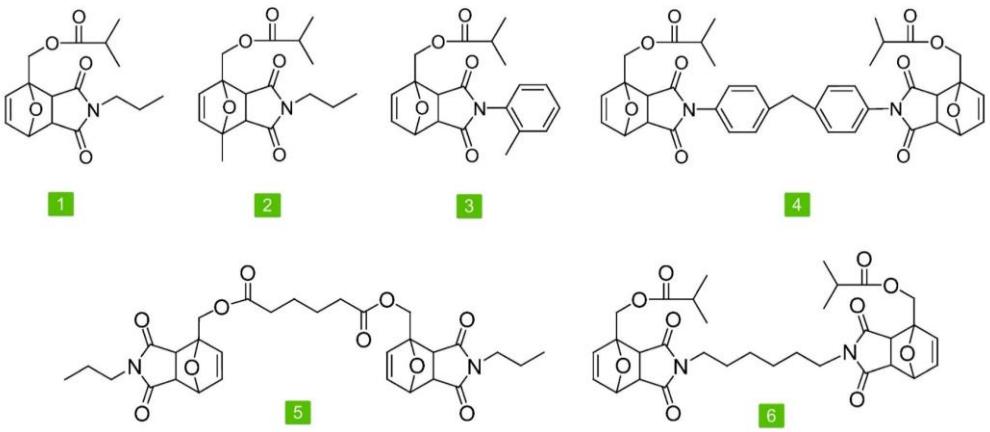

Figure 8. A series of DA model cross-links.[245]

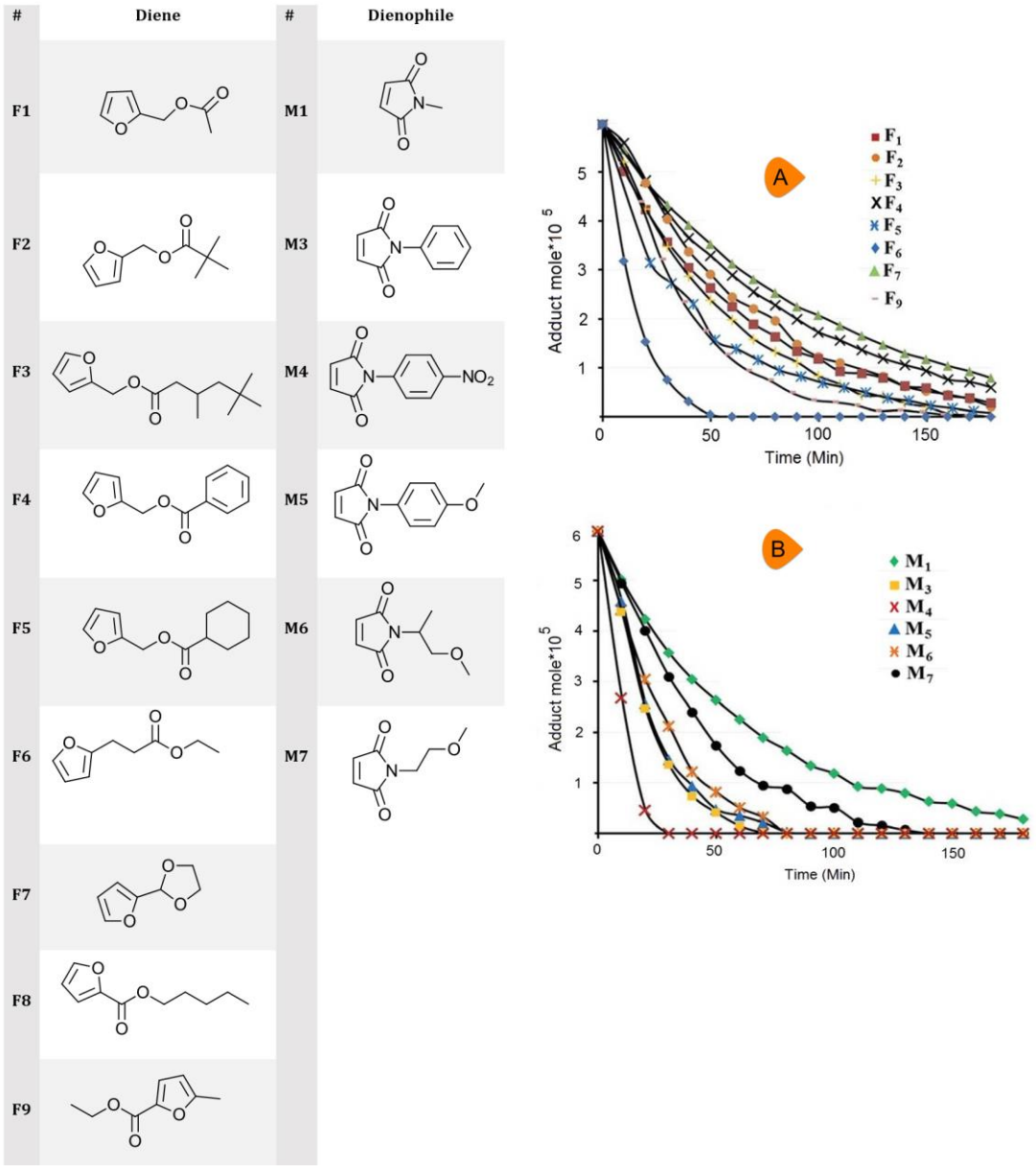

Figure 9. Retro-DA reaction profile for series of DA adducts based on A) M1 and different furan derivatives (F1-F9) B) F1 and different maleimide derivatives(M1-M7).[219] *(Adapted from the reference with permission)*

While substituting the furan ring with strong ED substituents greatly increased the furan's affinity for the maleimide, the significantly low free energy barriers cause strong obstacles against the retro-DA reactions. Therefore, depending on the desired application, the △G should be adjusted to optimize the extent of DA/retro-DA equilibrium at a given temperature. Based on Differential Scanning Calorimetry (DSC) measurements, the highest temperature reported for the model adducts (**1-6**) shown via **Figure 8** in which the compounds greatly undergo the retro-DA reaction, are 138°C, 114°C, 126°C, 157°C, 134°C, and 130°C, respectively.[245] Isothermal ^{1}H NMR studies at 70°C for a variety of DA adducts based on maleimide and furan derivatives indicated placing rigid substituents at the 3rd or 2nd position of the furan ring lowers the RDA reaction tendency (**Figure 9A**). On the other hand, having EW mesomeric substitutions on maleimide results in faster decoupling reactions (**Figure 9B**).[219]

3.5.2 FM-DA Containing Siloxane Groups & Carbon Spacers

The strategy of utilizing siloxane moieties and carbon spacers in the Diels-Alder reaction has been a gateway to promote the molecular flexibility required for the self-healing process. In fact, enhancing the flexibility of FM-DA networks promotes reversible bond formation. In 2001, this strategy was used to obtain removable foams based on [4+2] cycloaddition where the networks were subsequently cross-linked via epoxide groups reacted with amine

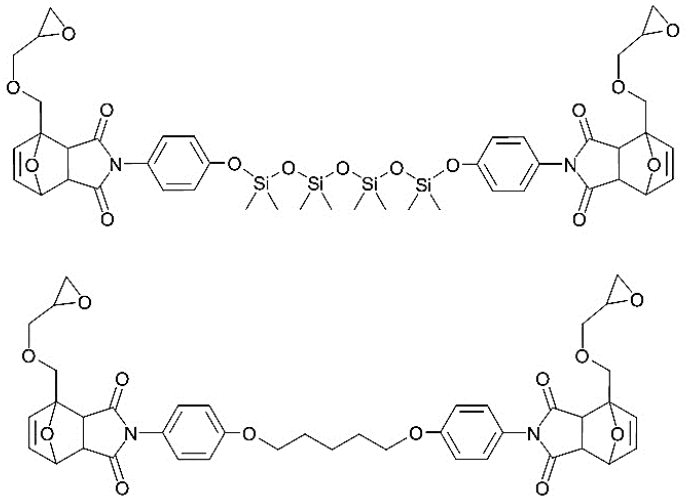

Figure 10. The siloxane- based maleimide derivatives synthesized to obtain removable foams.[185]

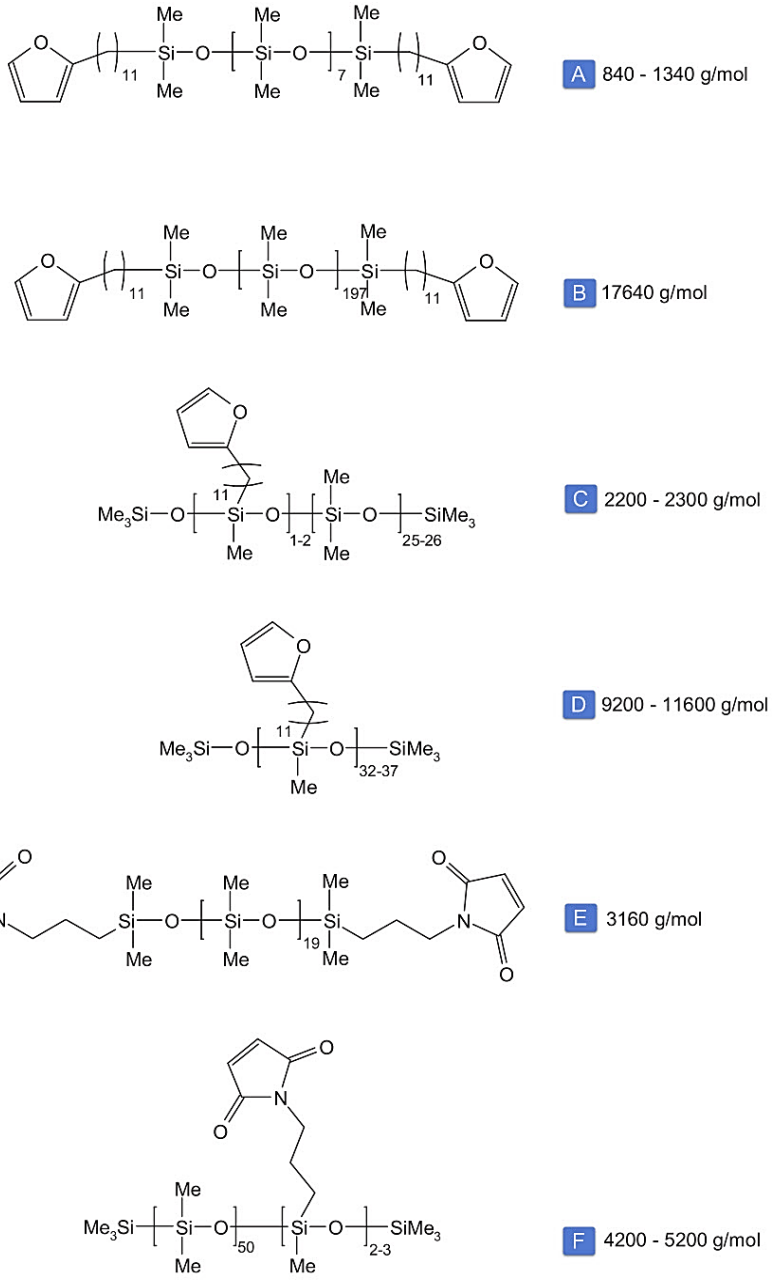

Figure 11. The furan- & maleimide-caped/grafted polysiloxanes prepared by Schäfer et al.[183]

functionalized compounds, **Figure 10**.[185] Moreover, Gheneim *et al.* provided a synthetic methodology to incorporate maleimide pendant groups into polysiloxanes through grafting two types of aminopropyl-functionalized siloxane copolymers.[246] Using commercially available copolymers with weight average molecular weights ($\bar{M}_w$) of 4,500 and 5,000 g/mol allowed only approximately 2.2 and 3.4 maleimide groups to be incorporated per chain,

respectively. The grafted polymeric dienophiles were reacted with a synthesized difuran compound to yield the target networks. However, although the DA reaction was confirmed via ^{1}H NMR, the intermolecular coupling was not sufficient to form a robust network.

More recently, Schäfer *et al.* illustrated that the flexibility and mobility added into the FM-DA networks by utilizing modified polysiloxanes increased the tendency of the RDA reaction, promoting the self-healing process.[183] In this comprehensive study, furan- or maleimide-functionalized silica nanoparticles cross-linked various maleimide- or furan-modified siloxane copolymers, **Figure 11.**[185] Similarly, Zhao *et al.* used the flexibility of polydimethylsiloxane backbones to produce elastic networks cross-linked via a difuran-functionalized siloxane.[184] Analogous to previous research studies, a series of commercially available aminopropylmethylsiloxane–dimethylsiloxane copolymers were functionalized with propylmaleimide groups. Although the selected copolymer precursors had low molecular weights (i.e., $\bar{M}_w < 6100$ g/mol) elastomers were formed after several days as a result of insufficient amounts of functional moieties along with the negative impact of the amide bond directly tethered to the furan ring. As previously described, carbonyl groups originating from furoyl/furfural derivatives significantly reduced the tendency for the DA reaction. The polymer displayed a high degree of self-healing efficiency, as well as the remoldability of the damaged networks by utilizing the aforementioned strategy, **Figure 12**.

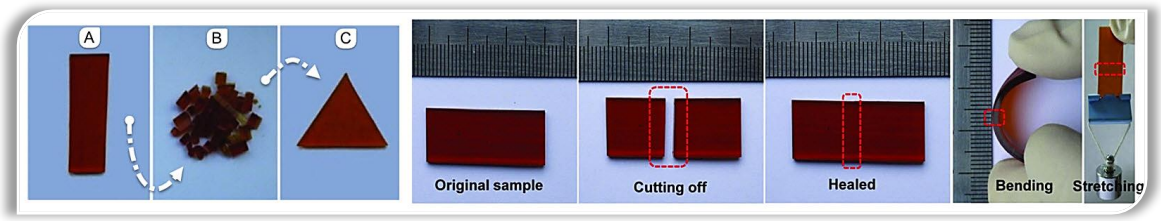

Figure 12. Illustration of the remoldability and high capacity for self-healing through the usage of flexible siloxane backbones.[184] *(Adapted from the reference with permission)*

3.6 Summary

The design of intrinsic self-healing systems based on the Diels-Alder reversible chemistry opens a wide window to the parameters that can be selected to adjust the network's properties concerning the target applications. In other words, altering the reactants

structures (i.e., the diene and dienophile structures) is a precious tool to optimize the state of the DA/RDA equilibrium at a given temperature. In fact, the extent of the coupling/decoupling reaction rate can be pushed toward the point where the readily reversible DA adduct becomes a robust adduct heavily hindered to undergo the RDA reaction at high temperatures. On the other hand, the functional groups can also be adjusted to access a RDA-controlled equilibrium where the adducts rapidly undergo cycloreversion at low temperatures. Furthermore, the strategy of using flexible polysiloxanes and carbon spacers extends the optimization capacity of DA adducts. Likewise, utilizing furan derivatives originating from renewal biomass sources elevates these structures toward an even more valuable level. Mechanically triggered RDA reactions of FM-DA adducts upon damage could be an important factor in selecting suitable, reversible DA adducts for a given application. All in all, Diels-Alder chemistry establishes an appealing opportunity for obtaining intrinsic self-healing polymeric networks for various operating conditions.

Chapter 4 Results & Discussion

A major portion of the current chapter is taken from the author's article published in *Polymer Chemistry* with minor changes.[247,†] This chapter deals with the evaluation of thermally reversible nature of a novel cross-link synthesized[‡] by the author. In order to better understand the complex polymeric system, a model system was purposed to represent the target macromolecules. Various measurements are discussed in this chapter including nuclear magnetic resonance (NMR) spectroscopy experiments and DSC analysis of the model system. The self-healing properties of the silicone elastomers are evaluated using scanning electron microscopy (SEM) and variable-temperature (VT) solid-state NMR experiments.

4.1 Introduction

Damage is an unavoidable aspect of polymers during their operation. Unlike many living organisms, self-healing ability is not a generic feature of synthetic materials. Engineered materials have been designed and developed on the basis of the damage suppression/management to expand the lifetime and reliability of materials. In fact, cross-linking has been a method of choice to achieve an enhancement in physical and mechanical properties of polymers. Compared to thermoplastics, superior properties can be provided through this approach such as higher durability, extended lifetime, solvent resistance, and dimension stability. However, the formation of conventional polymeric networks may result in drawbacks, including lack of recyclability, and remould-ability which would appear to be a major concern on environmental issues. Self-healing polymers are a class of smart materials capable of responding to a specific stimulus, commonly thermal and mechanical energies, to heal damaged areas through a chemical reaction or physical interaction.[105] The intrinsic self-healing approach is a desirable strategy replacing the classical chemical cross-linkers with thermally reversible bonds that can be repeatedly broken and re-connected chemically[183] or

---

† ***Nasresfahani, A.*** *& Zelisko, P. M. Synthesis of a self-healing siloxane-based elastomer cross-linked via a furan-modified polyhedral oligomeric silsesquioxane: investigation of a thermally reversible silicon-based cross-link. Polym. Chem. (2017), 8, 2942-2952.*

‡ *Please find the details in the next chapter Experimental*

physically[248,249]. Due to their high bonding strength, Diels–Alder (DA) and similar cycloaddition reactions are good candidates for equipping polymers with intrinsic self-repairing criteria, and enhancing the mechanical toughness of materials, as well.[118,250] Thus, upon utilizing these reversible bonds, networks could be prepared to have favorable physical and mechanical features of thermosets as well as the process-ability of thermoplastics which in fact may lead to drastically cut down the overall costs spent on preparations of self-healing materials through saving a considerable amount of resources and energy used. However, the main challenge in this area has been designing linkages having fast enough reversible reactions at lower temperature zones through a high yielding synthetic route.

DA chemistry has been a promising approach to prepare thermosets with self-healing criteria, in particular, remold-ability.[62,178,229] Furan derivatives are described in the literature as a valuable reactive diene for the DA reaction. The coupling reaction could happen even at room temperature while the decoupling reaction called retro-DA (RDA) starts to begin at higher temperatures. Several factors can affect these two temperatures (i.e., T_{DA} & T_{RDA}), the rate of reactions, and the final state of DA/RDA equilibrium at a given temperature.[231] The furan's oxygen atom facilitates the diene double bonds to relocate, resulting a reactivity increment towards dienophiles. In addition, withdrawing substituents with one carbon spacer to the furan ring can elevate the reactivity. Electron attracting groups attached to maleimide derivatives, specifically a phenyl ring appended to an ester group, enhance dienophile reactivity.[219,245,251,252] Although the commercially available bismaleimide with phenylene rings (1,1′-(Methylenedi-4,1-phenylene) bismaleimide) markedly enhanced the tensile strength, the lack of flexibility caused polymeric networks with T_g well above room temperature, and hindered the decoupling reaction at low tempertures.[182,253,254] In contrast, bis-maleimides with flexible molecular structures tend to improve the polymer elongation, affording polymers with an excellent healing capability. It is shown that the self-healing ability of such systems depends primarily on the mobility of the functional groups and the ratio of maleimide to furan. Owing to flexibility of polysiloxanes backbones, these networks have been shown to display reversible cross-linking process through DSC analysis.[183,184]

These results revealed that mobility and flexibility of the polymer backbones is crucial for a reasonable fast self-healing process. Thus, promoting the healing process could be achieved by considering a certain level of flexibility.

Although carbon-based polymeric backbones have been investigated quite thoroughly,[62,178,188,229,250,252,255–260] a small number of reports have discussed the potential application of polysiloxane units in developing intrinsic self-healing materials.[183,184] The majority of polydimethylsiloxane (PDMS) self-healing studies have focused on extrinsic approaches, where physical defects were healed through the application of encapsulated reagents embedded in the siloxane matrix.[129,214,261] Gheneim *et al.* attempted to impart intrinsic self-healing properties to a silicone matrix by grafting maleimide groups onto polysiloxane copolymers.[246] However, their efforts were not successful which was attributed to a lack of grafting and DA reaction efficiency along the siloxane backbone. More recently, Kickelbick's group conducted a comprehensive study in which a series of novel polysiloxanes were modified using both maleimide and furan as a pendant or/and terminal groups.[183] These results demonstrated that the flexible nature of the polysiloxanes facilitates Diels-Alder chemistry in polymeric systems. Xia *et al.* addressed the biocompatibility and remoldability of polysiloxane elastomers cross-linked with Diels-Alder linkages.[184] Another successful approach to self-healing silicones was developed through the introduction of dynamic coordination bonds utilizing a Co(II)/Fe(III) triazole complex. This type of self-healing PDMS resulted in the production of a highly elastic material having solvatochromic behaviors.[248,249]

In the context of intrinsic self-healing materials, few studies have employed modified polyhedral oligomeric silsesquioxanes (POSS, POSS®) as a cross-linking agent.[182,262] The rigid framework of POSS® closely resembles the smallest possible silica particle that can be incorporated into a siloxane network. The incorporation of POSS units into polymeric networks offers a unique opportunity for preparing truly dispersed nanocomposites with enhanced thermal stability, mechanical properties, and flame resistance.[98,263] The inorganic

nature and multiple reactive functionalities of POSS, make these modifiable nanoparticles ideal for the construction of hybrid nanomaterials with improved self-healing properties.[96,98]

4.2 Instrumentation

Mass Spectrometry (MS). Electron Impact (EI) and Fast Atom Bombardment (FAB) mass spectrometry were carried out on a Thermo DFS high-resolution mass spectrometer in positive ion mode. Matrix Assisted Laser Desorption Time of Flight (MALDI-ToF) spectra of the modified POSS (**12**) was acquired on a Bruker Autoflex MALDI-ToF mass spectrometer in the positive ion mode.

Nuclear Magnetic Resonance (NMR) Spectroscopy. ^{1}H, ^{13}C, and ^{29}Si NMR spectra were acquired using a Bruker AV-300 and AV-400 NMR spectrometer equipped with a PABBO broadband probe. Variable-temperature 1D proton magic angle spinning (MAS) solid-state NMR experiments were performed on a Bruker AV-600 SB spectrometer equipped with a BL4 NMR probe. The spin rate was set to 7kHz.

Differential Scanning Calorimetry (DSC). Thermal analysis was conducted using a Shimadzu DSC-60 and a TA-60WS thermal analyzer. The calorimeter was calibrated using octadecane, which has a melting temperature of 27.95°C. Aluminium was used as the standard.

Scanning Electron Microscopy (SEM). Samples were mounted onto SEM stubs, sputter-coated with gold and then viewed in a Tescan Vega II LSU scanning electron microscope (Tescan USA, PA) operating at 20kV.

Infrared Spectroscopy (IR). Attenuated Total Reflectance Fourier Transform IR (ATR FT-IR) spectra were acquired on a Bruker Alpha Optic GmbH 2012. All spectra were an average of 24 scans at 2cm^{-1} resolution using neat samples on a diamond window.

Durometer Test. Shore OO values were measured using a digital durometer (*Check-Line® RX-OO*) according to ASTM D-2240.

4.3 Evaluating the Model System

The components of the model system were synthesized as outlined in the next chapter. In the model study (**Figure 1**), compounds **10** and **5** represent the furan-modified POSS (**12**) and the maleimidocarboxyphenyl pendant group grafted onto the PDMS backbones, respectively. The model study was undertaken to characterize the DA and RDA reactions of the cross-link before applying the strategy to the target polymeric matrix.

Equimolar amounts of **10** and **5** were reacted without solvent at 40˚C. Consumption of the maleimide was confirmed by the disappearance of the maleimide ring-deformation signal at 680-700 cm^{-1} in the ATR-IR spectrum (see **Chapter 6**). The structure of the model adduct (**11**) was confirmed principally by ^{1}H and gradient ^{1}H homonuclear correlation (gCOSY) NMR spectroscopy (see **Chapter 6**).

In the ^{1}H NMR spectrum, the resonances associated with the adduct alkene's protons (C and D) were located at 6.48–6.63 ppm and the resonance for the bridgehead proton (G) was at 5.4 ppm. The relative proportion of *endo* and *exo* Diels-Alder products was determined by referencing integral values in the spectrum to the protons of the phenyl ring (8.15-8.13 ppm). Since the dihedral angle between the bridgehead proton and the proton which belongs to the exo Diels-Alder adduct is approximately 90˚, no observable spin-spin coupling was found for these two sets of protons in the gCOSY ^{1}H NMR spectrum (see **Chapter 6**).[245] Therefore, the protons of the Diels-Alder fused ring systems were assigned as follows: 3.08 ppm (E-*exo*), 3.16 ppm (F-*exo*), 3.58 ppm (E-*endo*), 3.82 ppm (F-*endo*), 5.41 ppm (G), 6.48 ppm (C), and 6.63 ppm (D), which is in agreement with the data reported for similar compounds.[219,245] Presumably, the steric bulk associated with the siloxane moieties is enough to disrupt the secondary orbital interactions that would favour the formation of the *endo* adduct, resulting in the *exo* adduct being the major product, even at relatively low temperatures.

In order to optimize the conversion of the maleimide to the Diels-Alder adduct (**11**), the reaction between **10** and **5** was performed at 40˚C (**A**), 50˚C (**B**), 60˚C (**C**), and 80˚C (**C**) under solvent-free conditions. Each reaction contained 1:1 furan:maleimide mole ratio (12 µL:10 µL) in a small test tube (0.75mL, 6 × 50mm) which was heated at the specified temperature

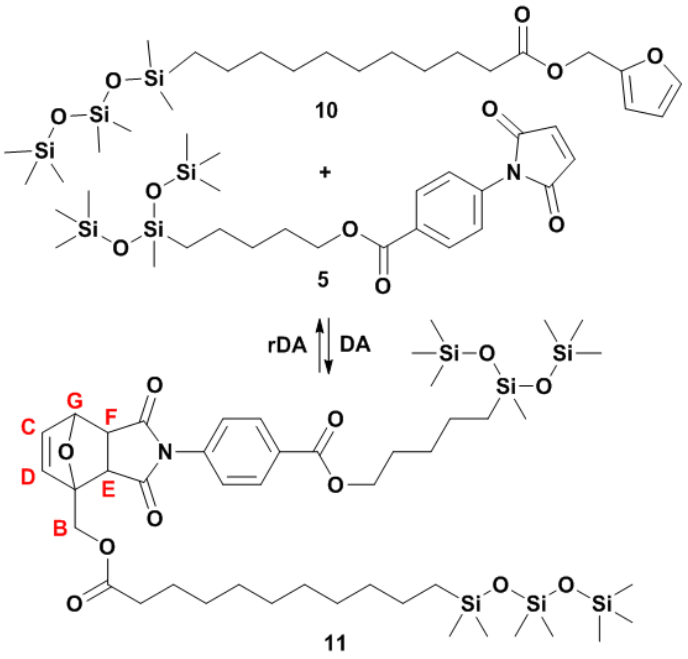

Figure 1. The model Diels-Alder/retro-Diels-Alder equilibrium involving appended furan rings (diene) and a maleimidocarboxyphenyl (dienophile). The Diels-Alder and retro-Diels-Alder reactions were favoured at 40°C and 110°C, respectively.[247] (See Chapter 6 for the synthetic details)

for 24h. The ^{1}H NMR data revealed that the equilibrium is predominantly favourable toward the DA reaction from 40˚C to 50˚C (**Table 1**, **Figure 2**). Extending the time to 48h for each sample produced approximately the same integral values, addressing that in the first 24h the model Diels-Alder/retro-Diels-Alder reactions had reached equilibrium conditions (**Figure 3**, also see **Chapter 6**). Consumption of the maleimide was calculated by comparing the integrals of the alkene protons (C, D) with the 2H resonance associated with the phenyl ring at 8.12-8.15 ppm. The relative proportion of *endo* product decreased significantly as the temperature was increased from 40˚C to 60˚C while the *exo* adduct became more abundant, suggesting the transition of *endo* to *exo* adduct significantly expanded within the mentioned temperature range. However, since the *endo* and *exo* adduct ratio has a negligible influence on the bulk properties of a polymeric material, the *endo* and *exo* isomers can be treated as a single adduct in terms of the macromolecular chemistry.[187,253]

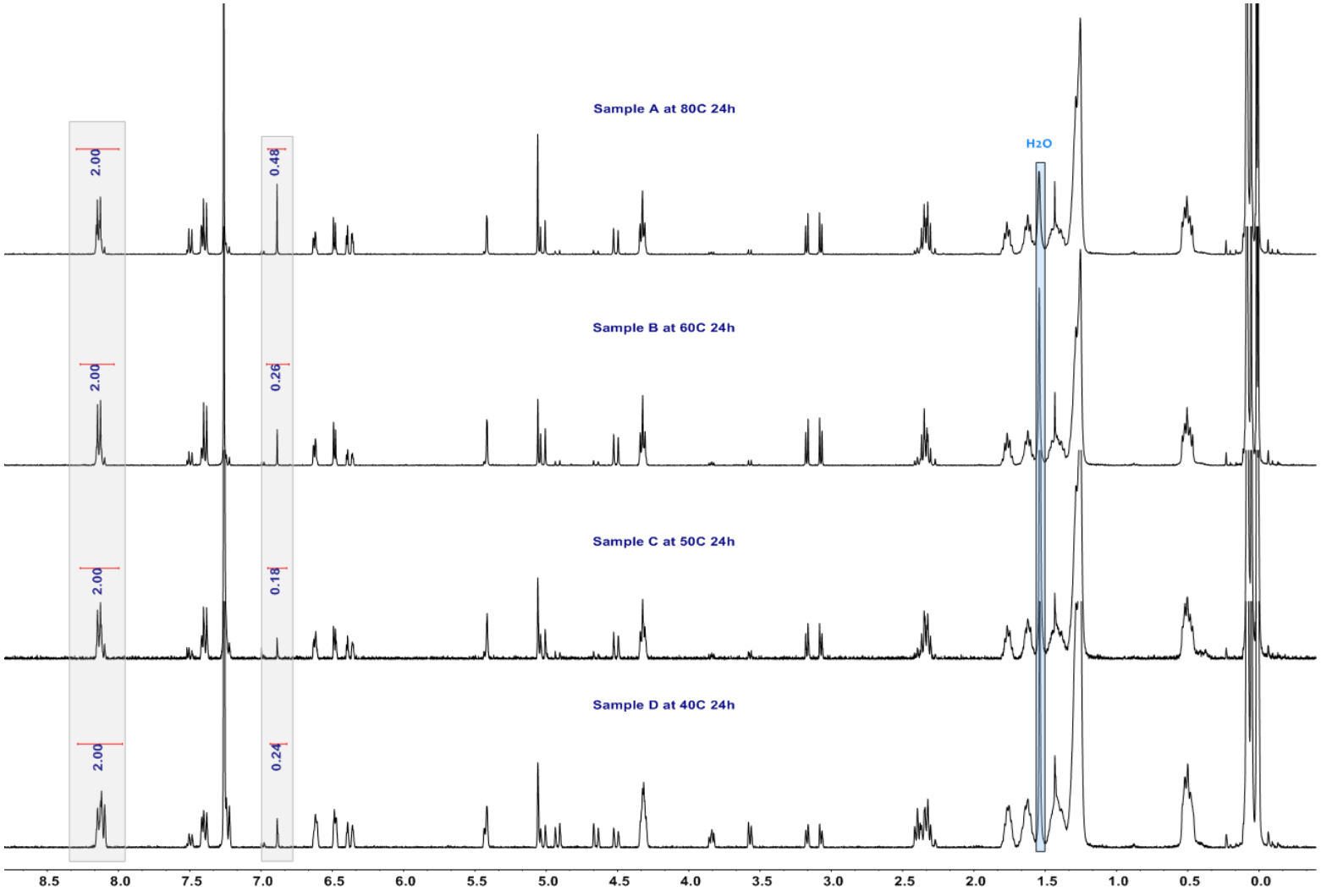

Figure 2. *^{1}H NMR spectra of samples (A,B,C,D) at different temperatures (80°C, 60°C, 50°C, and 40°C) after 24 h.* [247]

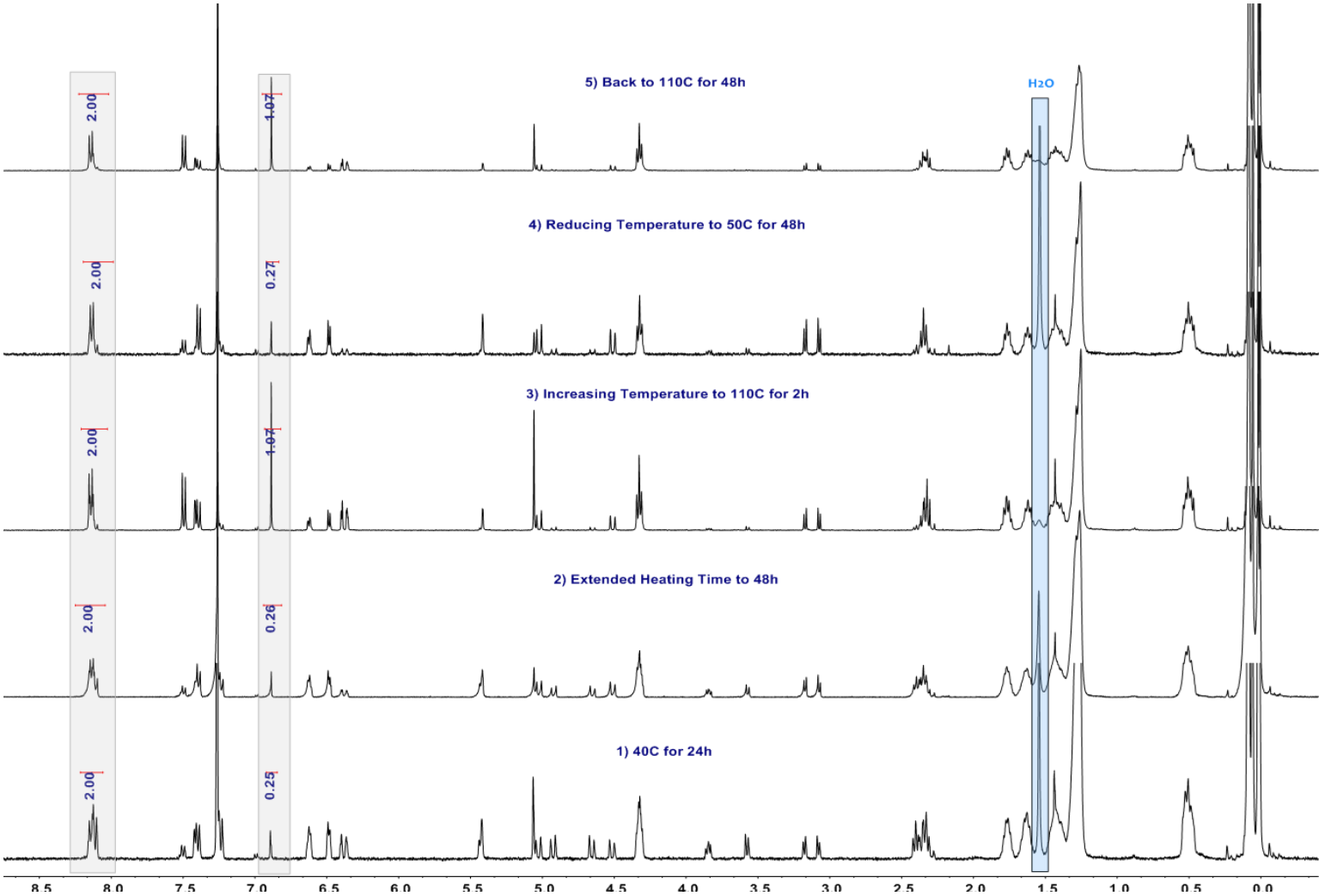

Figure 3. *[1]HNMR spectra illustrating the reversible nature of the Diels-Alder reaction over multiple cycles for the Diels-Alder adduct formed between 10 and 5 at 40°C (sample D).*[247]

Sample	Temperature (°C)	Maleimide Consumption (%)	Exo(%)
A	80	74	91
B	60	86	91
C	50	90	82
D	40	87	46

Table 1. The maleimide consumption in sample A, B, C, and D at different temperatures after 24h.[247]

To study the feasibility of having a system which undergoes multiple Diels-Alder/retro-Diels-Alder cycles, samples **A**, **B**, and **D** were subjected to elevated temperatures of up to 110˚C to facilitate the RDA reaction, prior to cooling down to 50˚C. According to the ^{1}H NMR data obtained for sample **D** (**Figure 3**), in just 2 h the amount of maleimide conversion altered to 42% from 87% proving the RDA reaction was profoundly favoured at 110˚C, shifting the equilibrium towards the starting materials. Lowering the reaction temperature to 50˚C led to reproduce 99% of the consumed adducts (**Figure 3**). Similarly, the reversible reactions for sample **A** and **B** were also studied (see **Chapter 6**). Looking at the data for sample **A**, the reaction needed less than 2h at 50˚C to reach its initial equilibrium values. Considering the data from retro-Diels-Alder reaction for sample **D** at 110˚C, the Diels-Alder reaction occurred in a comparable time frame.

Equimolar amounts of **5** and **10** were used to prepare a sample that contained almost 96% of the adduct. After exposure to 136˚C for 2 min the sample was quenched at 4˚C. A 66% decline in the concentration of the Diels-Alder adduct was observed by ^{1}H NMR (see **Chapter 6**).

Considering the thermal behavior of the linkage mentioned, the proposed cross-link was found to be similar to those of which previously described as ultrafast DA/RDA cross-links.[186] It needs to be noted that the diene was unstable at temperatures above 120˚C for extended time periods (i.e., if the diene from retro-Diels-Alder reaction remained at temperatures of 120˚C or greater for several hours, the reaction produced a black solid that was insoluble in conventional solvents). However, this instability did not provide a barrier in terms of the

$$\text{Diene + Dienophile} \underset{k_2}{\overset{k_1}{\rightleftharpoons}} \text{Adduct}$$

$$\frac{dx}{dt} = (k_1 F_0)(1 - x) - \left(k_2 {M_0}^{m-1}\right)x^m$$

$$k_1 = 0.4844 \ \ (h^{-1})(L/mol)$$

$$k_2 = 0.0019 \ (h^{-1})(L/mol)^{\approx -1}$$

$$m = 5.2 \times 10^{-5} \approx 0$$

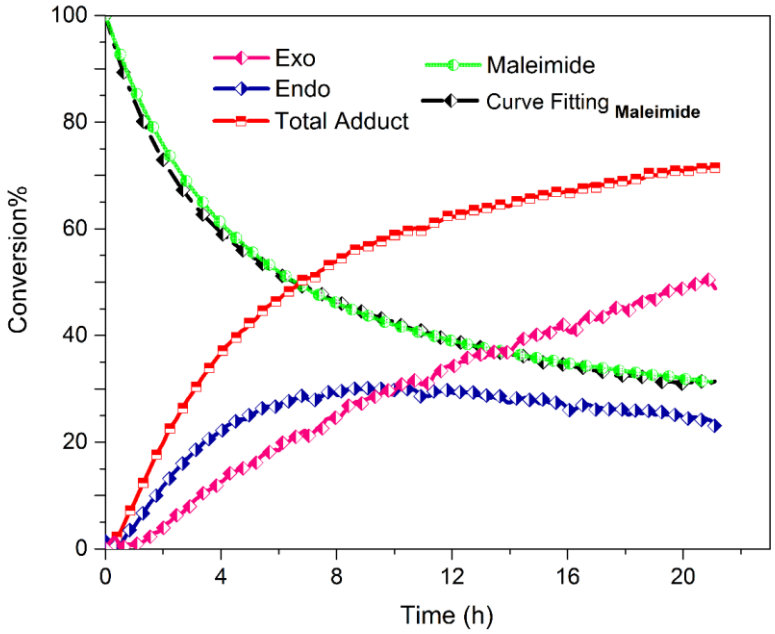

Figure 4. Conversion of the maleimide (5) to the adduct (11) in excess amount of the diene (10) monitored by Dynamic ^1H NMR experiment at 50°C. $CDCl_3$ was used as the reaction solvent. The total amount of the observed adduct is the summation of exo and endo products.[247]

adduct reversibility, as the retro-Diels-Alder reaction occurs within a few minutes. Analogous irreversible reactions have been also reported for furan derivitives[182,258,262,264–266]

In an effort toward an understanding of the reaction profile, the Diels-Alder reaction conducted at 50°C was studied by isothermal ^{1}H NMR spectroscopy (**Figure 4**). Spectra were acquired every 5 min resulting in 187 total acquisitions. An excess amount of the furan (10 mol equiv.) (F_0 = 10 M_0 ≈ 0.5 mol/L) in $CDCl_3$ was chosen to establish a pseudo-first-order DA reaction conditions and minimize the reaction time. Curve fitting of the maleimide conversion rate, dx/dt, confirmed the pseudo-first-order rate profile for the DA reaction. In contrast to the *exo* isomer, which showed relatively linear behaviour through the course of the reaction, the *endo* adduct was observed to reach its highest concentration in

approximately 10h, reaching a maximum concentration of approximately 30%. Following the reaction from this point, the *endo*:*exo* ratio started to increase from 1:1 to 1:2 whereas the *endo* adduct's amount gradually decreased to 24%. As the Diels–Alder reaction is a balance between the adduct and the starting materials, the maleimide consumption, as well as the adduct production, was expected to ultimately reach a plateau at the equilibrium state. The forward reaction (Diels-Alder) was almost $k_1/k_2 \approx 255$ $(L/mol)^{\approx 2}$ more favourable than the reverse reaction (retro-Diels-Alder) at 50°C. The rate constant for the Diels-Alder reaction at 50°C (k_1) is among the highest values reported for [4+2] cycloaddition reactions of furan and maleimide derivatives in the literature.[219,267] The curve fitting formula and constants are shown in **Figure 4**.

DSC measurements were also used to visualize the Diels-Alder and retro-Diels-Alder reactions. The sample prepared for DSC analysis was obtained from a 1:1 ratio of diene: dienophile that was kept at 50°C for 5 days. ^{1}H NMR spectroscopy analysis of the sample indicated approximately 88% consumption of the maleimide prior to being analyzed by DSC. The sample was equilibrated at -15°C for 10 min before being subjected to seven heating/cooling cycles ranging from -13°C to 116°C. All cycles had the same heating/cooling rate of $\pm$4°C/min. Comparing the first heating/cooling cycle with subsequent ones, there were three conspicuous areas (shaded) in **Figure 5**. Reports in the literature[186,219,245,250,254,257,258,264,268,269] as well as the ^{1}H NMR data presented above, indicated that the first, second, and third shaded areas can be attributed to the reduction of alignment between the aliphatic carbons bonded to the siloxane moieties (**Figure 5**, **Area 1**), the retro-Diels-Alder reaction of the endo isomers (**Figure 5**, **Area 2**), and the endo- to exo-isomerization along with crystallization of the exo-adduct before going through the exo-retro-Diels-Alder reaction at approximately 60°C (**Figure 5**, **Area 3**).

It is important to note that there were several parameters governing the material's overall response in the thermal analysis, including the amount of heat injected or extracted from the system by the DSC instrument, the quantity of adduct available, and the isothermal experience at 116°C in each cycle. The isothermal time periods for the first three cycles, the

"**4th & 5th**" and the "**6th & 7th**" cycle were 10, 20, and 40 min, respectively. According to the aforementioned ^{1}H NMR experiments, the Diels-Alder reaction at 50°C and the retro-Diels-Alder reaction at 110°C should be quite comparable to a given time scale in the DSC. However, since the holding time at 116°C was deliberately extended, the equilibrium tended to shift towards retrieving the amount of adduct that had been consumed. Thus, the exothermic peak

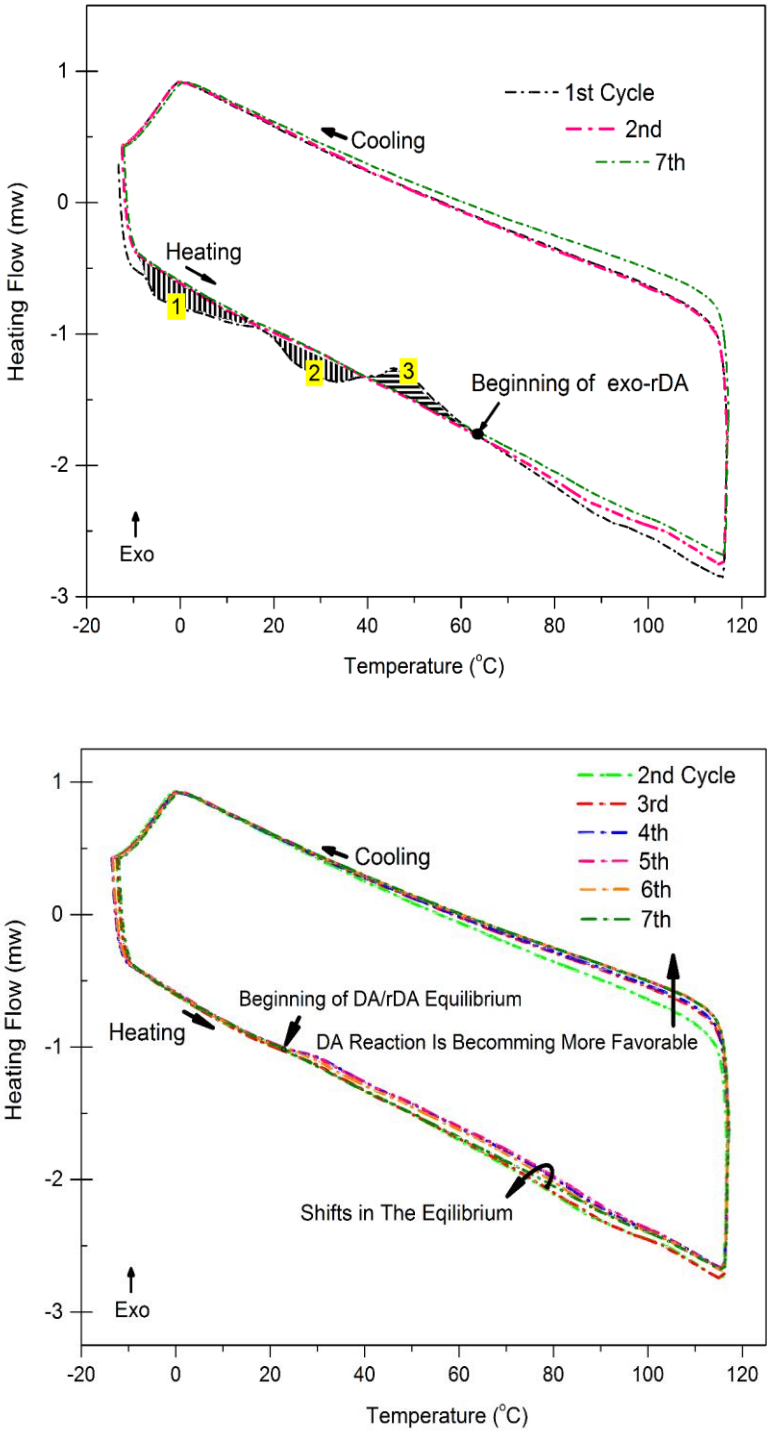

Figure 5. DSC analysis of a sample of the model cross-link containing 88% adduct (11). Both retro-Diels-Alder and Diels-Alder reactions were detected after the 2nd cycle.[247]

gradually increased. Consequently, the Diels-Alder reaction became more favourable in each cooling cycle. Furthermore, none of the cycles exhibited an endothermic peak to the same extent as the **1st cycle**. This can be attributed to the higher quantity of adduct available in the sample which motivated the equilibrium to favour the retro-Diels-Alder reaction in accoRDAnce with Le Châtelier's principle.

The data obtained from the ^{1}H NMR and DSC analyses demonstrated the capacity of the cycloaddition linkage to be considered as an excellent intrinsic self-healing cross-link.

4.4 The Diels-Alder Cross-Linked Siloxane Elastomer

The trimethylsiloxy terminated-methylhydrosiloxane-dimethylsiloxane copolymers used in these experiments had a number average molecular weight of 13,000 g/mol and possessed 3-4 mole% methylhydrosiloxane. Based on ^{1}H NMR data and elemental CH analysis, on average, there was one maleimidocarboxyphenyl side group for every 32 dimethylsiloxane units in the copolymer system. A homogenous solution of **PDMS-3** and furan-modified POSS (**12**) in chloroform with a maleimide: furan mol ratio of 1:3.5 was prepared. The solvent was gradually removed *in vacuo* before casting the blend into an open poly(tetrafluorethylene) (PTFE) mould with three 37.6 × 13.8 × 3mm cavities. The highly viscous liquid was kept at ambient temperature for 24h after it was transferred to the cavities. The mould was then placed inside an oven for 2h at 80°C, followed by 24h at 50°C to yield an elastomer (**Figure 6**). The material exhibited an average Shore OO hardness of 74 ± 1.6. As phase separation was not observed, the POSS units within siloxane chains were homogeneously dispersed.

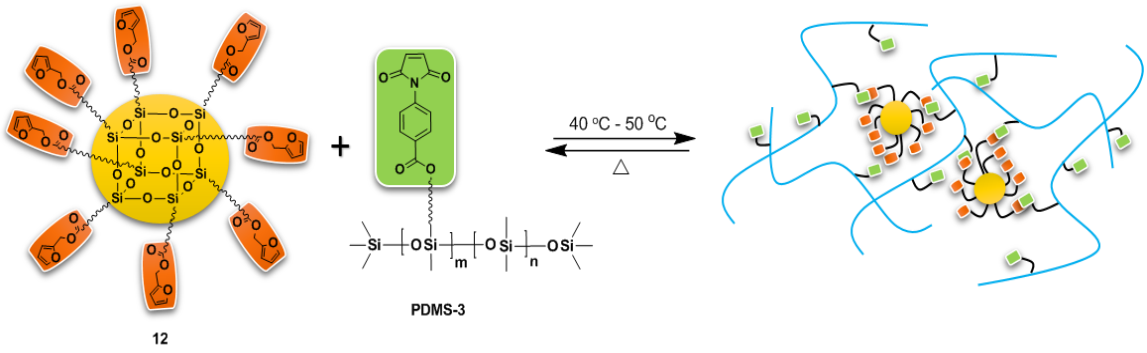

Figure 6. A graphical structure of the elastic network obtained from 12 and PDMS-3.[247]

Based on the model studies, 110˚C and 50˚C were selected as the optimal temperatures for the retro-Diels-Alder and Diels-Alder reactions in the self-healing process. To assess the self-healing capacity of the network, a specimen was cut completely in half and returned to the mould. Heating the cut elastomer for 2h at 110˚C prior to 5h at 50˚C was sufficient to fully rebind the cut pieces (**Figure 7**). At elevated temperatures, such as 110˚C, the specimen's surfaces became sticky as a result of retro-Diels-Alder reactions. The excess quantity of the diene in the system not only avoided deforming the specimen by supressing the retro-Diels-Alder reaction but also helped to efficiently heal the damaged surfaces at 50˚C. Retention of the overall integrity of the network at 110˚C can also be attributed to the rigidity of the furan-modified POS units and the reactivity of its flexible arms. The healed areas were assessed using scanning electron microscopy (SEM) (**Figure 7**). Although the cutline was faintly visible after healing, the healed surface exhibited almost a complete recovery. However, there were a number of spots that could not reconnect at the surface due to material loss during the cutting process. Variable temperature solid-state ^{1}H NMR analysis of the cross-linked PDMS elastomer provided a further evidence of the thermo-reversibility of cross-links at the molecular level. Although the peaks were heavily overlapped (**Figure 8**, **i, ii, iii, iv insets**), it was possible to observe reversible alterations in their locations as a result of the equilibrium exist among the functional groups. Retro-Diels-Alder and Diels-Alder reactions were detected by increasing the spectrometer temperature to 106˚C prior to decreasing it to

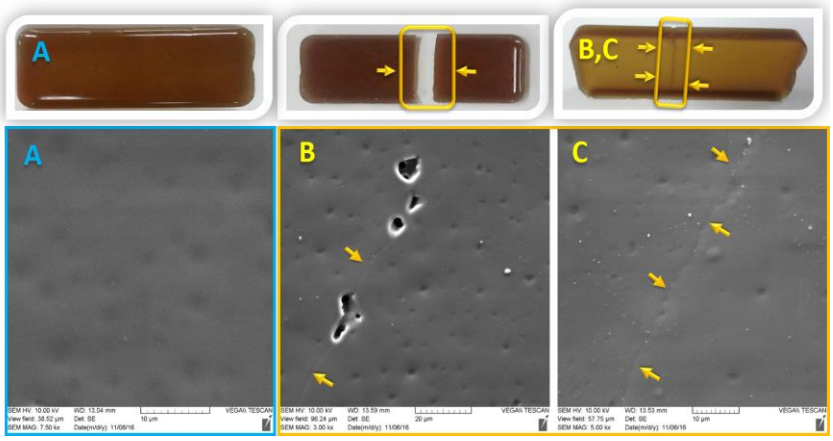

Figure 7. Illustration of the self-healing capacity of the siloxane network. A is the original, undamaged elastomer. B and C are the surface SEM images of the healed area. The arrows indicate the residual scar after healing. Due to the material loss upon the damage, some surface areas could not heal perfectly (SEM image B).[247]

ambient temperature (**Figure 8**). The spectra showed that the material recovered its initial state once the temperature reached 23˚C. The coupling and decoupling reactions within the silicone elastomer were found to occur at same relative rates as observed in the model systems.

To illustrate the material's recyclability and minimize the time needed for the self-healing process, a fully cut specimen was heated to 200˚C. The gap between the cut pieces was completely closed as the material subsequently became fluid when the surface temperature crossed 187˚C after 5 minutes. The heater was turned off after the gap closure and the healed specimen was allowed to cool. After an hour from the beginning of the process, the specimen was released from the mould. The material's hardness, Shore OO, experienced a ten-unit drop. Although 110˚C was sufficient for the process of healing, 187˚C was the temperature that the material not only could profoundly decouple the cross-links but also could overcome the molecular interactions to behave as a viscous fluid (see **the published video online**◉).§

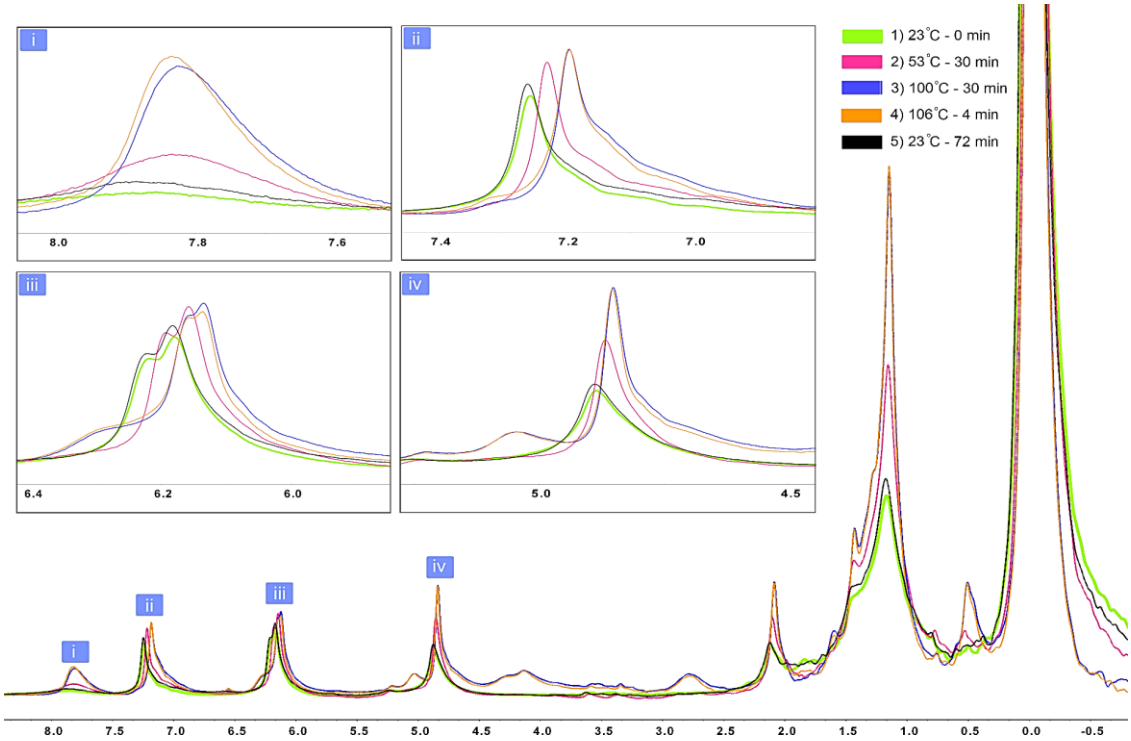

Figure 8. Variable temperature solid-state ^{1}H NMR analysis of the cross-linked silicone elastomer. The minutes indicate the amount of time passed from the previous depicted acquisition. i, ii, iii, and iv insets are the enlarged areas specified in the main spectrum.[247]

◉ *Please find the video here : http://www.rsc.org/suppdata/c7/py/c7py00215g/c7py00215g2.mp4*

4.5 Flexibility Impacts on Physical and Mechanical Properties

To study how the flexibility of the polymer chains affects the physical and mechanical properties and of the RDA reaction, **PDMS-T1** and **–T2** were prepared from **PDMS-3**. While **network-1** was obtained without the PDMS chains end-capped with maleimidocarboxyphenyl terminal groups, 12% w/w of **PDMS-T1** and **–T2** were included in **network-2** and **-3**, respectively (**Figure 9**). All networks were prepared by casting the mixtures into a silicone mould having three cavities with the dimensions of 76 × 25.4 × 2.2mm. Subsequently, the mould was exposed to ambient temperature (~30˚C) for about 17h prior to being placed in an oven for 24h at 50-60˚C. The molar ratio of maleimide: furan was kept 1:3.5 for all networks. Similarly, shapeless samples of the networks were prepared in 4mL vials for the DSC and thermogravimetric analysis (TGA) measurements. To study the self-healing process at 110˚C, rectangular specimens were cut into halves and placed into the mould and returned to the oven. The specimens experienced ~10h of 110˚C before the temperature was set to 50˚C-60˚C for approximately 20h. Due to the lack of a sufficient thermal conductivity within the silicone mould, the same process was followed for the other surfaces of the specimens previously exposed to the air. Consequently, the specimens were healed to the point where the cut-lines were almost hardly recognizable (**Figure 10**). In terms of hardness, **network-1**, **network-2**, and **network-3** exhibited average Shore OO values of 80.4±0.5, 80.7±4, and 78.2±3, respectively. The hardness values were higher in case

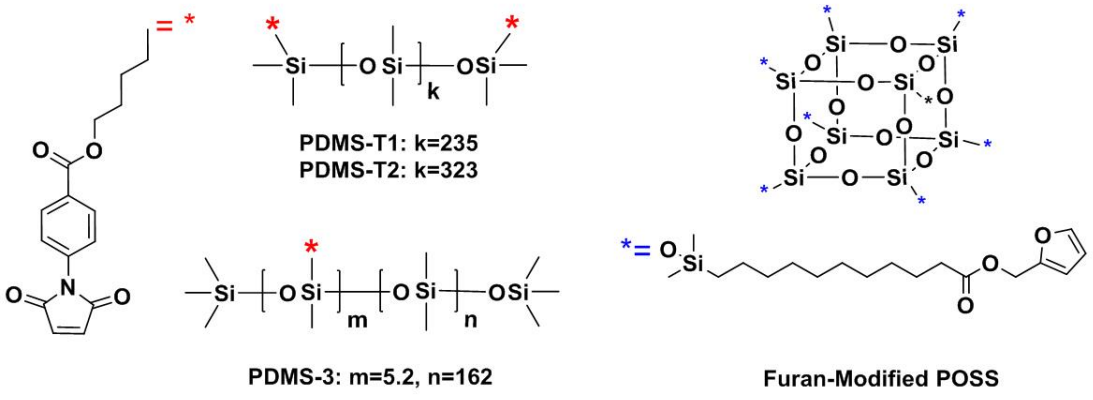

Figure 9. The macromolecules used to assess the flexibility and bimodality impacts on physical & mechanical properties.

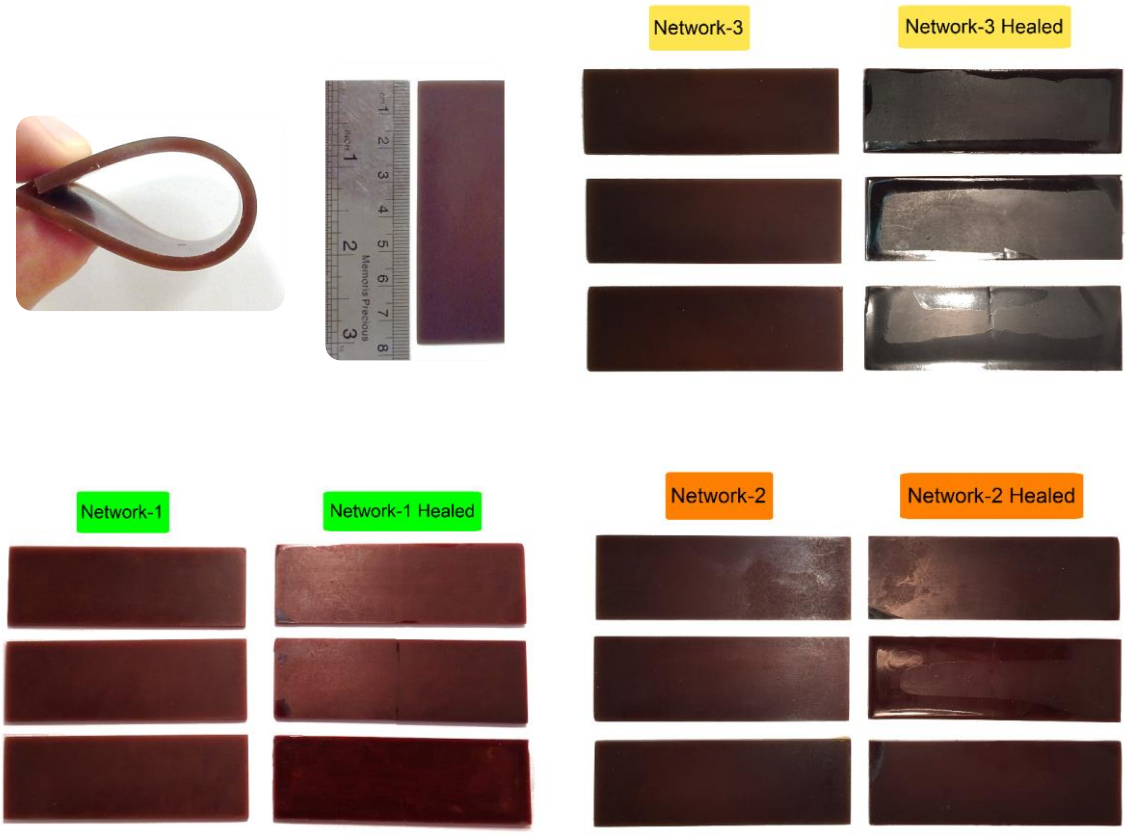

Figure 10. The images of the network prepared by casting method for the Tensile and DMA tests. The healed specimens became darker in comparison with the original ones.

of the healed specimens; 85.7±2, 83.8±5, and 84.6±3 for **network-1**, **network-2**, and **network-3**, accordingly. Such increases indicated the materials possessed higher cross-linking densities after the self-healing process.

4.5.1 DSC & TGA Measurements

The prepared shapeless networks were subjected to three cycles where the samples were heated from the ambient temperature (~25˚C) to 150˚C via DSC machine. The isothermal intervals were 2 and 5 min at 150˚C and -20˚C, respectively. A rate of 10˚C/min was used as the cooling or heating rate. Eventually, another cycle was performed to designate the glass transition region by cooling the sample to -130˚C from ~25˚C before returning to 20˚C with the rate of ±10˚C/min. The data reported in **Table 2** comprise the average results of four separate measurements. Comparing the glass transition regions, **network-1** and **-2** had roughly the same values whereas the addition of 12% w/w **PDMS-T2** lowered the region by approximately 4˚C for **network-3** (**Table 2**). Moreover, the addition of flexible backbones

#Network Furan: Maleimide Molar Ratio Used: [3.5:1]	Ave. Glass Transition (Onset \ End)	Cycloreversion $\overline{\triangle H}$ (J/g) for 4 Cycles
#1: (PDMS-3) + Furan-Modified POSS	- 64 ˚C \ -52.7 ˚C	4.22
#2: (PDMS-3 + 12wt% PDMS-T1) + Furan-Modified POSS	- 64.2 ˚C \ -52.6 ˚C	5.51
#3: (PDMS-3 + 12wt% PDMS-T2) + Furan-Modified POSS	- 68 ˚C \ -56.2 ˚C	5.48

Table2. The DSC measurements results regarding T_gs and cycloreversion enthalpies of the shapeless networks. The cycloreversion peaks occurs approximately at 140˚C.

resulted in increasing the $\overline{\triangle H}$ of the RDA reaction occurred at ~140˚C. Therefore, promoting flexibility in the polymer chains facilitated the [4+2] cycloreversion reaction.

Thermogravimetric analysis (TGA) of the samples indicated that the thermal stabilities are in the order of **network-3**, **-2**, and **-1** (**Figure 11**). Such behavior can be attributed to an increased tendency for the RDA reaction due to having **PDMS-T1** and **–T2** within **network-2** and **-3**. In fact, RDA reaction retards the onset of destructive decomposition behavior by consuming the thermal energy injected via TGA machine into the polymeric system. Therefore, a higher thermal stability can be achieved by increasing RDA reaction tendency through more flexible backbones.

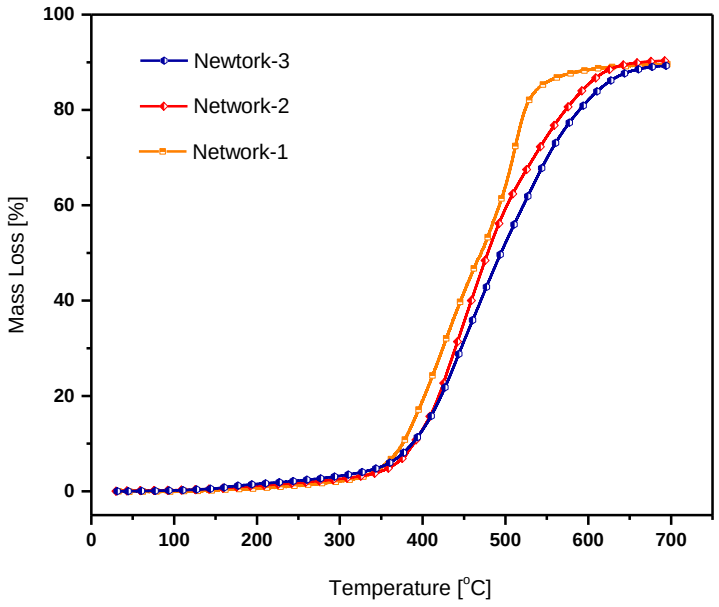

Figure 11. Thermogravimetric analysis of the prepared networks. The heating rate was set to 10˚C/min.

4.5.2 Dynamic Mechanical Analysis & Tensile Tests

The instrument used for the tensile strength was a Instron 5943 with a load cell of 1kN. The analysis rate was set to 5mm/min. A PerkinElmer DMA8000 on single cantilever mode also used for the dynamic mechanical analysis (DMA). The temperature was set to range from -50°C to 110°C. Samples for the tensile and DMA experiments were cut from the original cast specimens. The prepared specimens had relatively smooth edges with the dimensions of 50 × 12.5 × 2mm and 25 × 10 × 2mm for the tensile and DMA specimens, respectively. The tensile tests of the healed specimens showed an unexpected result. In the tensile tests of healed materials the ruptured areas was most often at a place other than the healed part of the specimens, indicating high recoveries were achieved at the damaged zone. Also, the impact of bimodality of siloxane chains was only observable in the healed specimens of **network-2**. The DMA and tensile measurements are depicted in the following pages (**Figure 13-18**).** The tensile modulus and yield strengths were calculated by using the data below 5% elongation. Comparing to the Larson equation††, the measured elastic modulus was quite higher than the estimated ones for the prepared networks:

$$\boldsymbol{Elastic\ Modulus = A\ exp(B \times Shore\ OO), A = 0.0037, B = 0.0718}$$

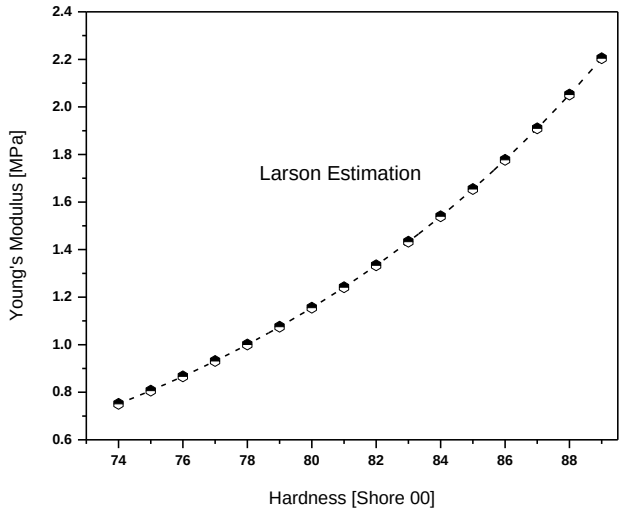

Figure 12. The estimated E values calculated for Shore OO in the range of 74 - 89 using the Larson equation.

** *The results were obtained through collaborating with a group at the University of Alberta. Dan Li, an undergraduate student at the department of material and chemical engineering, under the supervision of Dr. Anastasia Elias, was responsible for running the tests whose data are presented in this section. This section is a part of an ongoing project.*

†† *K. Larson, Can You Estimate Modulus From Durometer Hardness for Silicones?, Dow Corning internal publication, 2016. Form No. 11-3716-01.*

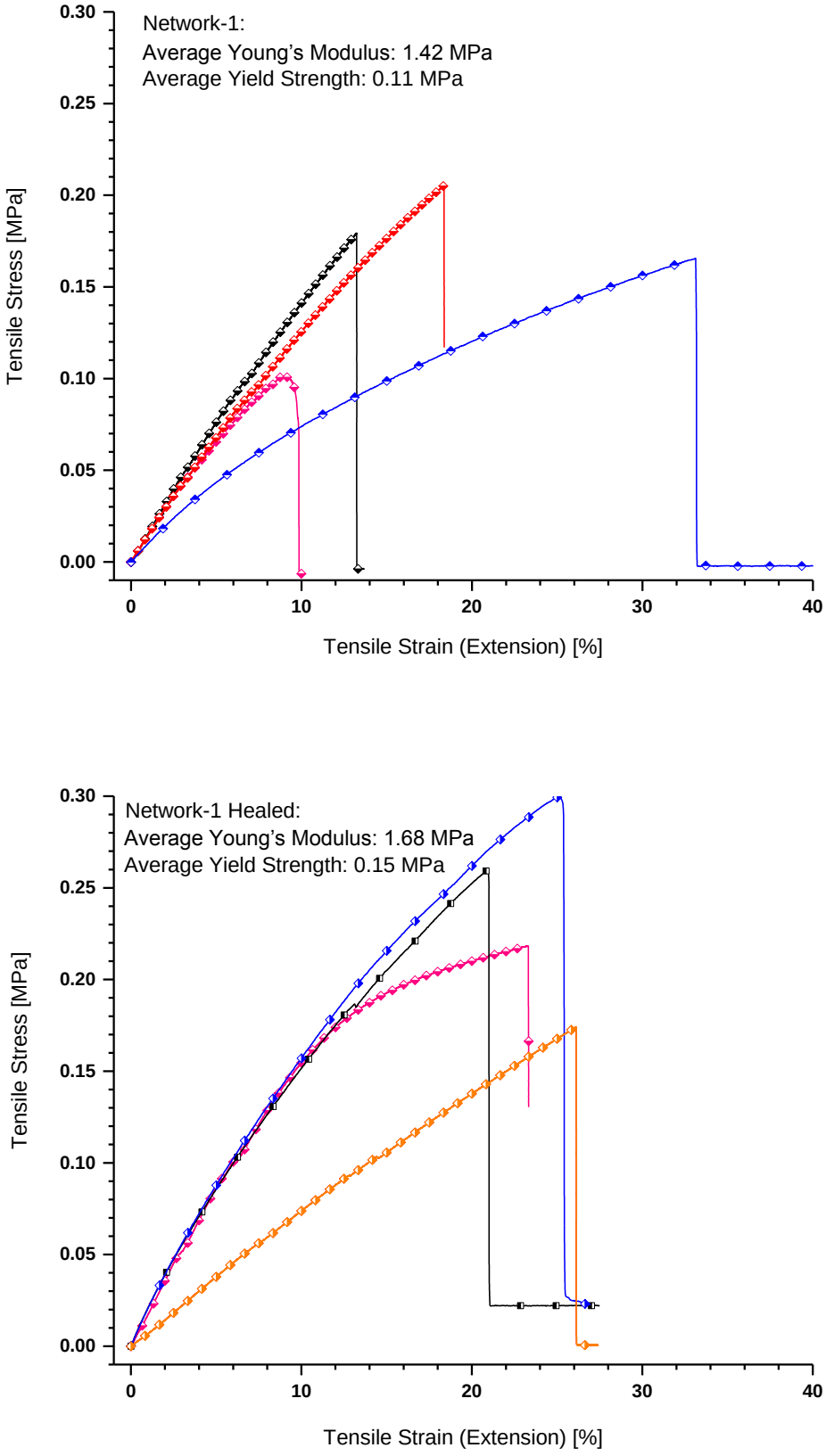

Figure 13. The tensile (Young's modulus) tests results for network-1 and its healed specimens.

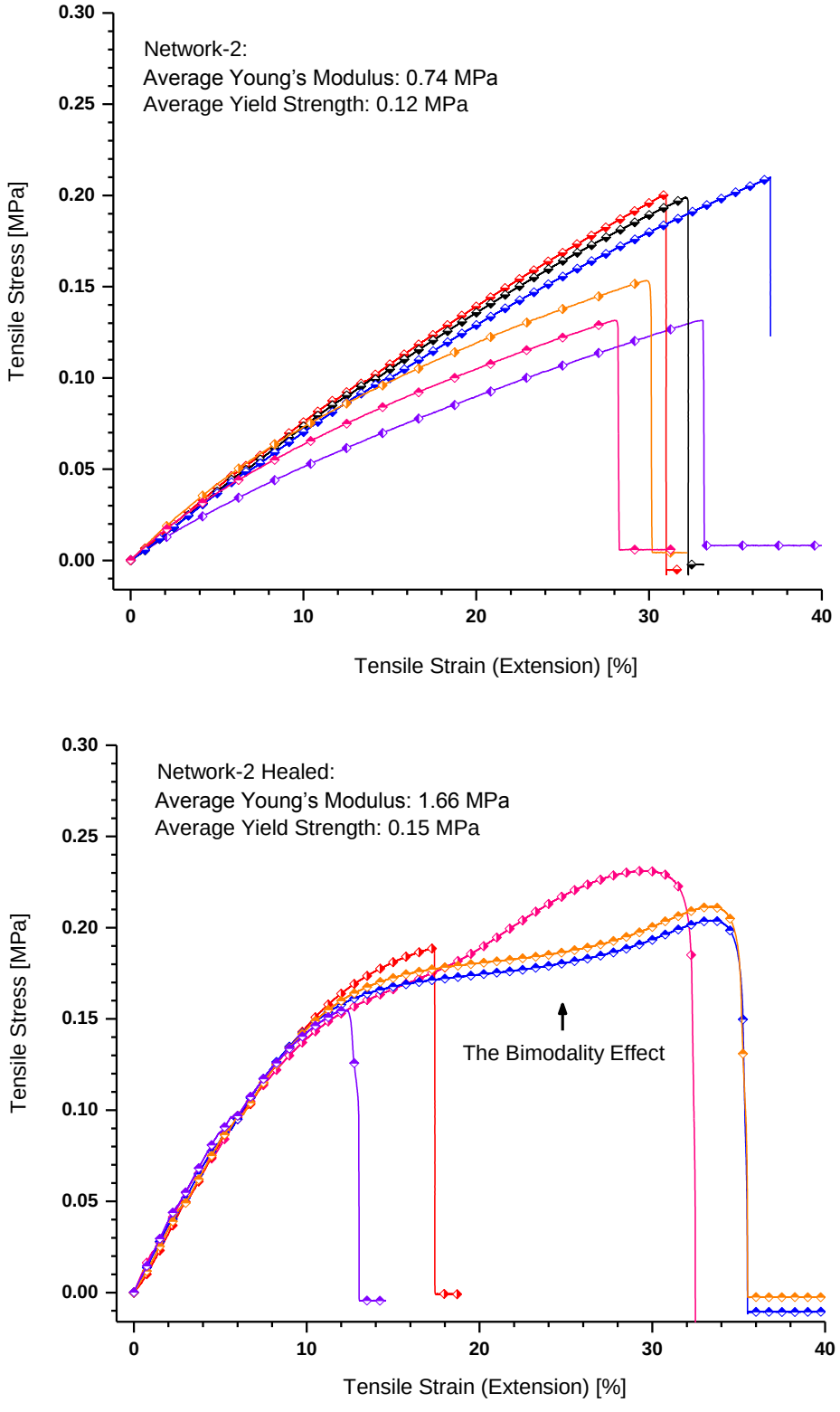

Figure 14. The tensile tests (Young's modulus) results for network-2 and its healed specimens.

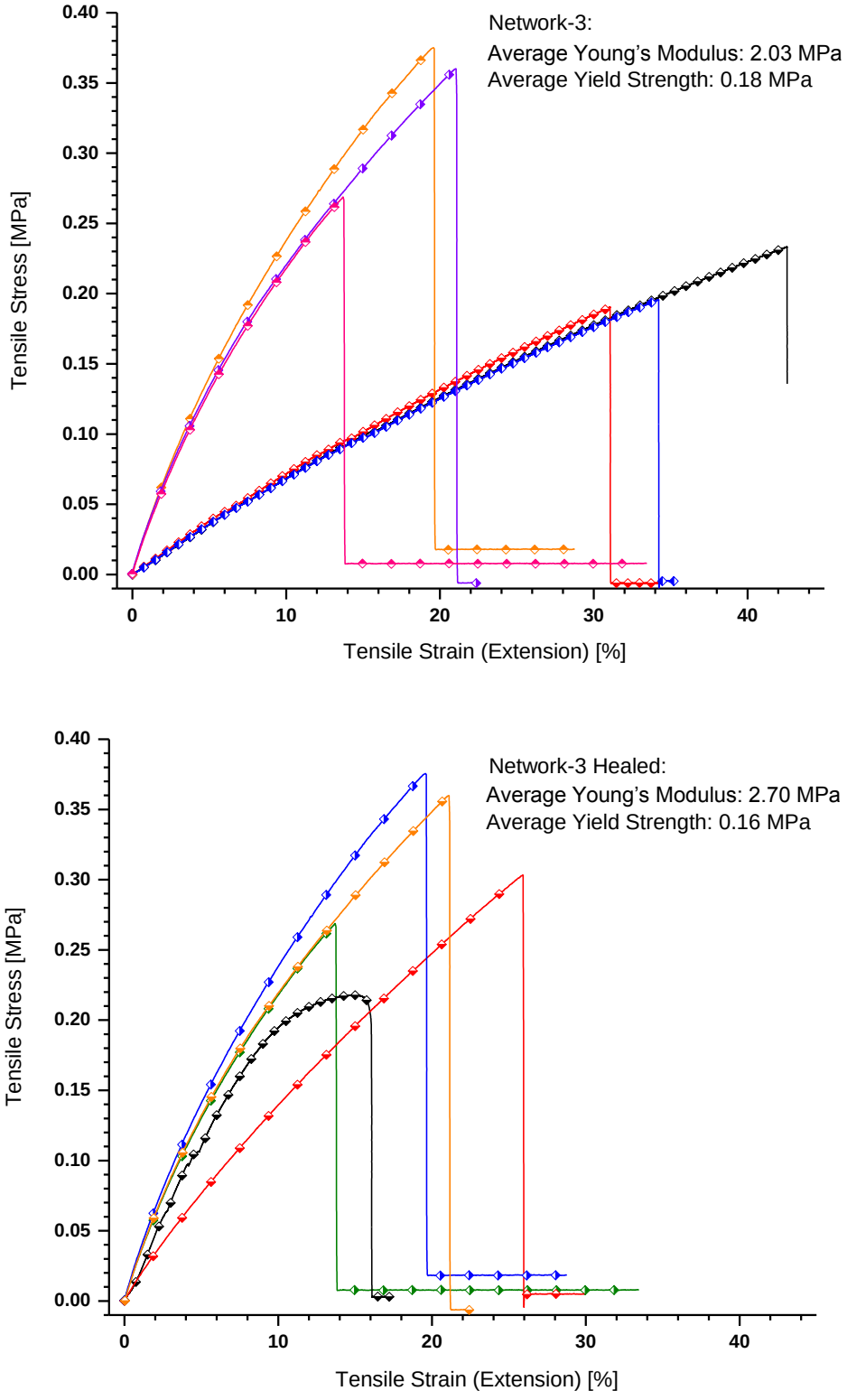

Figure 15. The tensile (Young's modulus) tests results for network-3 and its healed specimens.

As it was previously discussed in chapter 1 through bimodality effect, **network-2** and **network-3** were expected to exhibit higher tensile strains as a result of having the flexible terminal polysiloxanes (i.e., **PDMS-T1** and **PDMS-T2**).

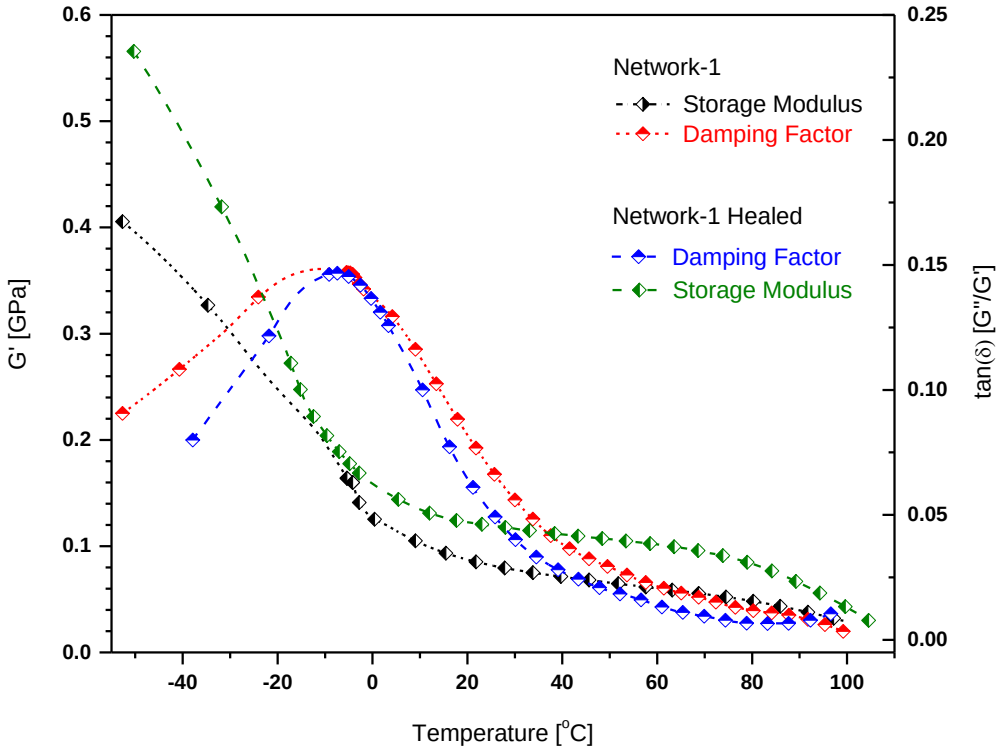

Figure 16. The DMA results for network-1 and its healed specimens.

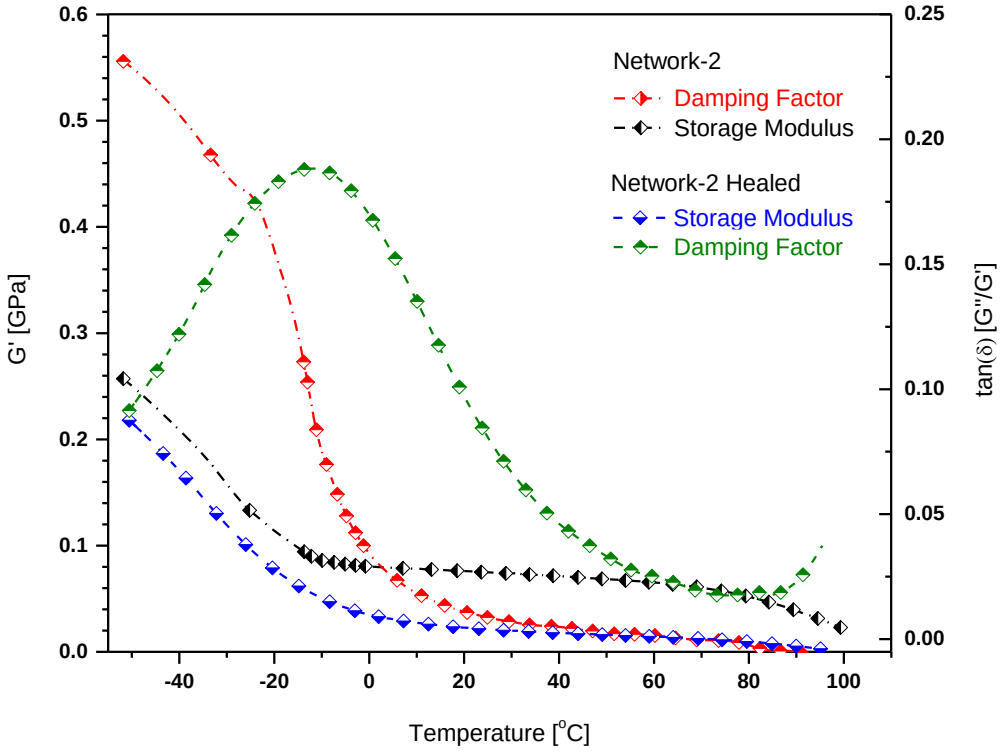

Figure 171. The DMA results for network-2 and its healed specimens.

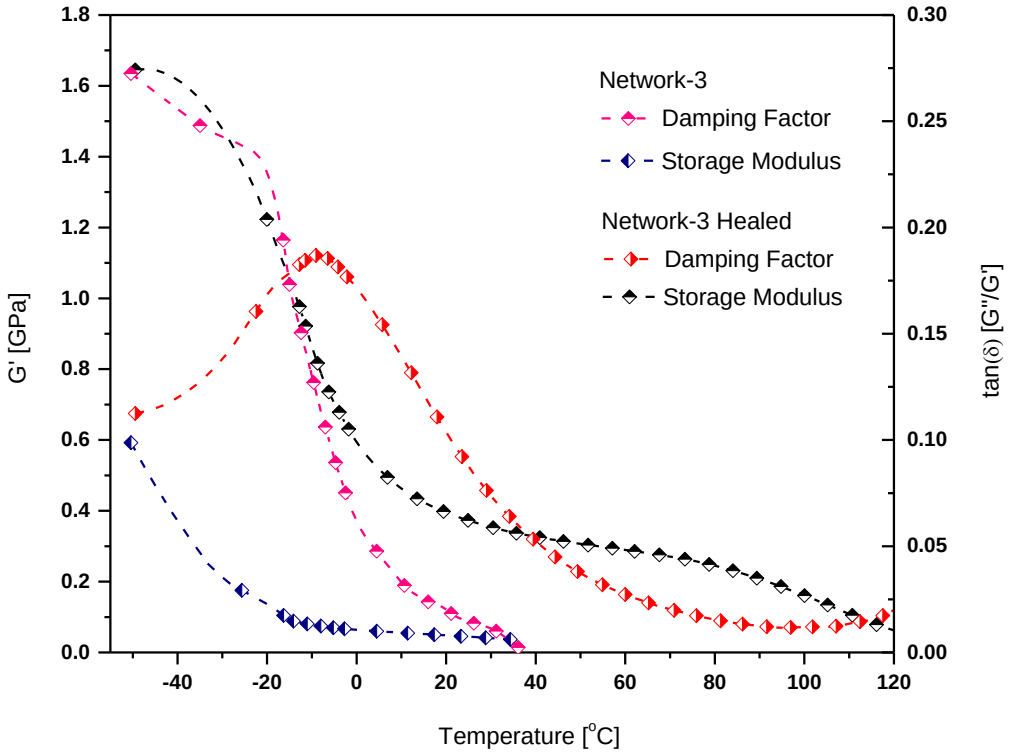

Figure 18. The DMA results for network-3 and its healed specimens.

4.6 Conclusion

The capacity of the Diels-Alder silicon-based linkage to be used for the intrinsic self-healing materials was illustrated through various thermal studies, including ^{1}H NMR analysis and DSC measurements. The author grafted siloxane chains with a pendant maleimidocarboxyphenyl attached to a five-carbon spacer to avoid the rigidity of the bismaleimide while gaining its high reactivity towards the diene. The electronics of the diene and dienophile, along with the flexibility and mobility factors in structural design allowed to obtain an elastic network exhibiting excellent temperature-controlled self-healing characteristics. SEM confirmed the complete reconnection of the two cut pieces in the absence of any solvent. The rigid POSS units and the ratio of maleimide:furan resulted in a material that retained its structural integrity at elevated temperatures without hindering the self-healing process. SEM imaging of the elastomeric samples, as well as solid-state ^{1}H NMR experiments, demonstrated the reversible nature of the DA reaction on macroscopic and microscopic scales, respectively. In addition, the author successfully prepared a recyclable

Healing Mechanism	*Self-healing Condition*	*Healing Efficiency*	*Ref.*
Cyclopentadiene Diels–Alder	*120°C, 12h*	*60%*	270
Maleimide/furan Diels–Alder with CrO_2	*110°C, 12h*	*100%*	271
Radical fission/recombination Alkoxyamines	*130°C, 2.5h*	*75%*	272
Maleimide/furan Diels–Alder Epoxy resin	*120°C, 20min & 80°C, 72h*	*96%*	273
Maleimide/furan Diels–Alder	*120–150°C, 24h*	*57%*	274
Maleimide/furan Diels–Alder Coatings	*175°C, 1h*	*100%*	275
Maleimide/furan Diels–Alder Polyketone	*120–150°C (5 min–1h)*	*100%*	276,277
Maleimide/furan Diels–Alder Polystyrene	*150°C (2,5 min)*	*80%*	266
Maleimide/furan Diels–Alder Polyethylene	*60–140°C (20 min–5d)*	*100%*	179,278,279
Maleimide/furan Diels–Alder Polyamides	*100–150°C (10 min–2h)*	*Not mentioned*	280,281
Maleimide/furan Diels–Alder Poly(methylmethacrylate)	*100–150°C (4h)*	*80–100%*	275,282,283
Anthracene-maleimide Diels–Alder	*100–200°C (1–3d)*	*50%*	283,284
Maleimide/furan Diels–Alder Epoxy	*90–120°C (1–3d)*	*37–100%*	285–289
Anionic Siloxanes	*90°C (24h)*	*100%*	186
Cyclopentadiene Diels–Alder	*120°C (20h)*	*63%*	235
Photochemical [2+2] cycloaddition Chitosan-Polyurethane	*hν (280–400nm) (15–30min)*	*100%*	290,291
Photochemical [4+4] cycloaddition	*hν(>360 nm) (15min)*	*Not mentioned*	190
Maleimide/furan Diels–Alder Polysiloxane	*110°C, 2hr & 50°C, 5hr*	*100%*	*This Work*[247]

Table 3. Comparison of the current project with previously reported dynamic covalent systems.

elastomeric material exhibiting excellent temperature-controlled self-healing characteristics. **Table 3** provides a simple comparison between the current work with the previously reported self-healing polymers based on the dynamic covalent bonds. In the table, the type of the damage can be a scratch or even a complete cut while the self-healing efficiency is often defined as a ratio of the healed specimen's Young's or storage modulus over the original (i.e., virgin) one.

4.7 Future Work

The goal of the research presented in this thesis was the investigation of a means of extending the lifetime of polymeric silicone materials through a process known as self-healing. A model system was designed to study the thermally reversible nature of Diels-Alder adduct cross-linked siloxane compounds utilizing NMR spectroscopy and differential scanning calorimetry. The knowledge gained from the model systems was applied to the synthesis of silicone-based elastomers cross-linked by a furan-modified polyhedral oligomeric silsesquioxane utilizing the Diels-Alder reaction and evaluating their self-healing capacity. Additionally, the research assessed the capacity of silicone-based elastomers to heal even after seemingly catastrophic damage. These healed materials were studied regarding their physicomechanical properties and compared with virgin silicone elastomers that were not damaged. Although the thesis attempted to investigate the prepared networks thoroughly, still there are plenty of new grounds to discover. Investigating the macromolecules properties before the cross-linking reaction (i.e., knowledge of the molecular distribution, $\overline{Mn}$, and $\overline{Mw}$ before & after each step in functionalizing the macromolecules) provide a better understanding of the materials self-healing and recyclability behaviors. Usage of different quantities of flexible macromolecules to obtain the optimized values, which are necessary for the emergence of the bimodality effect in the tensile test, is crucial to improving the materials physical and mechanical properties. Additionally, comparisons of self-healing efficiency and recyclability must be considered from studying higher molecular weight polysiloxane chains (>320 repeating units) and oligosiloxane (<30 repeating units). Since time and temperature are the two important factors in a self-healing process, their optimized values must be found to minimize the required time while accessing to a complete repair. To develop the materials, the remote self-healing concept might be a precious strategy to localize heat in the damaged area via embedding superparamagnetic nanoparticles triggered by remote sources of energy (i.e., electric or magnetic fields).

Chapter 5 *Experimental*[‡‡]

The chapter reports the in-detail information regarding the raw materials used in the experiments and the synthetic procedures used to obtain model systems as well as the polymeric compounds.[§§]

5.1 Materials

Celite®545, tetrahydrofuran (THF), toluene, pentane, diethyl ether, aluminium oxide (type WN-6, neutral), molecular sieves (4Å beads, 8-12 mesh), pyridine, 10-decenoic acid, furfuryl alcohol, 4-aminobenzoic acid, acetic anhydride, sodium acetate, Pt(0)-1,3-divinyl-1,1,3,3-tetramethyldisiloxane complex (Karstedt's catalyst, Pt(dvs)) in xylenes, lipase B from *C. antarctica* immobilized on Lewatit VPOC1600 cross-linked divinylbenzene resin (Novozym-435, N435), trimethylsilyl terminated-poly(dimethylsiloxane-co-methylhydrosiloxane) (3-4% methylhydrosiloxane) with an average $\overline{Mn}$ of 13,000 g/mol (**PDMS-1**), **PDMS-TS1**, and **PDMS-TS2** were obtained from Sigma–Aldrich (Oakville, Ontario, Canada). Maleic anhydride, 4-penten-1-ol, and thionyl chloride were obtained from Alfa-Aesar (Ward Hill, NJ, USA). Heptamethyltrisiloxane and octakis(dimethylsiloxy)-T8-silsesquioxane were obtained from Gelest (Morristown, PA, USA). All compounds and solvents were used as received unless otherwise noted.

5.2 Synthesis of Model Compounds

Activated carbon was kept at 120°C four days before being used. All reactions were performed under a nitrogen atmosphere. THF and pyridine were kept over molecular sieves at least seven days prior to usage.

---

‡‡ *The chapter is mainly based on* ***Nasresfahani, A.*** *& Zelisko, P. M. Synthesis of a self-healing siloxane-based elastomer cross-linked via a furan-modified polyhedral oligomeric silsesquioxane: investigation of a thermally reversible silicon-based cross-link. Polym. Chem. (2017), 8, 2942-2952.*

§§ *Please find the related characterizations in the next chapter Selected Spectra & Graphs*

5.2.1 Synthesis of The Dienophile

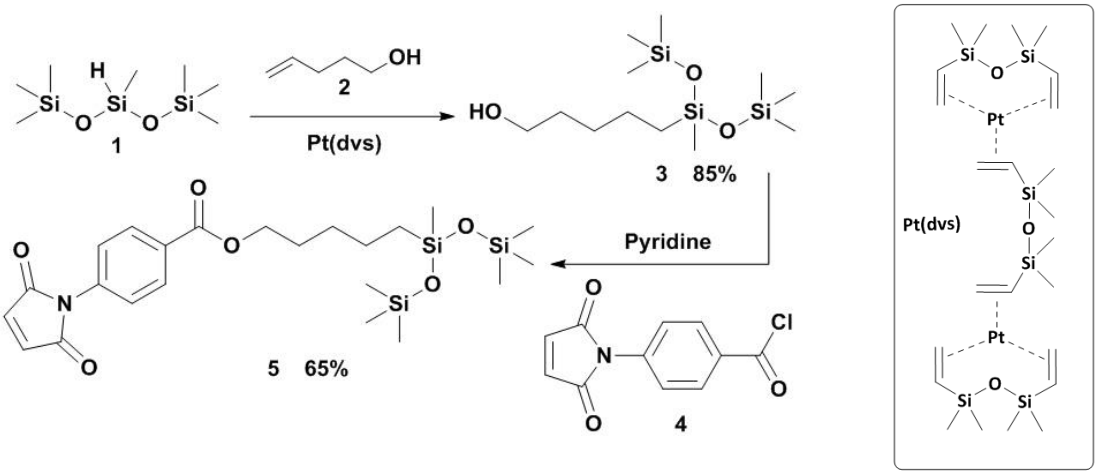

Scheme 1. Synthesis of the dienophile.[247]

Synthesis of 5-(1,1,1,3,5,5,5-heptamethyltrisiloxan-3-yl) pentan-1-ol (3)

To a solution of 4-penten-1-ol (**2**) (0.91 g, 11 mmol) in pentane (14 mL) 1,1,1,3,5,5,5-heptamethyltrisiloxane (**1**) (2.34 g, 10.6 mmol) was added followed by the addition of Karstedt's catalyst (20 µL). The resulting solution was allowed to reflux for 4 h. Activated charcoal was added to the reaction and the system stirred for 4 h at ambient temperature before being filtered through a pad of Celite® using a medium porosity fritted Büchner funnel. Toluene and any residual starting materials were removed *in vacuo* to afford **3** exclusively (2.8 g, 9.0 mmol, 85%) as a colourless liquid.

^{1}H NMR (400 MHz, $CDCl_3$) δ = 3.63 (t, 3J=6.7 Hz, 2H), 1.56 (b, 2H), 1.48 (b, 1H), 1.35 (b, 4H), 0.46 (b, 2H), 0.08 (b, 18H), -0.01 (b, 3H).^{13}C NMR (101 MHz, $CDCl_3$) δ = 63.02, 32.53, 29.23, 22.92, 17.60, 1.85, -0.29.^{29}Si NMR (80 MHz, $CDCl_3$) δ =6.94, -21.50. IR: ν = 3330 cm^{-1} (OH). High-Res. MS-EI(+ve): 307.1569 amu. Elemental Analysis (%): Calculated: C:46.70, H:10.45, Found: C:46.41, H:10.33.

Synthesis of N-[4-(chlorocarbonyl) phenyl] maleimide (4)

The compound was synthesized as previously described.[292,293]

^{1}H NMR (400 MHz, $CDCl_3$) δ = 8.23-8.21 (b,2H), 7.66-7.64 (b,2H), 6.92 (b, 2H).^{13}C NMR (101 MHz, $CDCl_3$) δ = 168.59, 167.55, 137.69, 134.61, 132.25, 131.71, 125.15 ppm. High-Res. MS-EI (+ve): 235.0027 amu.

Synthesis of 5-(1,1,1,3,5,5,5-heptamethyltrisiloxan-3-yl) pentyl 4-(2,5-dioxo-2,5-dihydro-1H-pyrrol-1-yl) benzoate (5)

A solution of **3** (0.31 g, 1.0 mmol) in 5 mL of dried THF was cooled in an ice bath. Pyridine (0.16 g, 2.0 mmol) was added to the reaction flask and stirred for 10 min. Subsequently, a solution of **4** (0.47 g, 2.0 mmol) in dried THF (5 mL) was injected in a drop-wise manner into the reaction flask. After 15 h, the crude reaction mixture was diluted with 10 mL THF. The pyridinium salt was filtered through a pad of Celite® using a medium porosity fritted Büchner funnel. After evaporation of the THF in vacuo, the crude mixture was dissolved in 20 mL of pentane to precipitate the excess amount of **4**. The suspension was cooled and filtered three times before the pentane was removed in vacuo. After dissolving the resulting viscous liquid in 10 mL toluene, volatiles (including unreacted pyridine) were removed in vacuo to give **5** (0.33 g, 0.65 mmol, 65%) as a brown viscous liquid.

^{1}H NMR (400 MHz, $CDCl_3$) δ = 8.15-8.13 (b, 2H), 7.50-7.48 (b, 2H), 6.89 (b, 2H), 4.33 (t, 3J = 6.6 Hz, 2H), 1.77 (b, 2H), 1.43 (b, 4H), 0.49 (b, 2H), 0.09 (b, 18H), 0.01 (b, 3H).^{13}C NMR (101 MHz, $CDCl_3$) δ =168.94, 165.74, 135.34, 134.36, 130.37, 129.48, 125.18, 65.31, 29.49, 28.48, 22.84, 17.53, 1.87, -0.26.^{29}Si NMR (80 MHz, $CDCl_3$) δ = 6.97, -21.66. High-Res. MS-EI (+ve): 507.1930 amu. Elemental Analysis (%): Calculated: C:54.40, H:7.34, Found: C:54.19, H:7.47.

5.2.2 Synthesis of The Diene

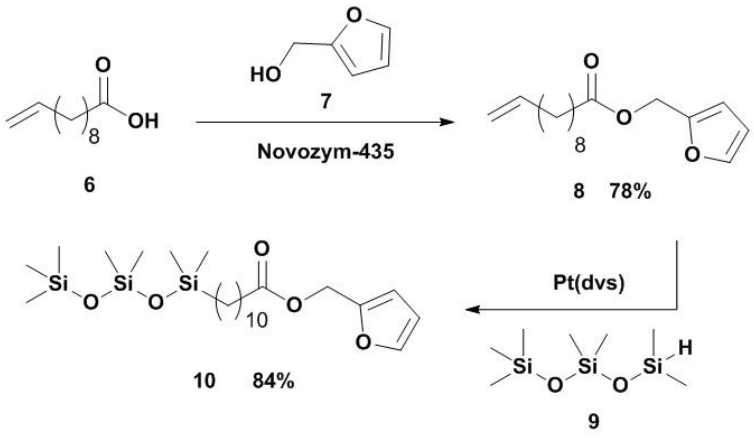

Scheme 2. Synthesis of the diene.

Synthesis of furan-2-ylmethyl undec-10-enoate (8)

10-Undecenoic acid (**6**) (24 g, 0.13 mol) was dissolved in toluene (160 mL) before the addition of furfuryl alcohol (**7**) (26 g, 0.26 mol). The enzymatic catalyst N435 (4% w/w, 0.90 g), as well as molecular sieves (2 g), were subsequently added to the reaction flask. After equipping the reaction flask with a Dean-Stark apparatus, the reaction mixture was heated to 85°C to stir for 48 h. The crude reaction mixture was filtered through a pad of Celite® using a medium porosity fritted Büchner funnel before removal of the solvent using a rotary evaporator. The resulting yellow liquid was dissolved in 50 mL of diethyl ether and washed with 80 mL of distilled water, 40 mL of a saturated solution of $NaHCO_3$, and 30 mL of brine (x3). Combined organic layers were dried over anhydrous Na_2SO_4 to yield **8** (27 g, 0.10 mol, 78%) as a yellow liquid.

^{1}H NMR (300 MHz, $CDCl_3$) $\delta = 7.42$ (b, 1H), 6.40-6.36 (b, 2H), 5.87-5.74 (b, 1H), 5.06 (s, 2H), 5.01-4.91 (b, 2H), 2.32 (t, J=7.5 Hz ,2H), 2.04 (b, 2H), 1.62 (b, 2H), 1.38-1.27 (b, 10H).^{13}C NMR (75 MHz, $CDCl_3$) $\delta = 173.46, 149.67, 143.18, 139.18, 114.14, 110.53, 110.46, 57.86, 34.14, 33.78, 29.25, 29.04, 28.89, 24.86$. High Res. MS-EI (+ve): 264.17 amu. Elemental Analysis (%): Calculated: C:72.69, H:9.15, Found: C:72.80, H:9.25.

Synthesis of furanyl-2-methyl 11-(1,1,3,3,5,5,5-heptamethyltrisiloxanyl) undecanoate (10)

To a solution of **8** (0.88 g, 3.3 mmol) in toluene (3 mL), Karstedt's catalyst (8 µL) was added and stirred for 10 min. Subsequently, 1,1,3,3,5,5,5-heptamethyltrisiloxane (**9**) (0.83 g, 3.7 mmol) was introduced to the flask, and the reaction mixture was allowed to reflux for 8 h. Activated charcoal was added to the reaction vessel and the contents were stirred for 2 h at ambient temperature before filtering the suspension through a pad of Celite® using a medium porosity fritted Büchner funnel. Toluene and residual starting material were removed in vacuo to afford **10** (1.36 g, 2.78 mmol, 84%) as a light yellow liquid.

^{1}H NMR (300 MHz, $CDCl_3$) $\delta =$ 7.42 (b, 1H), 6.40-6.35 (b, 2H), 5.06 (s, 2H), 2.33 (t, J=7 Hz, 2H), 1.62 (b, 2H), 1.26 (b, 14H), 0.52 (b, 2H), 0.08-0.02 (b, 21H).^{13}C NMR (101 MHz, $CDCl_3$) $\delta =$ 173.50, 149.68, 143.19, 110.54, 110.47, 57.86, 34.17, 33.45, 29.53, 29.49, 29.37, 29.25, 29.11, 24.90, 23.23, 18.30, 1.82, 1.29, 0.22. ^{29}Si NMR (60 MHz, $CDCl_3$) δ =7.45,7.01,-21.08. High-Res MS-FAB+ $[C_{23}H_{46}O_5Si_3+Na]^+$: 509.2545 amu. Elemental Analysis (%): Calculated: C:56.74, H:9.52, Found: C:57.01, H:9.52.

5.3 Synthesis of the Elastomers

Synthesis of pentan-1-ol-siloxane-dimethylsiloxane copolymers (PDMS-2)

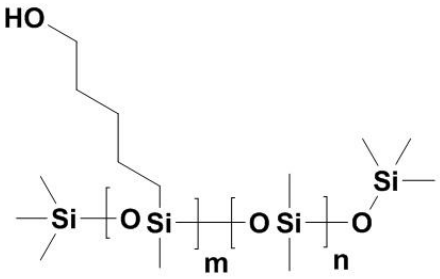

m~5.2, n~162

To a solution of **PDMS-1** (25 g, 10 mmol Si-H) in toluene (80 mL), 4-pentene-1-ol (**2**) (1.67 g, 19.3 mmol) was added. The solution was allowed to stir for 10 min. Karstedt's catalyst (197 µL) was introduced to the flask, and the reaction was stirred at ambient temperature. Completion of the reaction was confirmed by the disappearance of Si-H peak from the ^{1}H NMR spectrum. The crude reaction was diluted with 100 mL of toluene. Activated charcoal was added to the reaction vessel and the mixture was left to stir overnight at ambient temperature. The suspension was filtered three times through a layered pad of filtration agents, including Celite®, silica, and alumina (2 cm each) using a 150 mL medium porosity fritted Büchner funnel. Toluene and the residual starting materials were removed *in vacuo* to obtain **PDMS-2** (18 g, 7.0 mmol OH) as a slightly yellow, clear, viscous liquid.

^{1}H NMR (300 MHz, $CDCl_3$) δ =3.63 (t, J=6.7 Hz, 2H), 1.58 (b, 2.75H), 1.39 (bm, 4H), 0.54 (b, 2H), 0.09 (b, 215H).^{13}C NMR (101 MHz, $CDCl_3$) δ = 63.02, 32.53, 29.23, 22.92, 17.60, 1.85, -0.29. ^{29}Si NMR (60 MHz, $CDCl_3$) δ = 6.94, -21.50. Elemental Analysis (%): Calculated: C:33.50, H:8.27, Found: C:33.03, H:8.29.

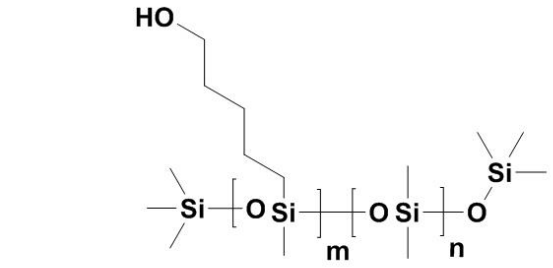

PDMS-2: m~5.2, n~162

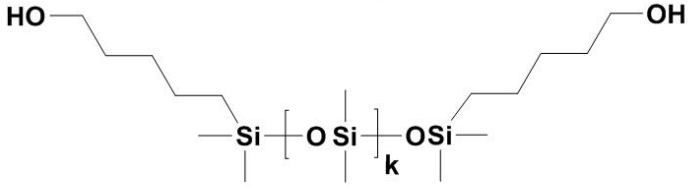

PDMS-TH1: k~ 235

PDMS-TH2: k~ 323

PDMS-B1S and **PDMS-B2S** were the two blends of **PDMS-1** comprising 12% (w/w) **PDMS-TS1** and **PDMS-TS2**, respectively. The PDMS chains with Si-H groups at the terminal positions had average repeat units of 235 and 323. The above procedure was also followed to synthesize **PDMS-B1H** and **PDMS-B2H** from **PDMS-B1S** and **PDMS-B2S**, accordingly.

PDMS-B1H: ^{1}H NMR (300 MHz, $CDCl_3$) δ=3.63 (b, 1.86H), 1.57(b,2.4H), 1.39(b,4H), 0.53(b,2H), 0.09(b,277H). ^{13}C NMR (101 MHz, $CDCl_3$) δ = 63.02, 32.53, 29.23, 22.92, 17.60, 1.85, -0.29. ^{29}Si NMR (60 MHz, $CDCl_3$) δ = 6.94, -21.50.

PDMS-B2H: ^{1}H NMR (300 MHz, $CDCl_3$) δ = 3.63 (b, 1.92H), 1.5(b,2.5H), 1.38(b,4.34H), 0.53(b,2H), 0.09(b,284H). ^{13}C NMR (101 MHz, $CDCl_3$) δ = 63.02, 32.53, 29.23, 22.92, 17.60, 1.85, -0.29. ^{29}Si NMR (60 MHz, $CDCl_3$) δ = 6.94, -21.50.

Synthesis of maleimidocarboxyphenylpentansiloxane - dimethylsiloxane copolymers (PDMS-3)

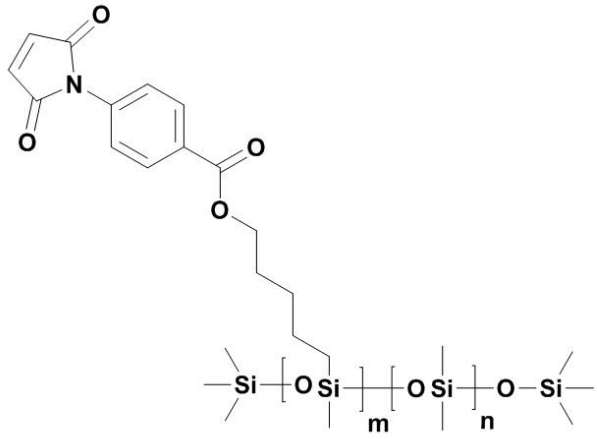

PDMS-3: m~5.2, n~162

To a solution of **PDMS-2** (16.4 g, 6.40 mmol -OH) in 40 mL of dried THF, pyridine (3.1 eq. per mol -OH) was added and the reaction was stirred for 15 min. A solution of **4** (3 eq. per mol -OH) in 160 mL of dried THF was introduced to the reaction media drop-wise. Completion of the reaction was confirmed by ^{1}H NMR when the resonance corresponding to the terminal methylene adjacent to the –OH group at 3.63 ppm was fully shifted to 4.32 ppm. At this point, the crude reaction mixture was diluted with 100 mL of THF. The pyridinium salt was filtered from the reaction mixture using a pad of Celite® in a medium porosity fritted Büchner funnel. Upon evaporating the THF, the crude mixture was dissolved in 200 mL of pentane to precipitate any remaining **4**. The suspension was cooled and filtered three times prior to evaporating the pentane from the filtrate *in vacuo*. After dissolving the resulting brownish viscous liquid in 50 mL toluene, the residual amount of unreacted pyridine was removed along with the toluene *in vacuo* to yield (15.2 g, 1.00 mmol maleimidocarboxyphenyl) **PDMS-3** as a brownish, highly viscous liquid**.**

^{1}H NMR (300 MHz, $CDCl_3$) $\delta =$ 8.15-8.12 (b, 2H), 7.50-7.47 (b, 2H), 6.88 (b, 1.66H), 4.32(b, 2H), 1.78 (b, 2H), 1.45 (b, 4.7H), 0.56 (b, 2H), 0.09 (b,238H).^{13}C NMR (101 MHz, $CDCl_3$) $\delta =$ 168.90, 165.75, 135.29, 134.37, 130.40, 129.55, 125.16, 65.31, 29.58, 28.51, 22.79, 17.41, 1.75,150,0.92,0.52 -0.50.^{29}Si NMR (60 MHz, $CDCl_3$) $\delta =$ 7.21, -21.95. Elemental Analysis (%): Calculated: C:35.89, H:7.80, Found: C:34.89, H:7.90.

The above procedure was also followed to synthesize **PDMS-B1M** and **PDMS-B2M** from **PDMS-B1H** and **PDMS-B2H**, respectively.

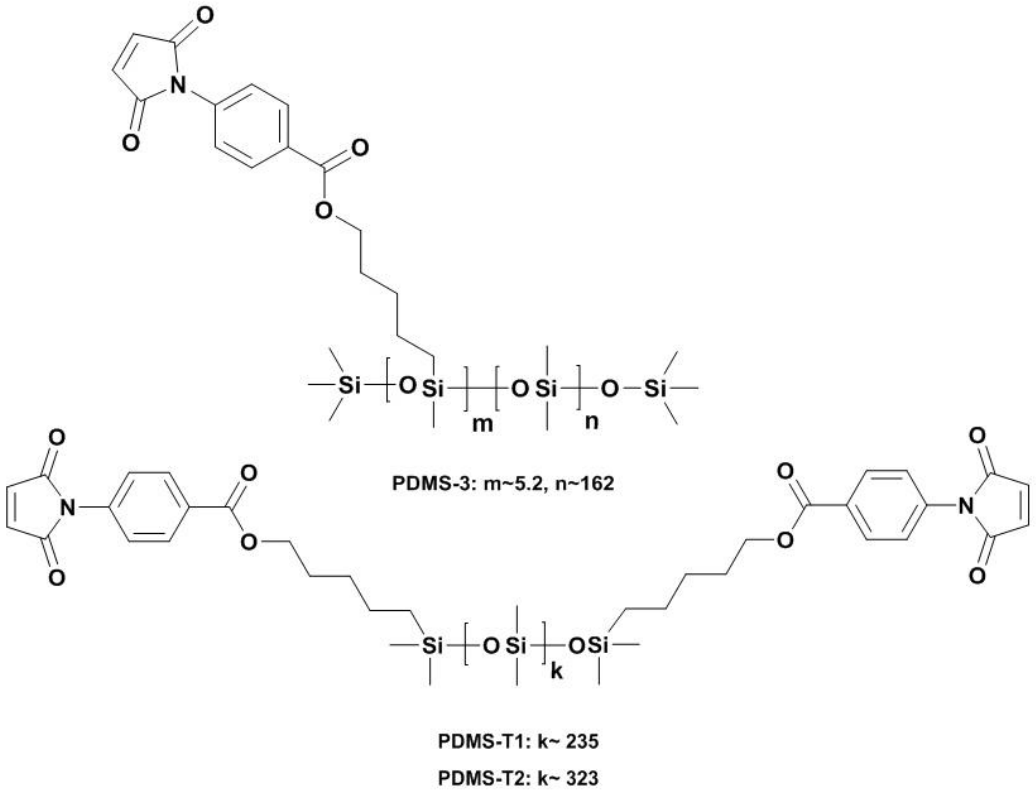

PDMS-B1M: ^{1}H NMR (300 MHz, CDCl3) δ = 8.15-8.12(b,2H), 7.50-7.47(b,1.86H), 6.88(b,2H), 4.32(b, 2H), 1.76(b,1.83H), 1.45(b,4.5H), 0.53(b,2H), 0.08(b,330H). ^{13}C NMR (101 MHz, $CDCl_3$) δ = 168.90, 165.75, 135.29, 134.37, 130.40, 129.55, 125.16, 65.31, 29.58, 28.51, 22.79, 17.41, 1.75, 150, 0.92, 0.52 -0.50. ^{29}Si NMR (60 MHz, $CDCl_3$) δ = 7.21, -21.95.

PDMS-B2M: ^{1}H NMR (300 MHz, CDCl3) δ = 8.15-8.12(b,2H), 7.50-7.47(b,2H), 6.88(b,1.85H), 4.32(b, 2H), 1.76(b,1.87H), 1.45(b,4.75H), 0.53(b,2H), 0.08(b,329H). ^{13}C NMR (101 MHz, $CDCl_3$) δ = 168.90, 165.75, 135.29, 134.37, 130.40, 129.55, 125.16, 65.31, 29.58, 28.51, 22.79, 17.41, 1.75, 150, 0.92, 0.52 -0.50. ^{29}Si NMR (60 MHz, $CDCl_3$) δ = 7.21, -21.95.

Synthesis of octakis(furan-2-ylmethyl)-functionalized polyhedral oligomeric silsesquioxane (12)

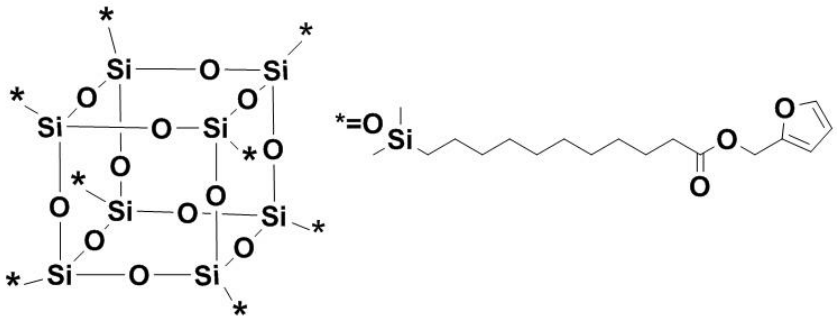

To a solution of octakis(dimethylsiloxy)-T8-silsesquioxane (3.25 g, 3.19 mmol) in pentane (50 mL), **8** (6.7 g, 25 mmol) was added. The solution was stirred for 10 min. Karstedt's catalyst (25 µL) was introduced to the flask, and the reaction mixture was allowed to reflux for 12 h, ultimately resulting in the appearance of two layers. After extracting the bottom layer, the liquid was dissolved in 50 mL of chloroform. Activated charcoal was added, and the reaction was stirred over night at ambient temperature before filtering the suspension through a pad of Celite® using a medium porosity fritted Büchner funnel. Chloroform was removed *in vacuo* to obtain **12** (7.14 g, 2.58 mmol, 71%) as a yellow viscous liquid.

^{1}H NMR (300 MHz, $CDCl_3$) δ = 7.41 (b, 1H), 6.39-6.34 (b, 2H), 5.05 (s,2H), 2.32 (t, 3J=7Hz, 2H), 1.63 (b, 2H), 1.24 (b, 14H), 0.58 (b, 2H), 0.12 (b, 6H).^{13}C NMR (101 MHz, $CDCl_3$) δ = 173.42, 149.66, 143.16, 110.52, 110.45, 57.83, 34.14, 33.49, 29.63, 29.55, 29.41, 29.30, 29.14, 24.89, 22.98, 17.70, -0.33. ^{29}Si NMR (60 MHz, $CDCl_3$) δ = 12.59, -108.88. MALDI: Theoretical mass of $[C_{144}H_{248}O_{44}Si_{16}+Na]^+$: 3152.337m/z, Measured mass: 3152.363 m/z. Elemental Analysis (%): Calculated: C:55.21, H:7.98, Found: C:55.49, H:7.96.

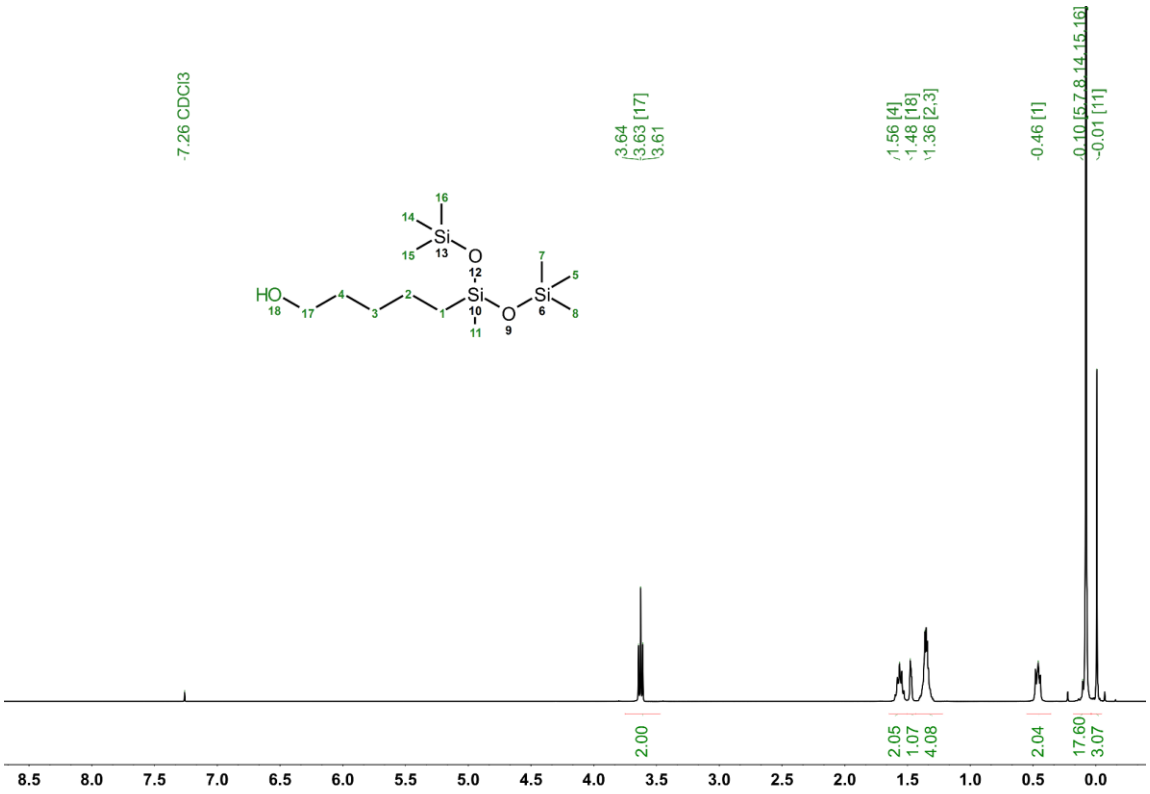

Figure 1. *^{1}H NMR spectrum of compound **3**.*[247]

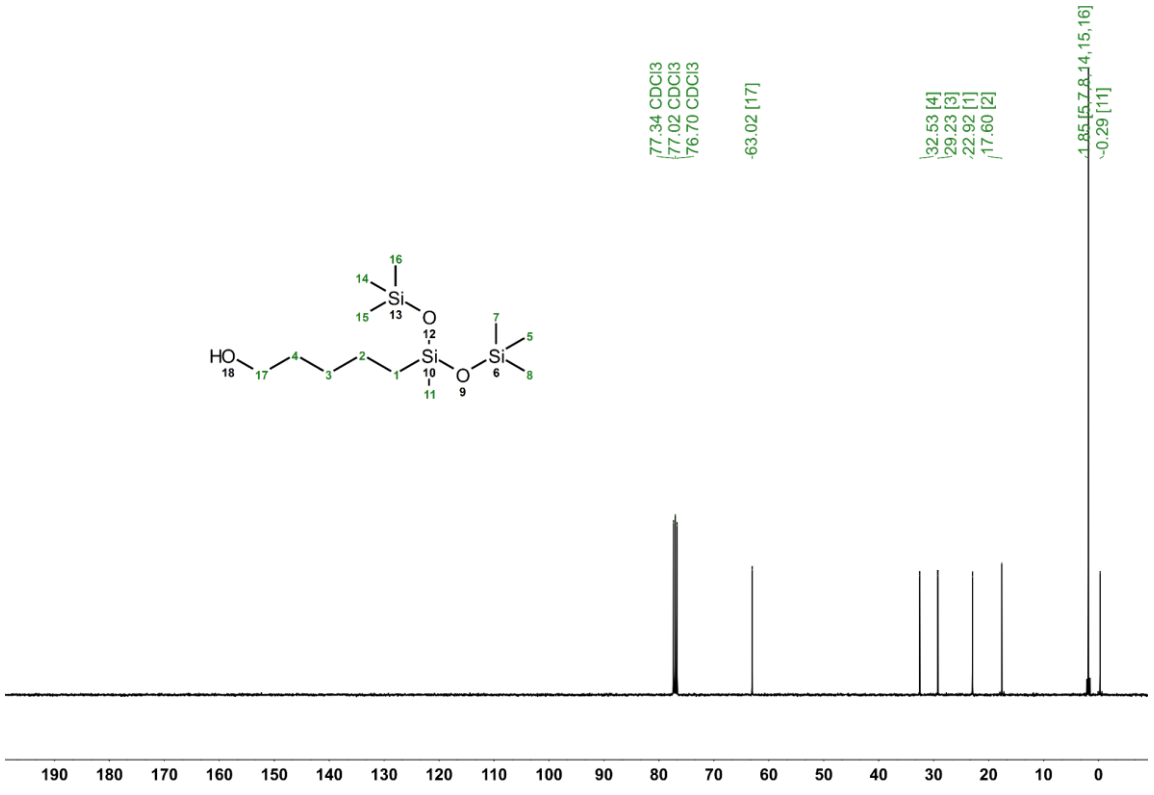

Figure 2. *^{13}C NMR spectrum of compound **3**.*[247]

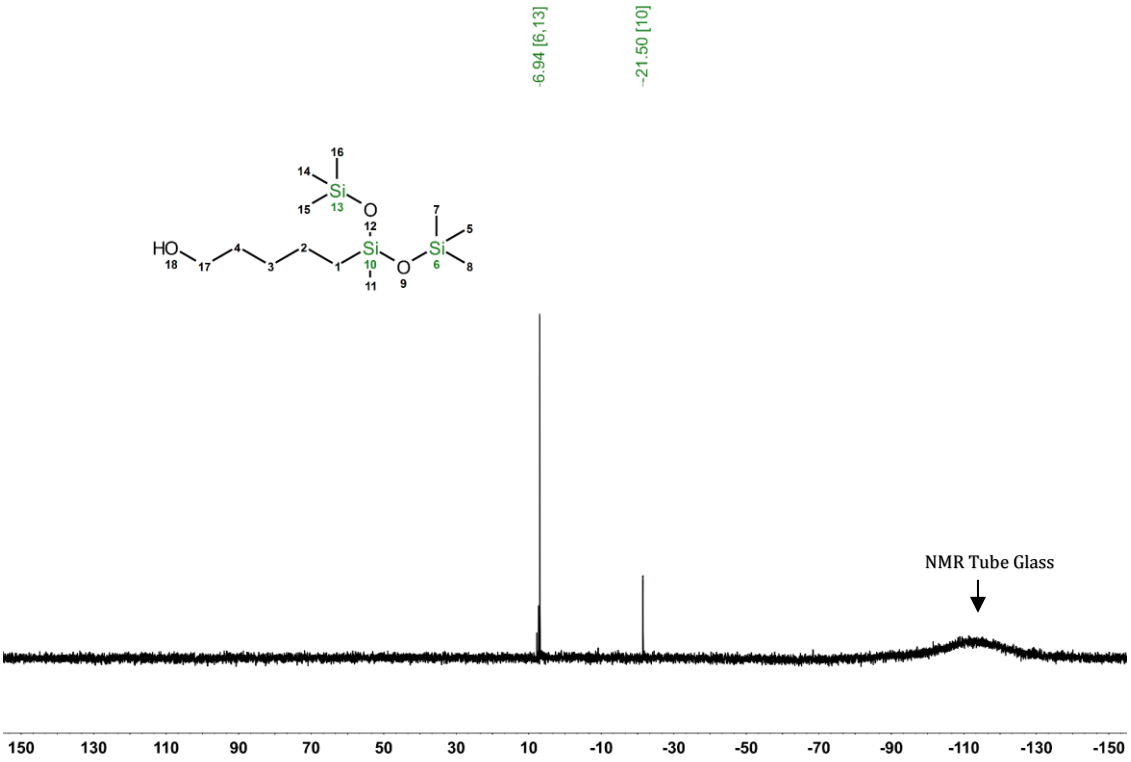

***Figure 3**. [29]Si NMR spectrum of compound **3**.*[247]

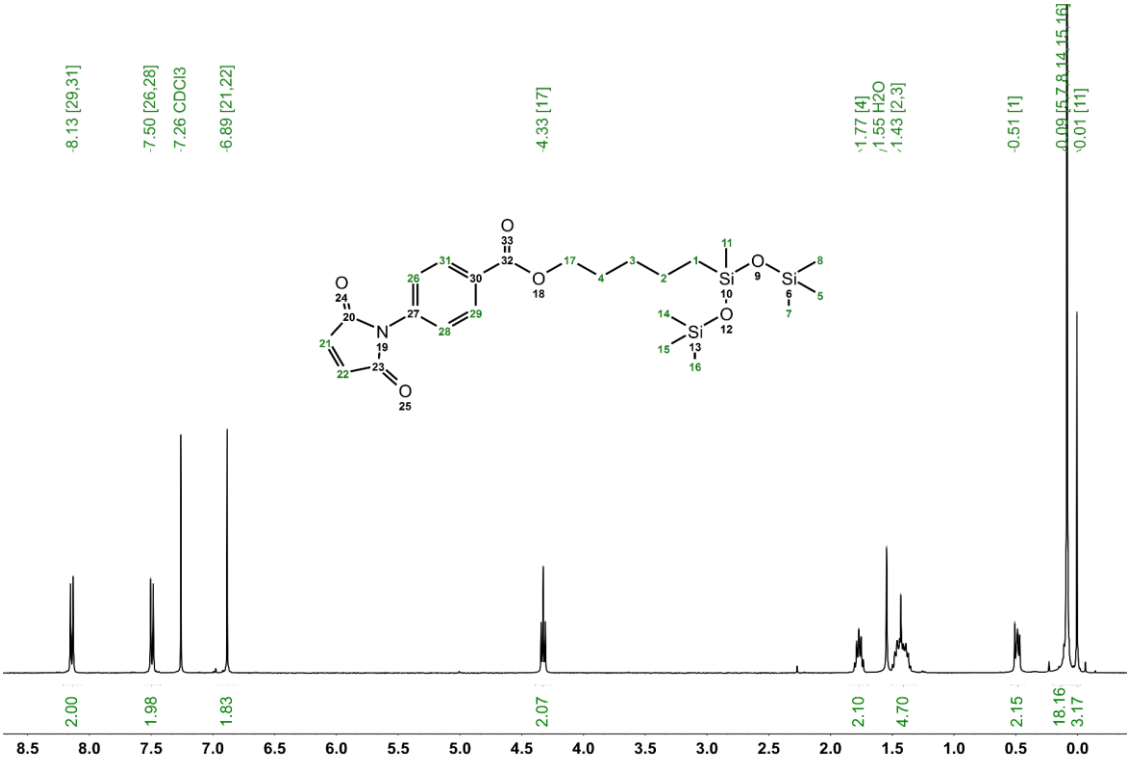

***Figure 4.** [1]H NMR spectrum of compound **5**.*[247]

Figure 5. *^{13}C NMR spectrum of compound* ***5****.*[247]

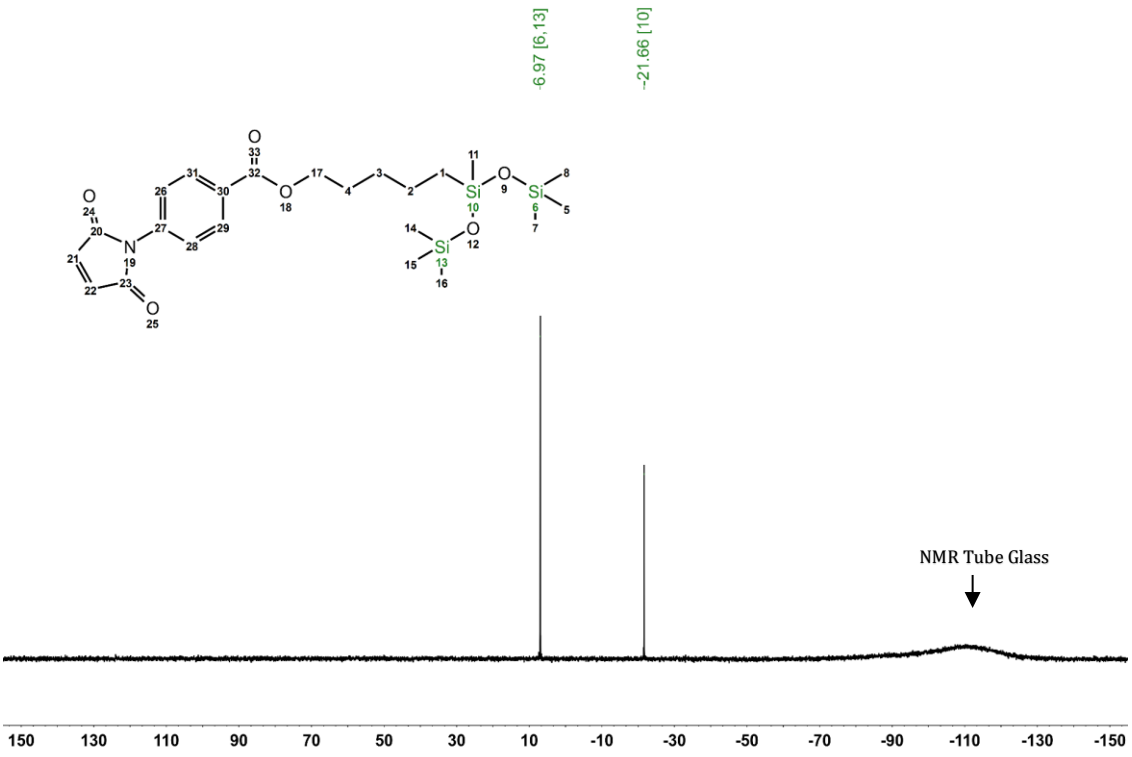

Figure 6.*^{29}Si NMR spectrum of compound* ***5****.*[247]

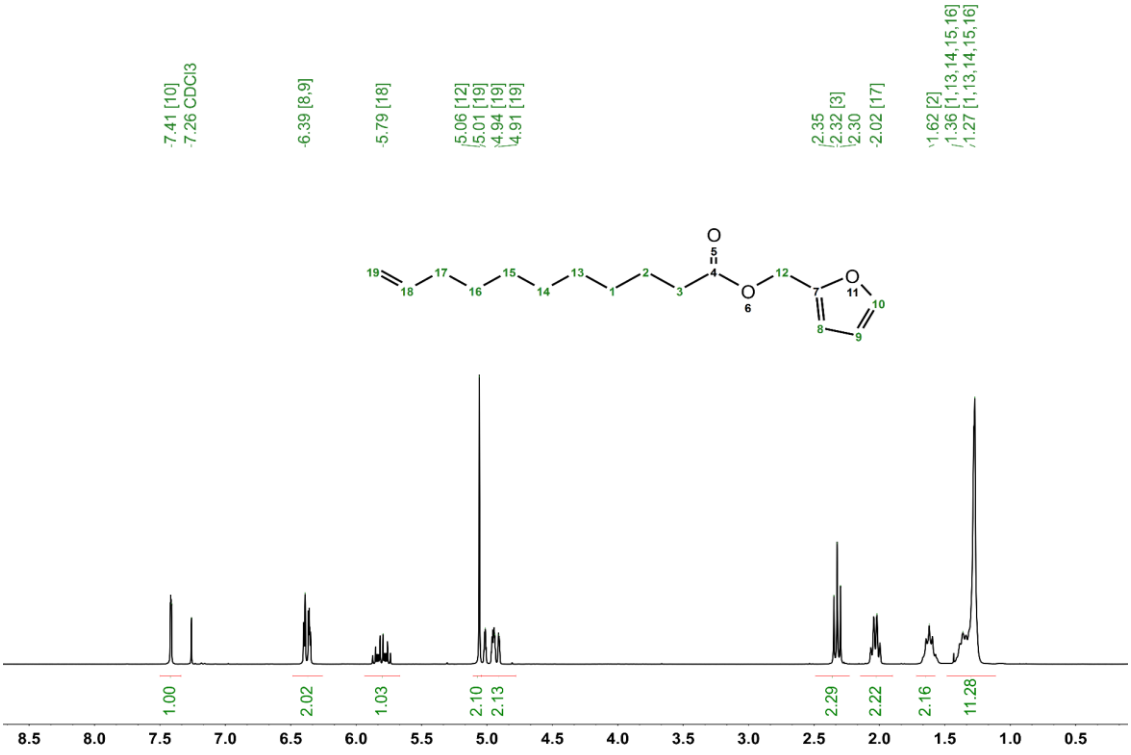

Figure 7. *^{1}H NMR spectrum of compound* ***8****.*[247]

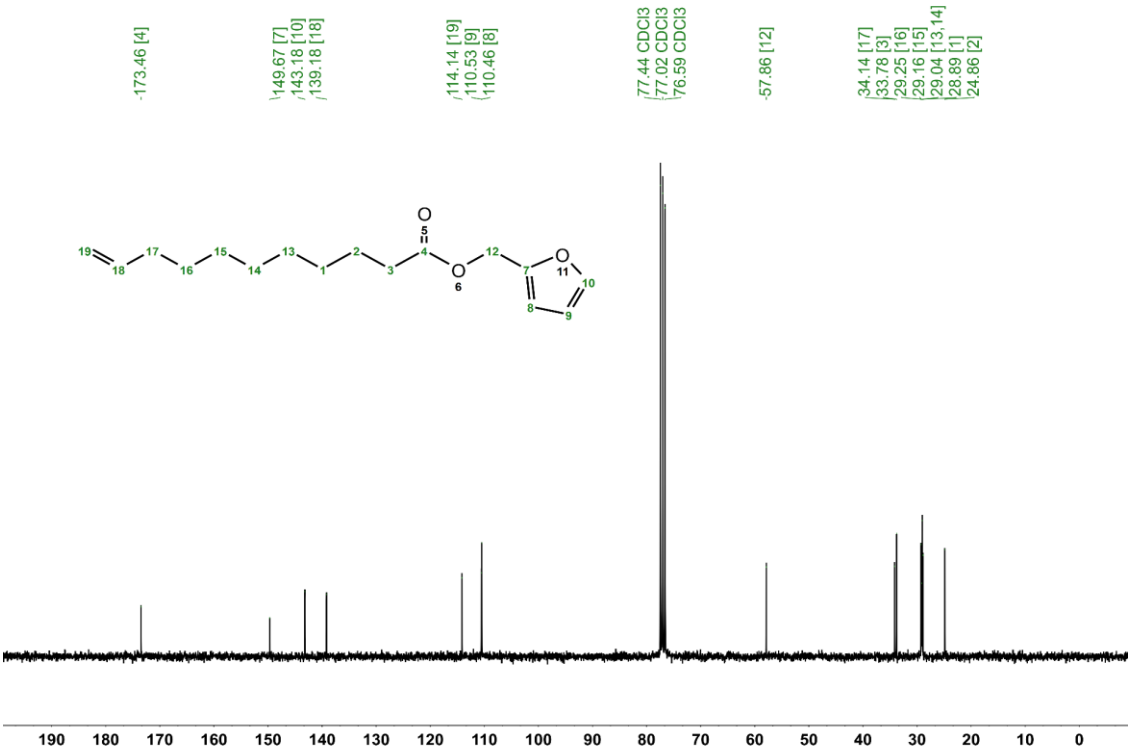

Figure 8. *^{13}C NMR spectrum of compound* ***8****.*[247]

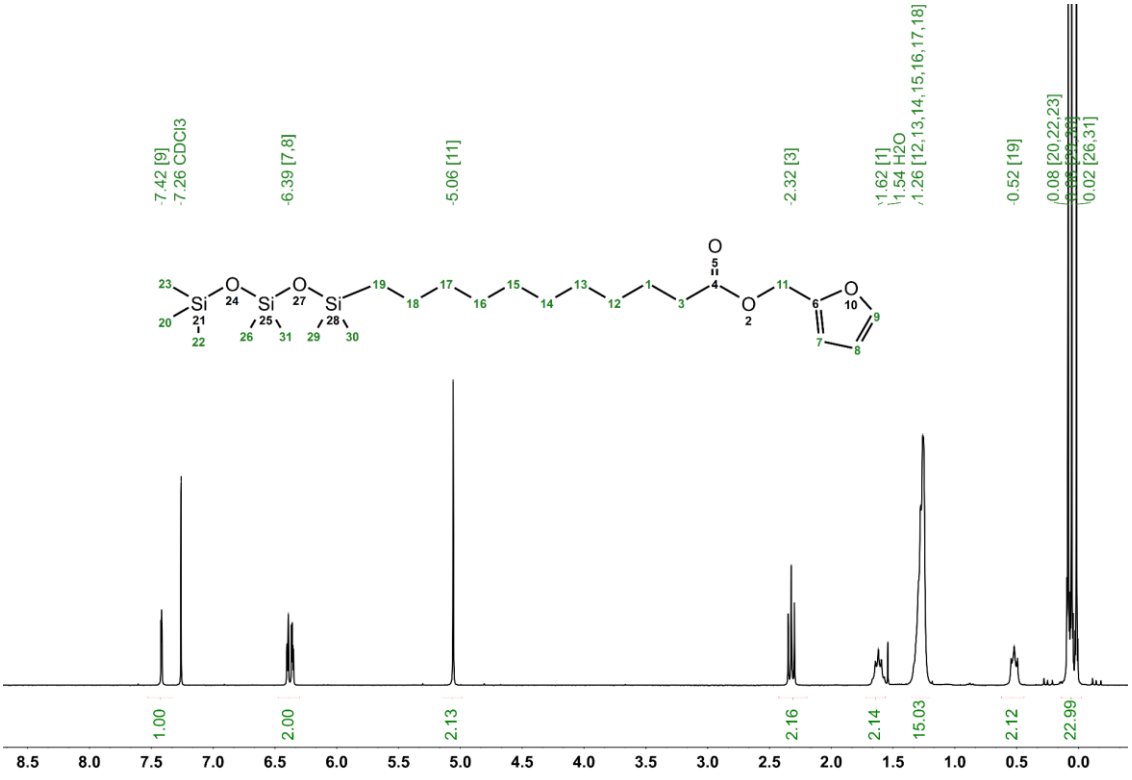

Figure 9. *^{1}H NMR spectrum of compound* ***10****.*[247]

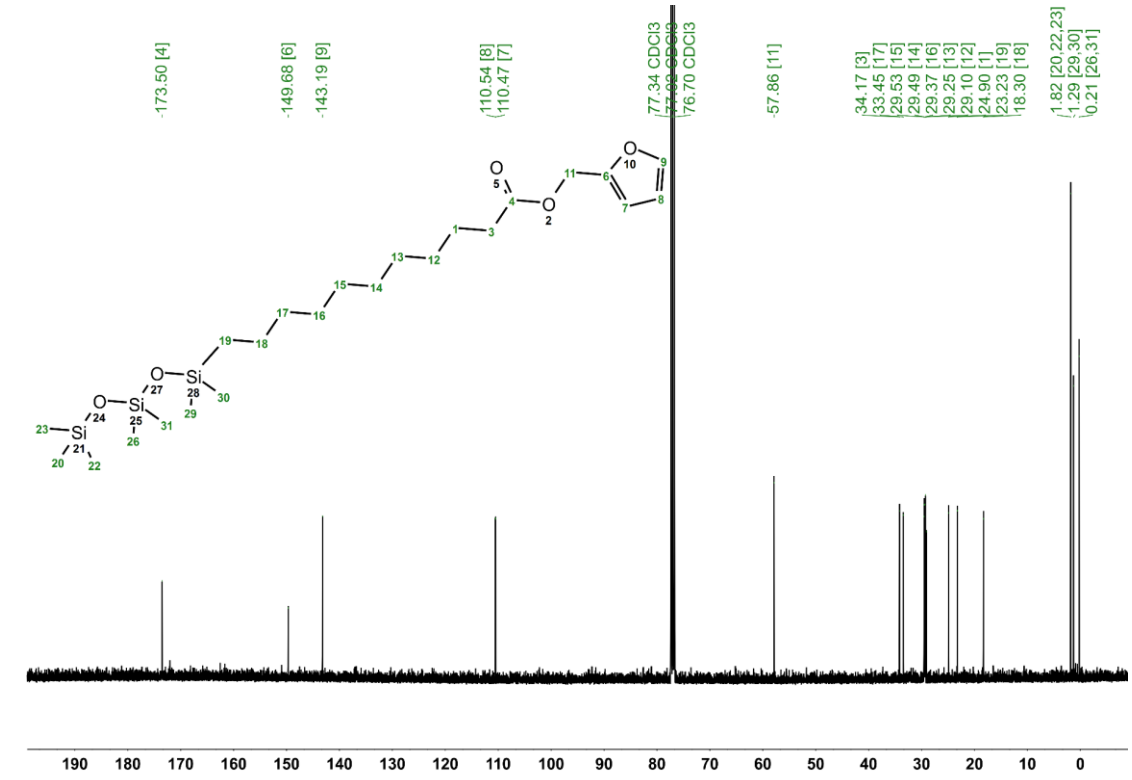

Figure 10. *^{13}C NMR spectrum of compound* ***10****.*[247]

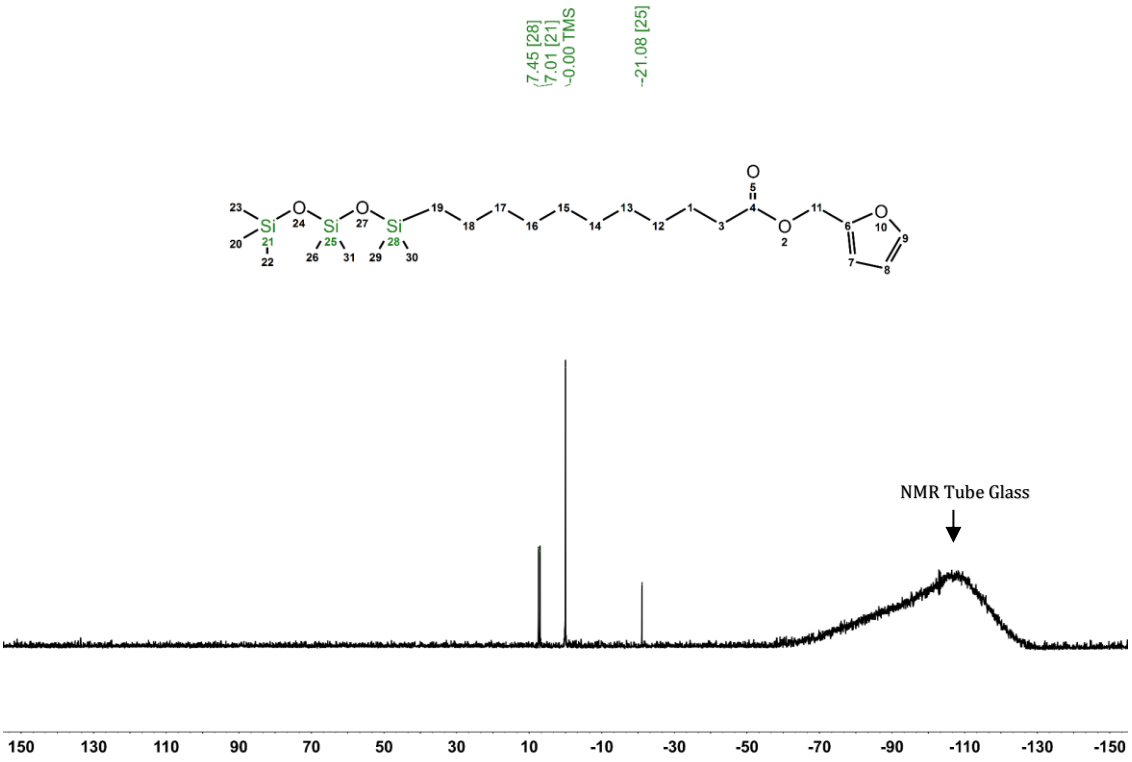

Figure 1. *[29]Si NMR spectrum of compound* ***10****.*[247]

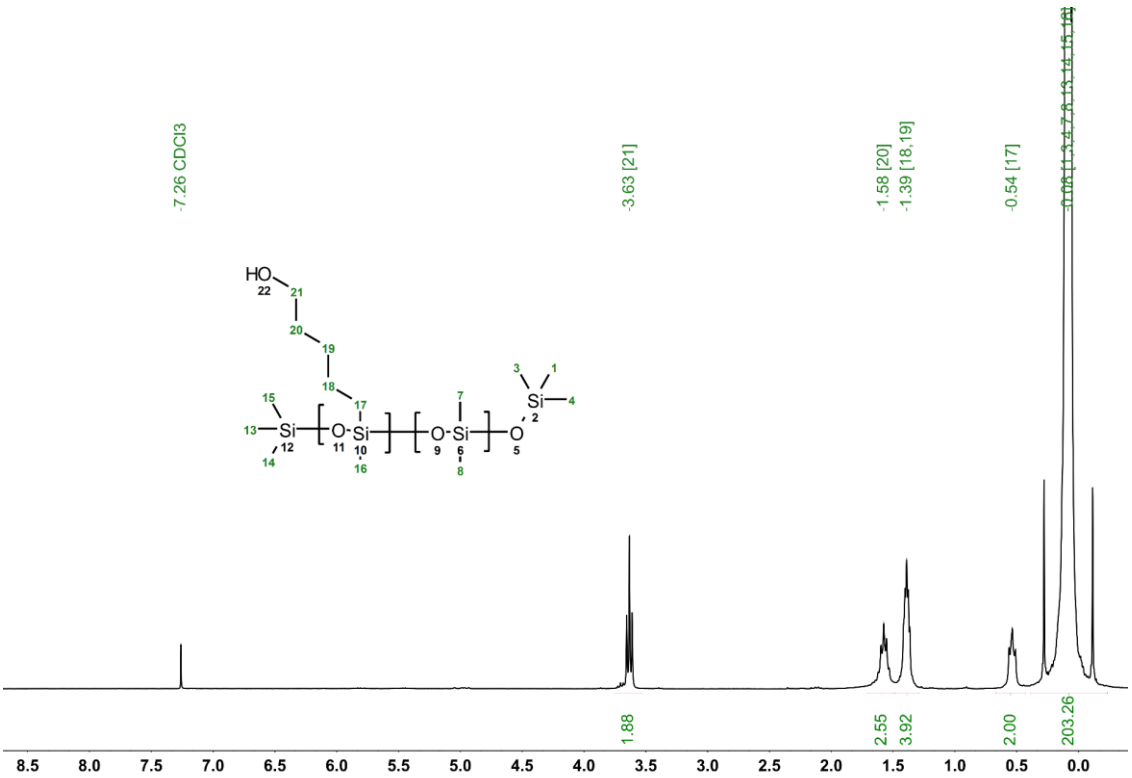

Figure 2. *[1]H NMR spectrum of* ***PDMS-2****.*[247]

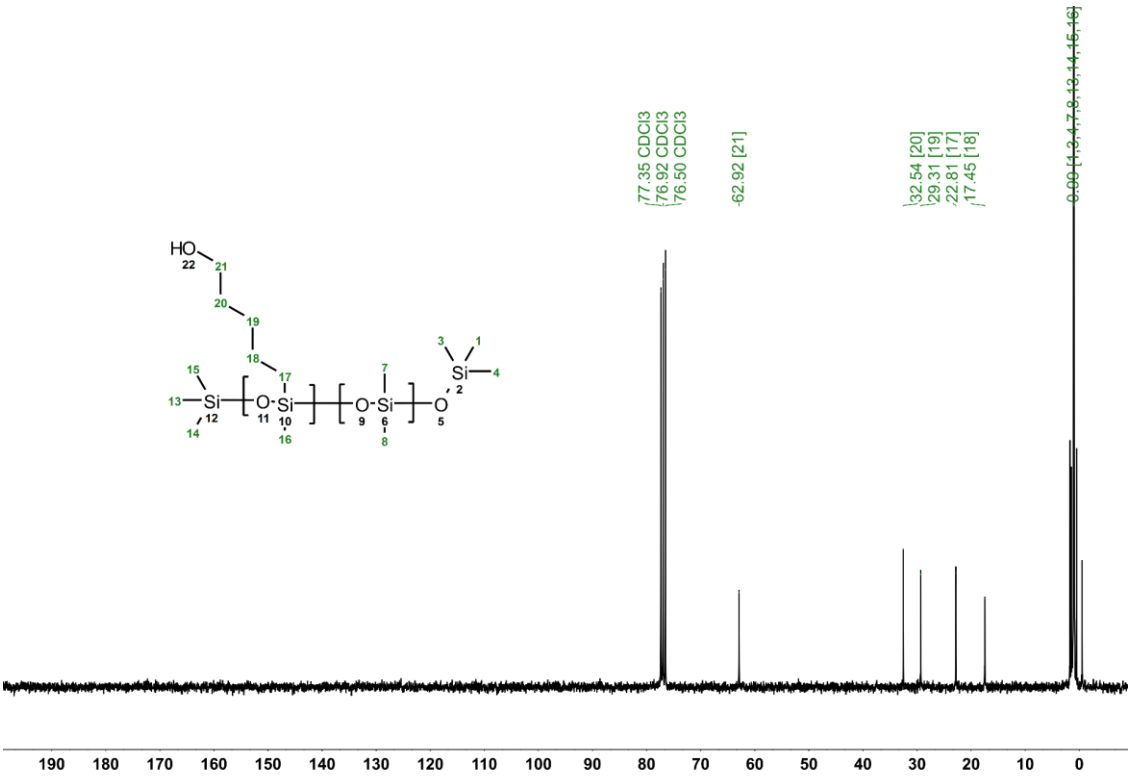

Figure 3. *^{13}C NMR spectrum of* ***PDMS-2****.* [247]

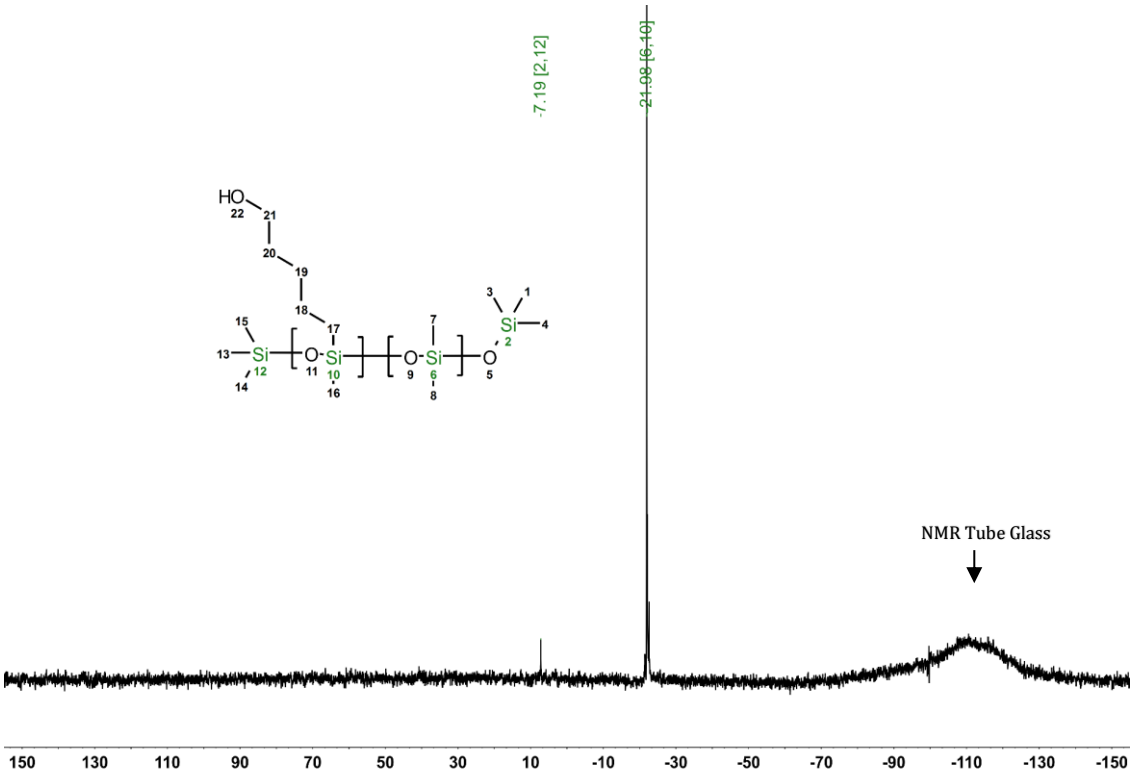

Figure 14. *^{29}Si NMR spectrum of* ***PDMS-2****.* [247]

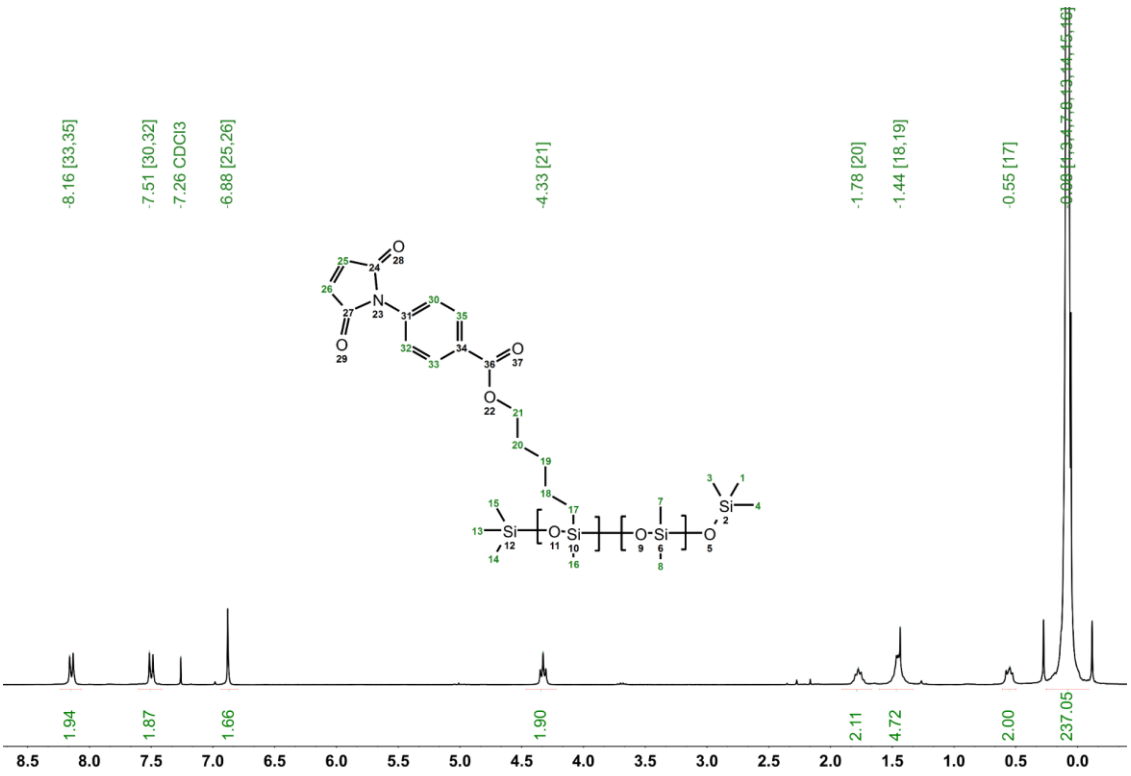

Figure 15. *^{1}H NMR spectrum of* ***PDMS-3****.* [247]

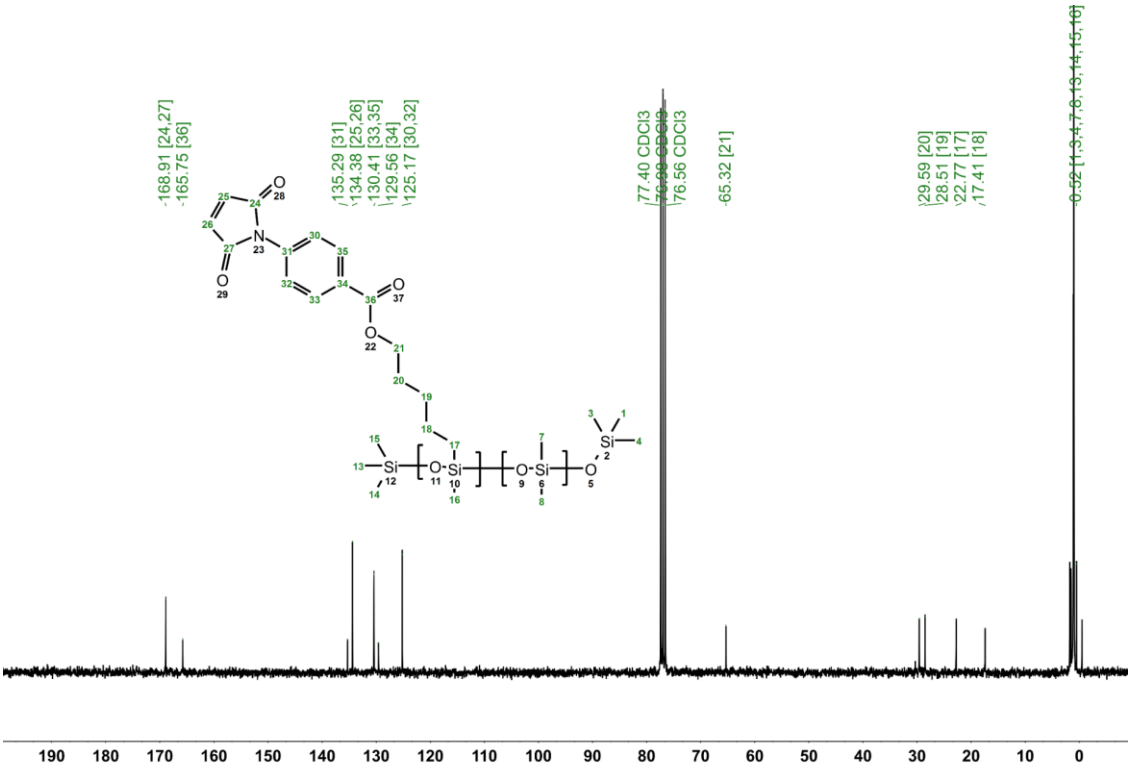

Figure 16. *^{13}C NMR spectrum of* ***PDMS-3****.* [247]

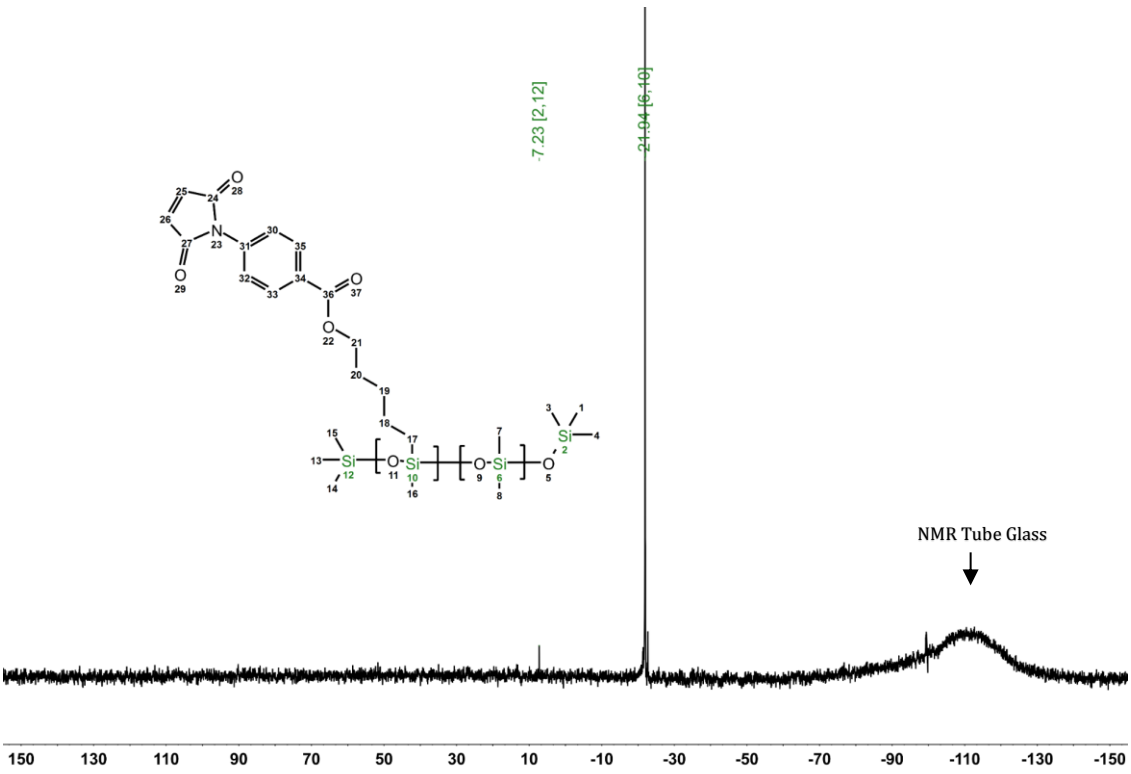

***Figure 17**. [29]Si NMR spectrum of **PDMS-3**.* [247]

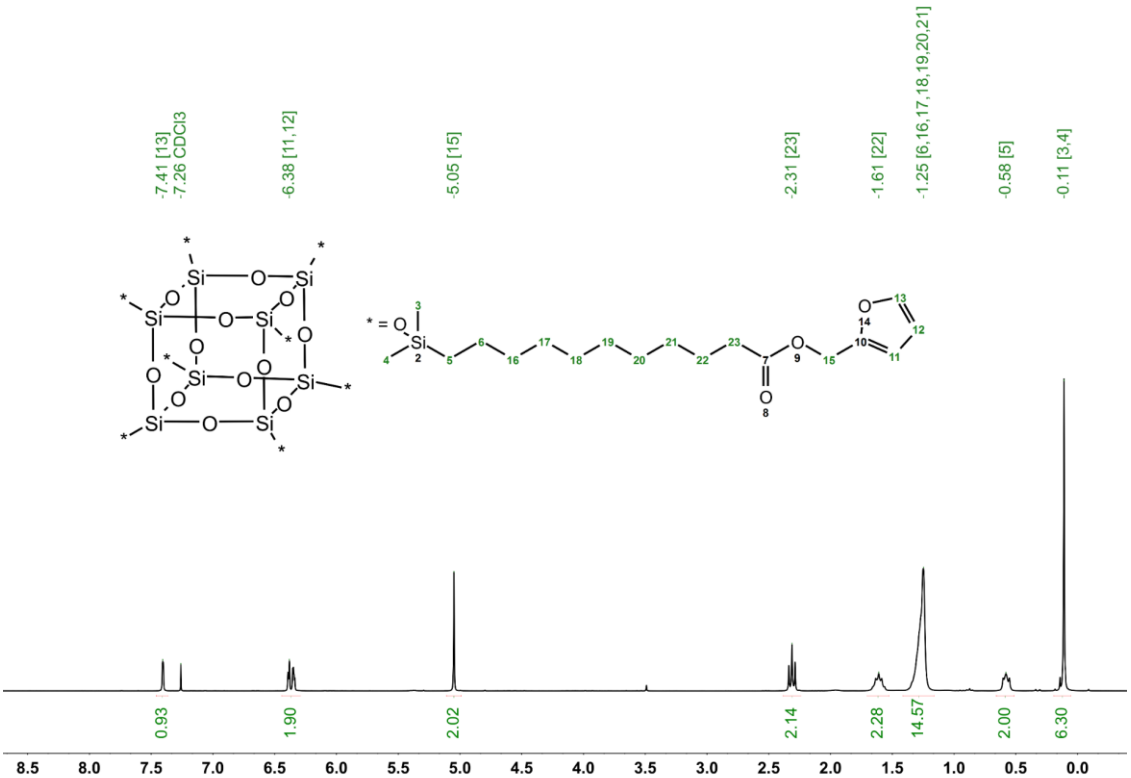

***Figure 18.** [1]H NMR spectrum of compound **12**.* [247]

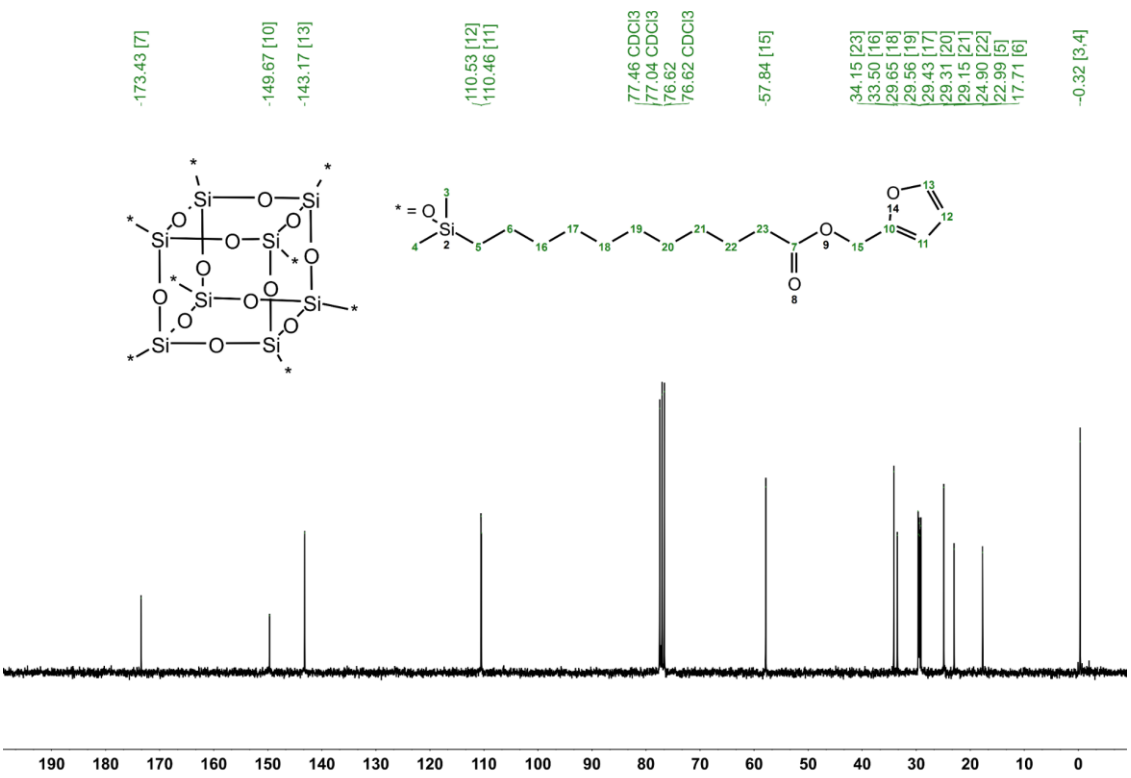

***Figure 19**. [13]C NMR spectrum of compound **12**.* [247]

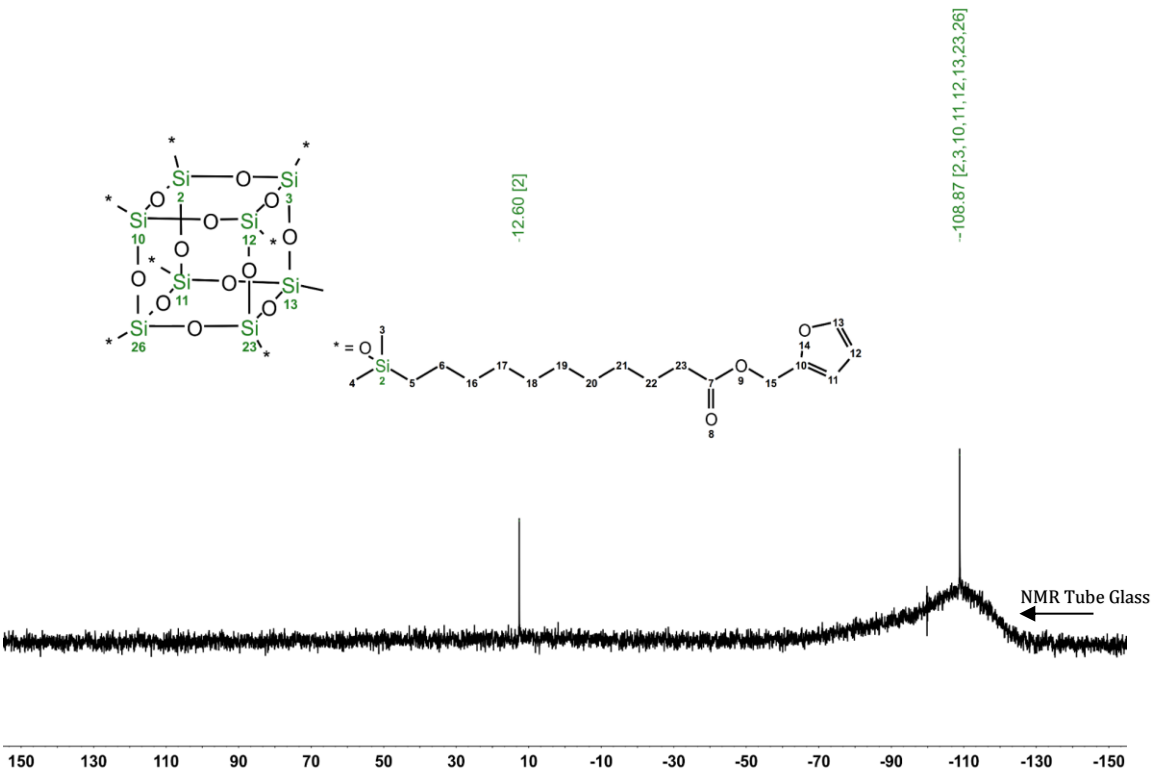

***Figure 4.** [29]Si NMR spectrum of compound **12**.* [247]

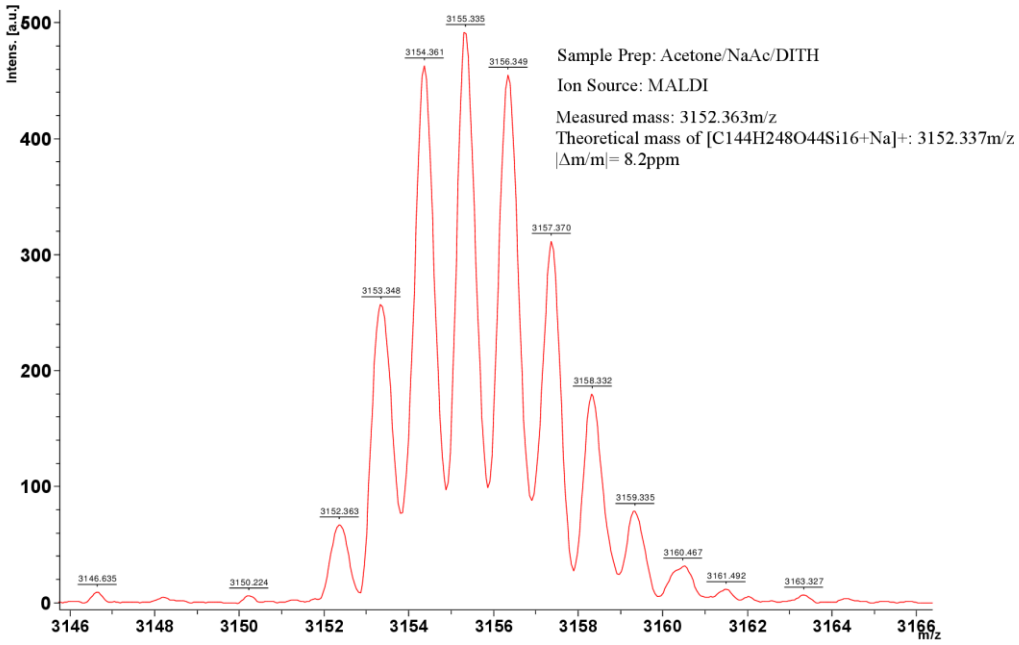

***Figure 5**. MALDI-ToF mass spectrometry of **12**.* [247]

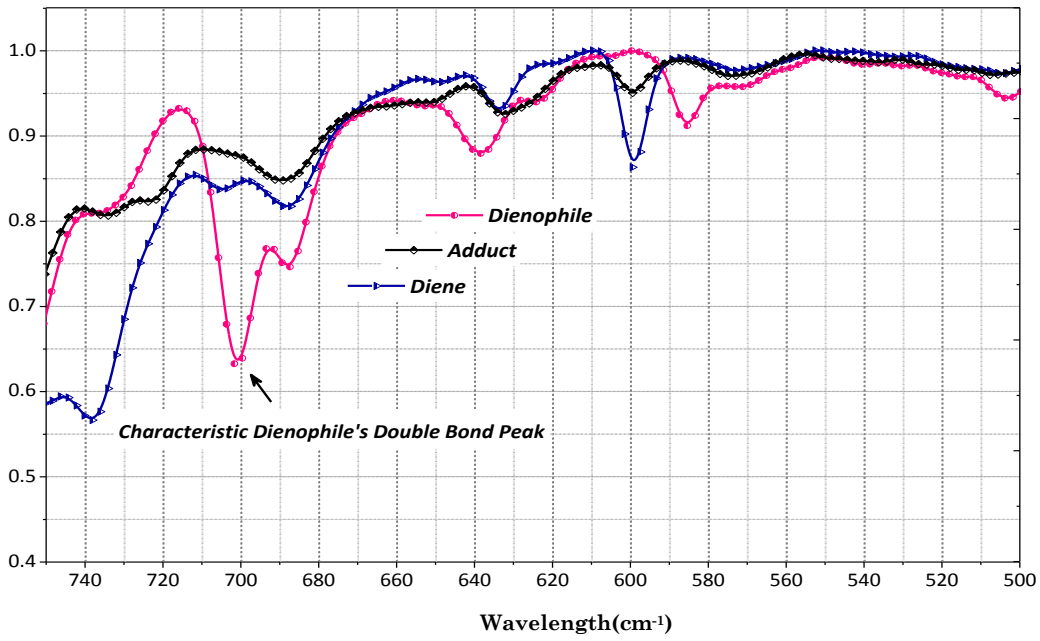

***Figure 22.** ATR-IR spectrums of the diene(**10**), the dienophile (**5**) and a DA reaction mixture which contained 88% adduct (**11**) according to ^{1}H NMR.* [247]

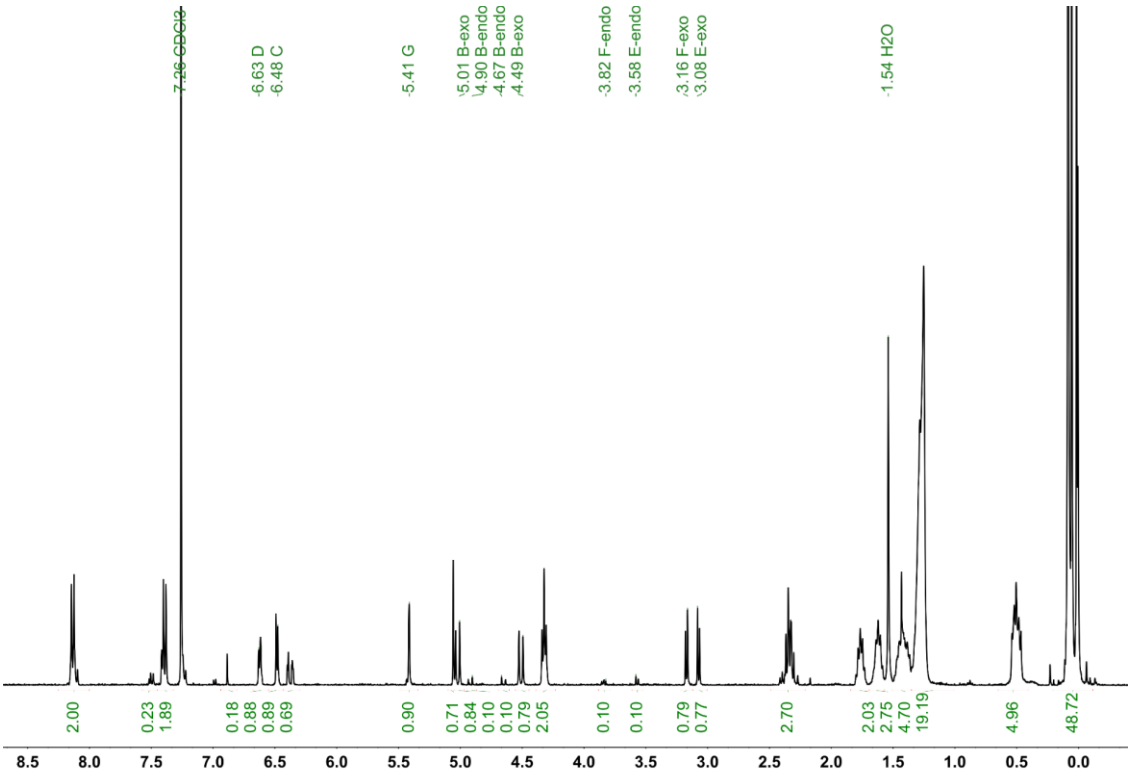

Figure 6. *^{1}H NMR spectroscopy of a Diels-Alder reaction mixture containing **10**, **5**, and **11**.* [247]

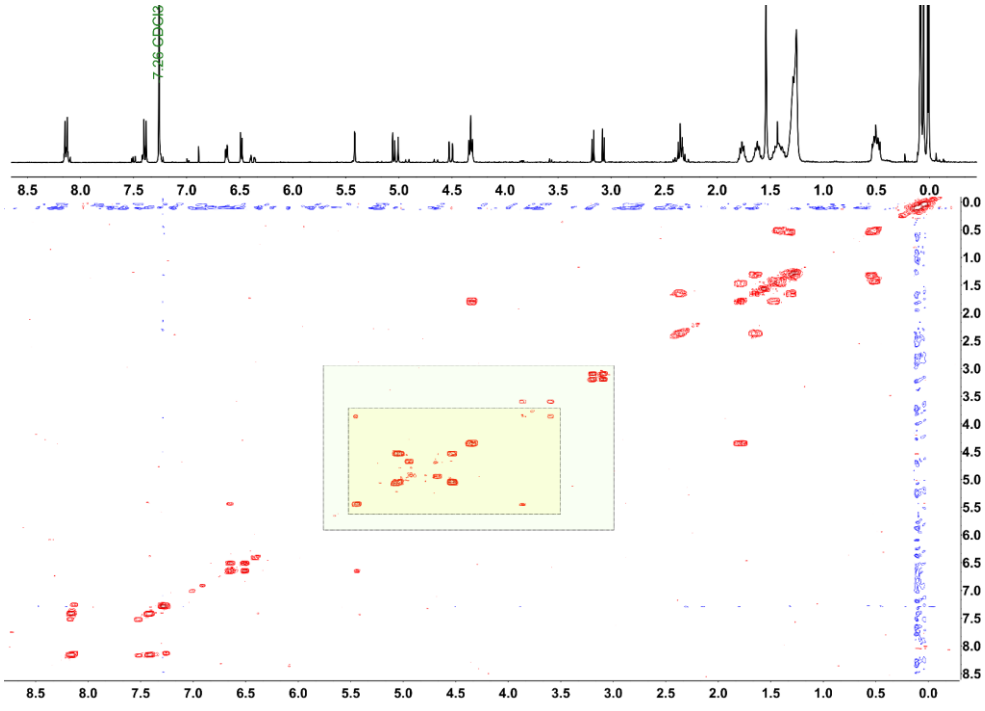

Figure 7. *gCOSY NMR spectroscopy of a Diels-Alder reaction mixture. Only the endo isomer correlates with the bridge's hydrogen.* [247]

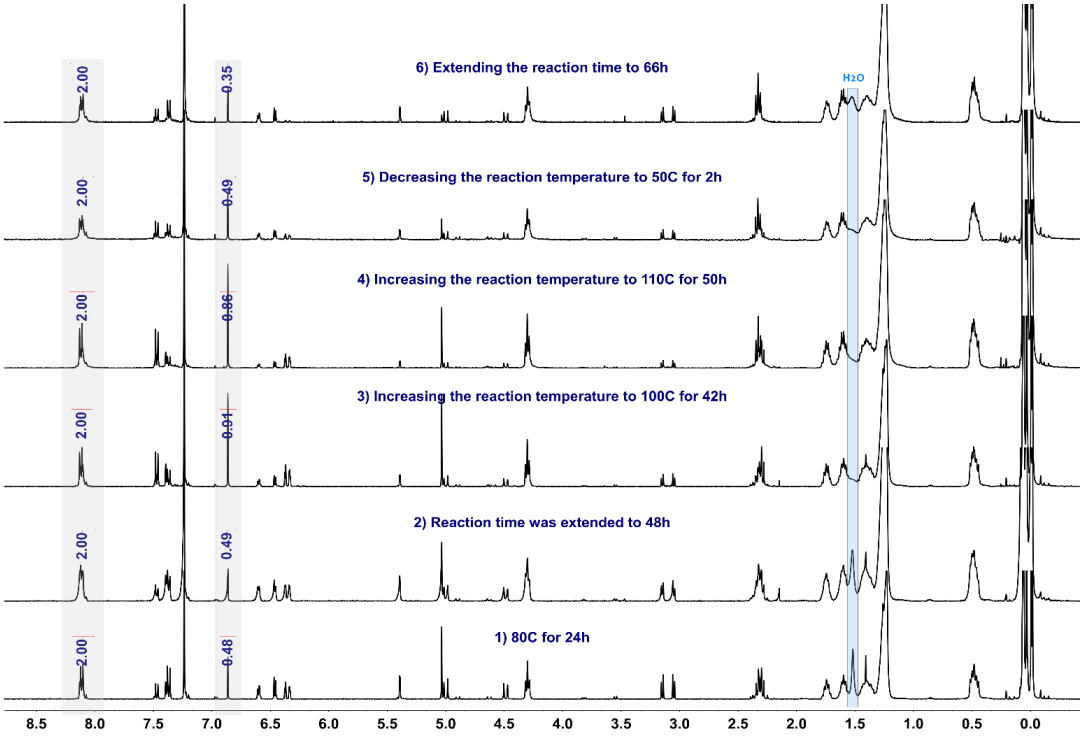

Figure 8. *A series of ^{1}H NMR spectra acquired for sample* ***B*** *in different time periods and various temperatures followed subsequently.* [247]

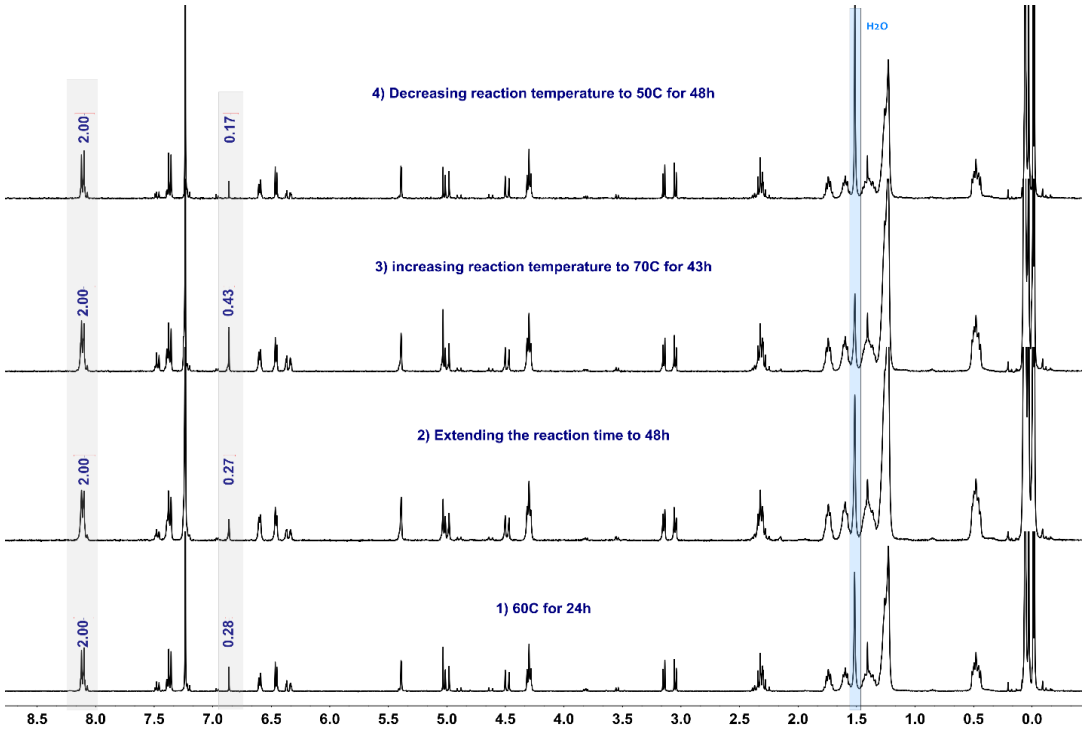

Figure 9. *A series of ^{1}H NMR spectra acquired for sample* ***A*** *in different time periods and various temperatures followed subsequently.* [247]

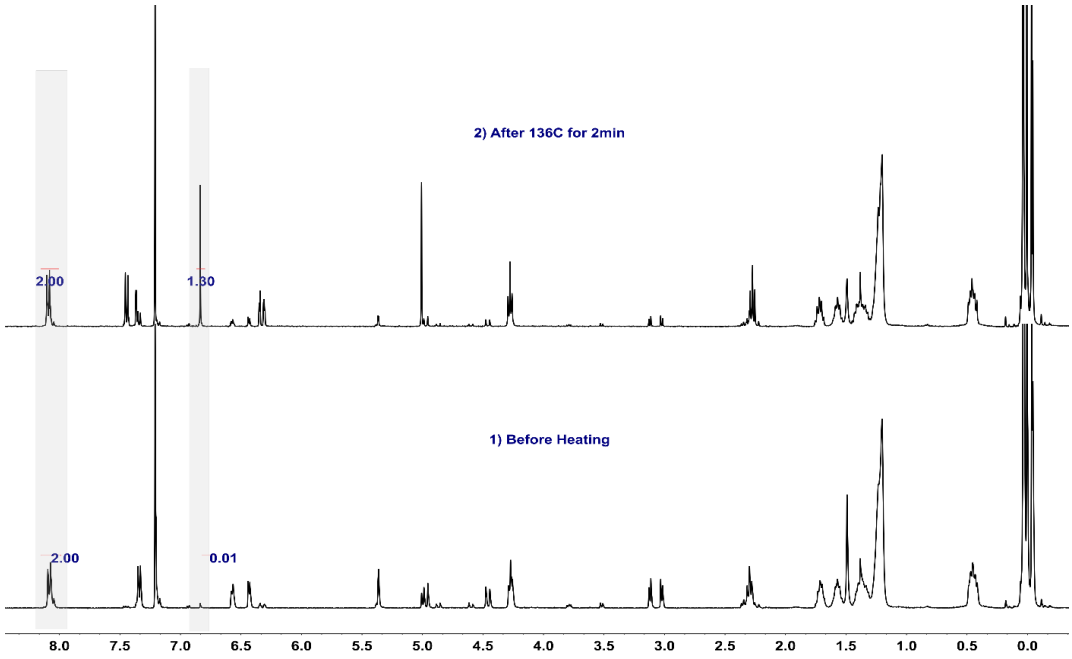

Figure 10. *^{1}H NMR spectra of a DA mixture sample contained a high quantity of the adduct (**11**) before and after exposing to 136°C for 2 min.* [247]

Chapter 7 Vita

Amin Nasresfahani was born on November 19, 1992 and grew up in a vibrant city called Esfahan in the heart of Iran. He obtained his B.Sc. Eng. in Polymer Engineering in July 2015 from one of Iran's most prestigious universities, Amirkabir University, located in Tehran, the capital of Iran. Upon completion of his M.Sc. in Chemistry with Dr. Paul Zelisko at Brock University in 2017, he decided to pursue a Ph.D. in Chemical Engineering at Queen's University with Prof. Robin Hutchinson.

Chapter 8 References

(1) Saul Patai, Z. R. *The Chemistry of Organic Silicon Compounds*; Rappoport, Z., Apeloig, Y., Eds.; The Chemistry of Functional Groups; John Wiley & Sons, Ltd: Chichester, UK, 1998; Vol. 2.

(2) Brook, M. a. In *Silicon in Organic, Organometallic and Polymer Chemistry*; John Wiley & Sons, Inc., 2000; pp 27–38.

(3) Nakamura, E.; Shimizu, M.; Kuwajima, I.; Sakata, J.; Yokoyama, K.; Noyori, R. *J. Org. Chem.* **1983**, *48* (7), 932–945.

(4) Lipowitz, J. *J. Am. Chem. Soc.* **1972**, *94* (5), 1582–1589.

(5) Adcock, W.; Aldous, G. L.; Kitching, W. *Tetrahedron Lett.* **1978**, *19* (36), 3387–3390.

(6) Cooper, D. L.; Cunningham, T. P.; Gerratt, J.; Karadakov, P. B.; Raimondi, M. *J. Am. Chem. Soc.* **1994**, *116* (10), 4414–4426.

(7) Giordan, J. C. *J. Am. Chem. Soc.* **1983**, *105* (22), 6544–6546.

(8) Ratner, M. A.; Sabin, J. R. *J. Am. Chem. Soc.* **1977**, *99* (12), 3954–3960.

(9) Reed, A. E.; Ragué Schleyer, P. Von. *J. Am. Chem. Soc.* **1990**, *112* (4), 1434–1445.

(10) Reed, A. E.; Schade, C.; Schleyer, P. v. R.; Kamath, P. V; Chandrasekhar, J. *J. Chem. Soc. Commun.* **1988**, No. 1, 67–69.

(11) Reed, A. E.; Schleyer, P. v. R. *Inorg. Chem.* **1988**, *27* (22), 3969–3987.

(12) Magnusson, E. *J. Am. Chem. Soc.* **1990**, *112* (22), 7940–7951.

(13) Magnusson, E. *J. Am. Chem. Soc.* **1993**, *115* (3), 1051–1061.

(14) Mo, Y.; Zhang, Y.; Gao, J. *J. Am. Chem. Soc.* **1999**, *121* (24), 5737–5742.

(15) Mitzel, N. W.; Oberhammer, H. *Inorg. Chem.* **1998**, *37* (14), 3593–3598.

(16) Albright, T. A.; Burdett, J. K.; Whangbo, M.-H. *Orbital Interactions in Chemistry*; John Wiley & Sons, Inc.: Hoboken, NJ, USA, 2013.

(17) Sini, G.; Ohanessian, G.; Hiberty, P. C.; Shaik, S. S. *J. Am. Chem. Soc.* **1990**, *112* (4), 1407–1413.

(18) Bovey, F.; Mirau, P.; Gutowsky, H. S. *Nuclear Magnetic Resonance Spectroscopy*, Second.; Academic Press, Inc., 1988.

(19) Nanny, M. A.; Knicker, H. *Nuclear Magnetic Resonance Spectroscopy in Environmental Chemistry (Topics in Environmental Chemistry)*; Mark A. Nanny, Roger A. Minear, J. A. L., Ed.; Oxford University Press, 1997; Vol. 1.

(20) Richards, S. A.; Hollerton, J. C. *Essential Practical NMR for Organic Chemistry*; John Wiley & Sons, Ltd: Chichester, UK, 2010.

(21) Balci, M. *Basic 1H- and 13C-NMR Spectroscopy*; Elsevier, 2005.

(22) Apeloig, Y. *The Chemistry of Organic Silicon Compounds*; Rappoport, Z., Apeloig, Y., Eds.; The Chemistry of Functional Groups; John Wiley & Sons, Ltd: Chichester, UK, 2001; Vol. 3.

(23) Brook, M. a. In *Silicon in Organic, Organometallic and Polymer Chemistry*; John Wiley & Sons, Inc., 2000; pp 3–26.

(24) Williams, E. A.; Cargioli, J. D. In *Annual Reports on NMR Spectroscopy*; Elsevier., 1979; pp 221–318.

(25) Marsmann, H. C. In *Encyclopedia of Magnetic Resonance*; John Wiley & Sons, Ltd: Chichester, UK, 2011.

(26) Hoffman, R. V. *Organic Chemistry: An Intermediate Text*; John Wiley & Sons, Inc.: Hoboken, NJ, USA, 2004.

(27) Wade, L. G. *Organic Chemistry*, 8th ed.; Advanced Organic Chemistry; Pearson, 2013.

(28) Kazlauskas, R. J.; Weissfloch, A. N. E.; Rappaport, A. T.; Cuccia, L. A. *J. Org. Chem.* **1991**, *56* (8), 2656–2665.

(29) Drauz, K.; Gro, H. *Enzyme Catalysis in Organic Synthesis*; Drauz, K., Gröger, H., May, O., Eds.; Wiley-VCH Verlag GmbH & Co. KGaA: Weinheim, Germany, 2012; Vol. 1.

(30) Raza, S.; Fransson, L.; Hult, K. *Protein Sci.* **2001**, *10* (2), 329–338.

(31) Smith, L. C.; Faustinella, F.; Chan, L. *Curr. Opin. Struct. Biol.* **1992**, *2* (4), 490–496.

(32) Poojari, Y.; Clarson, S. J. *Biocatal. Agric. Biotechnol.* **2013**, *2* (1), 7–11.

(33) Uppenberg, J.; Ohmer, N.; Norin, M.; Hult, K.; Kleywegt, G. J.; Patkar, S.; Waagen, V.; Anthonsen, T.; Jones, T. A. *Biochemistry* **1995**, *34* (51), 16838–16851.

(34) Sperling, L. H. *Introduction to Physical Polymer Science*; John Wiley & Sons, Inc.: Hoboken, NJ, USA, 2005; Vol. 31.

(35) Bower, D. I. *An Introduction to Polymer Physics*; Cambridge University Press: Cambridge, 2002; Vol. 21.

(36) Mouritz, P. A. In *Introduction to Aerospace Materials*; Elsevier, 2012; pp 268–302.

(37) Mark, J. E.; Schaefer, D. W.; Lin, G. *The Polysiloxanes*, Revised.; Oxford University Press, 2015.

(38) Mark, J. E. *Acc. Chem. Res.* **2004**, *37* (12), 946–953.

(39) Debolt, L. C.; Mark, J. E. *J. Polym. Sci. Part B Polym. Phys.* **1988**, *26* (5), 989–995.

(40) Taylor, D. *Mineral. Mag.* **1972**, *38* (297), 629–631.

(41) Stixrude, L.; Bukowinski, M. S. T. *Phys. Chem. Miner.* **1988**, *16* (2), 629–631.

(42) Awazu, K.; Kawazoe, H. *J. Appl. Phys.* **2003**, *94* (10), 6243–6262.

(43) Mark, J. E. *Prog. Polym. Sci.* **2003**, *28* (8), 1205–1221.

(44) Urayama, K.; Kohjiya, S. *Eur. Phys. J. B* **1998**, *2*, 75–78.

(45) Mark, J. E. *Acc. Chem. Res.* **2004**, *37* (12), 946–953.

(46) Dvornic, P. R.; Jovanovic, J. D.; Govedarica, M. N. *J. Appl. Polym. Sci.* **1993**, *49* (9), 1497–1507.

(47) Kataoka, T.; Ueda, S. *J. Polym. Sci. Part B Polym. Lett.* **1966**, *4* (5), 317–322.

(48) Fetters, L. J.; Lohse, D. J.; Richter, D.; Witten, T. A.; Zirkel, A. *Macromolecules* **1994**, *27* (17), 4639–4647.

(49) Fetters, L. J.; Lohse, D. J.; Colby, R. H. *Physical Properties of Polymers Handbook*; Mark, J. E., Ed.; Springer New York: New York, NY, 2007.

(50) Mark, J. E. In *American Chemical Society, Polymer Preprints, Division of Polymer Chemistry*; 2000; Vol. 39, pp 1–10.

(51) Mojsiewicz-Pieńkowska, K. In *Handbook of Polymers for Pharmaceutical Technologies*; John Wiley & Sons, Inc.: Hoboken, NJ, USA, 2015; Vol. 2, pp 363–381.

(52) Drobny, J. G. In *Introduction to Fluoropolymers*; Elsevier, 2013; pp 149–230.

(53) Mark, J. E. *Acc. Chem. Res.* **1994**, *27* (9), 271–278.

(54) Britcher, L. G.; Kehoe, D. C.; Matisons, J. G.; Swincer, A. G. *Macromolecules* **1995**, *28* (9), 3110–3118.

(55) Marciniec, B.; Matisons, J. *Hydrosilylation*; Marciniec, B., Ed.; Advances In Silicon Science; Springer Netherlands: Dordrecht, 2009; Vol. 1.

(56) Risangud, N.; Li, Z.; Anastasaki, A.; Wilson, P.; Kempe, K.; Haddleton, D. M. *RSC Adv.* **2015**, *5* (8), 5879–5885.

(57) Mani, S.; Cassagnau, P.; Bousmina, M.; Chaumont, P. *Polymer.* **2010**, *51* (17), 3918–3925.

(58) Baquey, G.; Moine, L.; Degueil-Castaing, M.; Lartigue, J.-C.; Maillard, B. *Macromolecules* **2005**, *38* (23), 9571–9583.

(59) Dworak, D. P.; Soucek, M. D. *Macromolecules* **2004**, *37* (25), 9402–9417.

(60) Kowalewska, A.; Kupcik, J.; Pola, J.; Stańczyk, W. A. *Polymer.* **2008**, *49* (4), 857–866.

(61) Rambarran, T.; Gonzaga, F.; Brook, M. A. *Macromolecules* **2012**, *45* (5), 2276–2285.

(62) Tasdelen, M. A. *Polym. Chem.* **2011**, *2* (10), 2133.

(63) Hoyle, C. E.; Bowman, C. N. *Angew. Chemie Int. Ed.* **2010**, *49* (9), 1540–1573.

(64) Troegel, D.; Stohrer, J. *Coord. Chem. Rev.* **2011**, *255* (13–14), 1440–1459.

(65) Marciniec, B. *Comprehensive Handbook on Hydrosilylation*, 1st ed.; Marciniec, B., Ed.; Pergamon, 1992.

(66) Speier, J. L. In *Advances in Organometallic Chemistry*; 1979; Vol. 17, pp 407–447.

(67) Lewis, L. N. *J. Am. Chem. Soc.* **1990**, *112* (16), 5998–6004.

(68) Sabourault, N.; Mignani, G.; Wagner, A.; Mioskowski, C. *Org. Lett.* **2002**, *4* (13), 2117–2119.

(69) Nakajima, Y.; Shimada, S. *RSC Adv.* **2015**, *5* (26), 20603–20616.

(70) Kubas, G. J. *J. Organomet. Chem.* **2001**, *635* (1–2), 37–68.

(71) Chalk, A. J.; Harrod, J. F. *J. Am. Chem. Soc.* **1965**, *87* (1), 16–21.

(72) Faglioni, F.; Blanco, M.; Goddard, W. A.; Saunders, D. *J. Phys. Chem. B* **2002**, *106* (7), 1714–1721.

(73) A. Schroeder, M.; S. Wrighton, M. *J. Organomet. Chem.* **1977**, *128* (3), 345–358.

(74) Sakaki, S.; Mizoe, N.; Sugimoto, M. *Organometallics* **1998**, *17* (12), 2510–2523.

(75) Roy, A. K.; Taylor, R. B. *J. Am. Chem. Soc.* **2002**, *124* (32), 9510–9524.

(76) Abdellah, L.; Boutevin, B.; Youssef, B. *Prog. Org. Coatings* **1994**, *23* (3), 201–236.

(77) Sommer, L. H.; Lyons, J. E. *J. Am. Chem. Soc.* **1969**, *91* (25), 7061–7067.

(78) Braun, F.; Willner, L.; Hess, M.; Kosfeld, R. *J. Organomet. Chem.* **1989**, *366* (1–2), 53–56.

(79) Braun, F.; Willner, L.; Hess, M.; Kosfeld, R. *J. Organomet. Chem.* **1987**, *332* (1–2), 63–68.

(80) Ghose, B. N. *J. Organomet. Chem.* **1979**, *164* (1), 11–18.

(81) Zhang, C.; Laine, R. M. *J. Am. Chem. Soc.* **2000**, *122* (29), 6979–6988.

(82) Zhu, Q.; Feng, S.; Chen, J. *J. Appl. Polym. Sci.* **2002**, *85* (11), 2431–2435.

(83) Mammeri, F.; Douja, N.; Bonhomme, C.; Ribot, F.; Babonneau, F.; Dirè, S. *MRS Proc.* **2004**, *847*, EE13.26.

(84) Mammeri, F.; Bonhomme, C.; Ribot, F.; Babonneau, F.; Dirè, S. *Chem. Mater.* **2009**, *21* (18), 4163–4171.

(85) Rutnakornpituk, M.; Ngamdee, P. *Polymer.* **2006**, *47* (23), 7909–7917.

(86) Sabourault, N.; Mignani, G.; Wagner, A.; Mioskowski, C. *Org. Lett.* **2002**, *4* (13), 2117–2119.

(87) Bartels, J. M. Inorganic Backbone Ionomers: Design and Dielectric Response of Single-ion Conducting Polymers, The Pennsylvania State University, 2015.

(88) Feinle, A.; Flaig, S.; Puchberger, M.; Schubert, U.; Hüsing, N. *Chem. Commun.* **2015**, *51* (12), 2339–2341.

(89) Putzien, S.; Louis, E.; Nuyken, O.; Kühn, F. E. *Catal. Sci. Technol.* **2012**, *2* (4), 725–729.

(90) Du, X.; Huang, Z. *ACS Catal.* **2017**, *7* (2), 1227–1243.

(91) Rakshit, D.; Daily, K. M.; Blume, D. *Phys. Rev. A - At. Mol. Opt. Phys.* **2012**, *85* (3), 567–571.

(92) Odian, G. *Principles of Polymerization*, 4th ed.; John Wiley & Sons, Inc, 2004.

(93) Chanda, M. *Introduction to Polymer Science and Chemistry: A Problem-Solving Approach, Second Edition*; Taylor & Francis Group, 2013.

(94) Montaudo, G.; Samperi, F.; Montaudo, M. S. *Prog. Polym. Sci.* **2006**, *31* (3), 277–357.

(95) Schwab, J. J.; Lichtenhan, J. D. *Appl. Organomet. Chem.* **1998**, *12* (10–11), 707–713.

(96) Pielichowski, K.; Njuguna, J.; Janowski, B.; Pielichowski, J. In *Advances in Polymer Science*; 2006; Vol. 201, pp 225–296.

(97) Li, G.; Wang, L.; Ni, H.; Jr., C. U. P. *J. Inorg. Organomet. Polym.* **2001**, *11* (3), 123–154.

(98) Zhou, H.; Ye, Q.; Xu, J. *Mater. Chem. Front.* **2017**, *1* (2), 212–230.

(99) *Applications of Polyhedral Oligomeric Silsesquioxanes*; Hartmann-Thompson, C., Ed.; Advances in Silicon Science; Springer Netherlands: Dordrecht, 2011; Vol. 3.

(100) Tanaka, K.; Chujo, Y. *Polym. J.* **2012**, *45* (3), 247–254.

(101) Zhang, C.; Babonneau, F.; Bonhomme, C.; Laine, R. M.; Soles, C. L.; Hristov, H. A.; Yee, A. F. *J. Am. Chem. Soc.* **1998**, *120* (33), 8380–8391.

(102) Leibler, L.; Rubinstein, M.; Colby, R. H. *Macromolecules* **1991**, *24* (16), 4701–4707.

(103) Romo-Uribe, A.; Mather, P. T.; Haddad, T. S.; Lichtenhan, J. D. *J. Polym. Sci. Part B Polym. Phys.* **1998**, *36* (11), 1857–1872.

(104) Shea, K. J.; Loy, D. a.; Webster, O. *J. Am. Chem. Soc.* **1992**, *114* (17), 6700–6710.

(105) Guimard, N. K.; Oehlenschlaeger, K. K.; Zhou, J.; Hilf, S.; Schmidt, F. G.; Barner-Kowollik, C. *Macromol. Chem. Phys.* **2012**, *213* (2), 131–143.

(106) Garcia, S. J. *Eur. Polym. J.* **2014**, *53* (1), 118–125.

(107) Speck, T.; Mülhaupt, R.; Speck, O. In *Self-Healing Polymers: From Principles to Applications*; John Wiley & Sons, Inc., 2013; pp 61–89.

(108) Harrington, M. J.; Speck, O.; Speck, T.; Wagner, S.; Weinkamer, R. In *Advances in Polymer Science*; Springer, Cham, 2015; pp 307–344.

(109) Stukalin, E. B.; Cai, L.-H.; Kumar, N. A.; Leibler, L.; Rubinstein, M. *Macromolecules* **2013**, *46* (18),

7525–7541.

(110) Döhler, D.; Michael, P.; Binder, W. In *Self-Healing Polymers*; Wiley-VCH Verlag GmbH & Co. KGaA: Weinheim, Germany, 2013; pp 5–60.

(111) Wool, R. P.; O'Connor, K. M. *J. Appl. Phys.* **1981**, *52* (10), 5953–5963.

(112) Wool, R. P. *Soft Matter* **2008**, *4* (3), 400.

(113) Zhang, M. Q.; Rong, M. Z. *J. Polym. Sci. Part B Polym. Phys.* **2012**, *50* (4), 229–241.

(114) Stokes, V. K. *Polym. Eng. Sci.* **1989**, *29* (19), 1310–1324.

(115) Vinson, J. R. *Polym. Eng. Sci.* **1989**, *29* (19), 1325–1331.

(116) Yang, Y.; Urban, M. W. *Chem. Soc. Rev.* **2013**, *42* (17), 7446.

(117) Hager, M. D.; Greil, P.; Leyens, C.; van der Zwaag, S.; Schubert, U. S. *Adv. Mater.* **2010**, *22* (47), 5424–5430.

(118) Yang, Y.; Ding, X.; Urban, M. W. *Prog. Polym. Sci.* **2015**, *49–50*, 34–59.

(119) Zhu, D. Y.; Rong, M. Z.; Zhang, M. Q. *Prog. Polym. Sci.* **2015**, *49–50*, 175–220.

(120) White, S. R.; Sottos, N. R.; Geubelle, P. H.; Moore, J. S.; Kessler, M. R.; Sriram, S. R.; Brown, E. N.; Viswanathan, S. *Nature* **2001**, *409* (6822), 794–797.

(121) Rule, J. D.; Brown, E. N.; Sottos, N. R.; White, S. R.; Moore, J. S. *Adv. Mater.* **2005**, *17* (2), 205–208.

(122) Fickert, J.; Rupper, P.; Graf, R.; Landfester, K.; Crespy, D. *J. Mater. Chem.* **2012**, *22* (5), 2286–2291.

(123) Fickert, J.; Makowski, M.; Kappl, M.; Landfester, K.; Crespy, D. *Macromolecules* **2012**, *45* (16), 6324–6332.

(124) Fickert, J.; Wohnhaas, C.; Turshatov, A.; Landfester, K.; Crespy, D. *Macromolecules* **2013**, *46* (3), 573–579.

(125) Xiao, D. S.; Yuan, Y. C.; Rong, M. Z.; Zhang, M. Q. *Polymer.* **2009**, *50* (13), 2967–2975.

(126) Xiao, D. S.; Yuan, Y. C.; Rong, M. Z.; Zhang, M. Q. *Polymer.* **2009**, *50* (2), 560–568.

(127) Yao, L.; Yuan, Y. C.; Rong, M. Z.; Zhang, M. Q. *Polymer.* **2011**, *52* (14), 3137–3145.

(128) Wang, H. P.; Yuan, Y. C.; Rong, M. Z.; Zhang, M. Q. *Macromolecules* **2010**, *43* (2), 595–598.

(129) Keller, M. W.; White, S. R.; Sottos, N. R. *Adv. Funct. Mater.* **2007**, *17* (14), 2399–2404.

(130) Crespy, D.; Landfester, K.; Fickert, J.; Rohwerder, M. In *Advances in Polymer Science*; 2016; pp 219–245.

(131) Wu, D. Y.; Meure, S.; Solomon, D. *Prog. Polym. Sci.* **2008**, *33* (5), 479–522.

(132) Bekas, D. G.; Tsirka, K.; Baltzis, D.; Paipetis, A. S. *Compos. Part B Eng.* **2016**, *87*, 92–119.

(133) Scheiner, M.; Dickens, T. J.; Okoli, O. *Polymer.* **2016**, *83*, 260–282.

(134) Chipara, M.; Zaleski, J.; Dragnea, B.; Shansky, E.; Onuta, T.-D.; Chipara, M. D. In *47th AIAA/ASME/ASCE/AHS/ASC Structures, Structural Dynamics, and Materials Conference 14th AIAA/ASME/AHS Adaptive Structures Conference 7th*; American Institute of Aeronautics and Astronautics: Reston, Virigina, 2006.

(135) Williams, G.; Trask, R.; Bond, I. *Compos. Part A Appl. Sci. Manuf.* **2007**, *38* (6), 1525–1532.

(136) Lehn, J.-M. *Angew. Chemie Int. Ed. English* **1988**, *27* (1), 89–112.

(137) Brunsveld, L.; Folmer, B. J. B.; Meijer, E. W.; Sijbesma, R. P. *Chem. Rev.* **2001**, *101* (12), 4071–4098.

(138) *Self-Healing Polymers*; Binder, W. H., Ed.; Wiley-VCH Verlag GmbH & Co. KGaA: Weinheim, Germany, 2013.

(139) Heinzmann, C.; Weder, C.; de Espinosa, L. M. *Chem. Soc. Rev.* **2016**, *45* (2), 342–358.

(140) Bode, S.; Sandmann, B.; Hager, M. D.; Schubert, U. S. In *Self-Healing Polymers*; Wiley-VCH Verlag GmbH & Co. KGaA: Weinheim, Germany, 2013; pp 301–314.

(141) de Espinosa, L. M.; Fiore, G. L.; Weder, C.; Johan Foster, E.; Simon, Y. C. *Prog. Polym. Sci.* **2015**, *49–50*, 60–78.

(142) Herbst, F.; Binder, W. H. In *Self-Healing Polymers*; Wiley-VCH Verlag GmbH & Co. KGaA: Weinheim, Germany, 2013; pp 273–300.

(143) Herbst, F.; Döhler, D.; Michael, P.; Binder, W. H. *Macromol. Rapid Commun.* **2013**, *34* (3), 203–220.

(144) Binder, W. H.; Zirbs, R. In *Hydrogen Bonded Polymers*; Springer Berlin Heidelberg, 2006; pp 1–78.

(145) Sijbesma, R. P. *Science (80-.).* **1997**, *278* (5343), 1601–1604.

(146) Binder, W. H.; Petraru, L.; Roth, T.; Groh, P. W.; Pálfi, V.; Keki, S.; Ivan, B. *Adv. Funct. Mater.* **2007**, *17* (8), 1317–1326.

(147) Herbst, F.; Schröter, K.; Gunkel, I.; Gröger, S.; Thurn-Albrecht, T.; Balbach, J.; Binder, W. H. *Macromolecules* **2010**, *43* (23), 10006–10016.

(148) Park, T.; Zimmerman, S. C. *J. Am. Chem. Soc.* **2006**, *128* (35), 11582–11590.

(149) Maes, F.; Montarnal, D.; Cantournet, S.; Tournilhac, F.; Corté, L.; Leibler, L. *Soft Matter* **2012**, *8* (5), 1681–1687.

(150) Zhang, R.; Yan, T.; Lechner, B.-D.; Schröter, K.; Liang, Y.; Li, B.; Furtado, F.; Sun, P.; Saalwächter, K. *Macromolecules* **2013**, *46* (5), 1841–1850.

(151) Hart, L. R.; Hunter, J. H.; Nguyen, N. A.; Harries, J. L.; Greenland, B. W.; Mackay, M. E.; Colquhoun, H. M.; Hayes, W. *Polym. Chem.* **2014**, *5* (11), 3680–3688.

(152) Burattini, S.; Greenland, B. W.; Hayes, W.; Mackay, M. E.; Rowan, S. J.; Colquhoun, H. M. *Chem. Mater.* **2011**, *23* (1), 6–8.

(153) Greenland, B. W.; Burattini, S.; Hayes, W.; Colquhoun, H. M. *Tetrahedron* **2008**, *64* (36), 8346–8354.

(154) Burattini, S.; Colquhoun, H. M.; Fox, J. D.; Friedmann, D.; Greenland, B. W.; Harris, P. J. F.; Hayes, W.; Mackay, M. E.; Rowan, S. J. *Chem. Commun.* **2009**, No. 44, 6717.

(155) Vaccaro, E.; Waite, J. H. *Biomacromolecules* **2001**, *2* (3), 906–911.

(156) Whittell, G. R.; Hager, M. D.; Schubert, U. S.; Manners, I. *Nat. Mater.* **2011**, *10* (3), 176–188.

(157) Eisenberg, A.; Hird, B.; Moore, R. B. *Macromolecules* **1990**, *23* (18), 4098–4107.

(158) Varley, R. J.; Shen, S.; van der Zwaag, S. *Polymer.* **2010**, *51* (3), 679–686.

(159) Rhaman, M. A.; Penco, M.; Spagnoli, G.; Grande, A. M.; Di Landro, L. *Macromol. Mater. Eng.* **2011**, *296* (12), 1119–1127.

(160) Kalista, S. J.; Ward, T. C.; Oyetunji, Z. *Mech. Adv. Mater. Struct.* **2007**, *14* (5), 391–397.

(161) Hohlbein, N.; Shaaban, A.; Bras, a R.; Pyckhout-Hintzen, W.; Schmidt, a M. *Phys. Chem. Chem.*

Phys. **2015**, *17* (32), 21005–21017.

(162) Wei, Z.; He, J.; Liang, T.; Oh, H.; Athas, J.; Tong, Z.; Wang, C.; Nie, Z. *Polym. Chem.* **2013**, *4* (17), 4601.

(163) Varley, R. J.; van der Zwaag, S. *Acta Mater.* **2008**, *56* (19), 5737–5750.

(164) Hohlbein, N.; von Tapavicza, M.; Nellesen, A.; Schmidt, A. M. In *Self-Healing Polymers*; Wiley-VCH Verlag GmbH & Co. KGaA: Weinheim, Germany, 2013; pp 315–334.

(165) Roy, N.; Bruchmann, B.; Lehn, J.-M. *Chem. Soc. Rev.* **2015**, *44* (11), 3786–3807.

(166) Cordier, P.; Tournilhac, F.; Soulié-Ziakovic, C.; Leibler, L. *Nature* **2008**, *451* (7181), 977–980.

(167) Jin, Y.; Yu, C.; Denman, R. J.; Zhang, W. *Chem. Soc. Rev.* **2013**, *42* (16), 6634.

(168) Ying, H.; Zhang, Y.; Cheng, J. *Nat. Commun.* **2014**, *5*, 3218.

(169) Ono, T.; Nobori, T.; Lehn, J. M. *Chem Commun* **2005**, No. 12, 1522–1524.

(170) Zheng, P.; McCarthy, T. J. *J. Am. Chem. Soc.* **2012**, *134* (4), 2024–2027.

(171) Schmolke, W.; Perner, N.; Seiffert, S. *Macromolecules* **2015**, *48* (24), 8781–8788.

(172) Cash, J. J.; Kubo, T.; Bapat, A. P.; Sumerlin, B. S. *Macromolecules* **2015**, *48* (7), 2098–2106.

(173) Yuan, C.; Rong, M. Z.; Zhang, M. Q.; Zhang, Z. P.; Yuan, Y. C. *Chem. Mater.* **2011**, *23* (22), 5076–5081.

(174) Imato, K.; Nishihara, M.; Kanehara, T.; Amamoto, Y.; Takahara, A.; Otsuka, H. *Angew. Chemie Int. Ed.* **2012**, *51* (5), 1138–1142.

(175) Amamoto, Y.; Otsuka, H.; Takahara, A.; Matyjaszewski, K. *Adv. Mater.* **2012**, *24* (29), 3975–3980.

(176) Diesendruck, C. E.; Moore, J. S. In *Self-Healing Polymers*; Wiley-VCH Verlag GmbH & Co. KGaA: Weinheim, Germany, 2013; pp 193–214.

(177) Yang, Y.; Ding, X.; Urban, M. W. *Prog. Polym. Sci.* **2015**, *49–50*, 34–59.

(178) Gandini, A. *Prog. Polym. Sci.* **2013**, *38* (1), 1–29.

(179) Yoshie, N.; Watanabe, M.; Araki, H.; Ishida, K. *Polym. Degrad. Stab.* **2010**, *95* (5), 826–829.

(180) Yu, F.; Cao, X.; Du, J.; Wang, G.; Chen, X. *ACS Appl. Mater. Interfaces* **2015**, *7* (43), 24023–24031.

(181) Imbesi, P. M.; Fidge, C.; Raymond, J. E.; Cauët, S. I.; Wooley, K. L. *ACS Macro Lett.* **2012**, *1* (4), 473–477.

(182) Engel, T.; Kickelbick, G. *Eur. J. Inorg. Chem.* **2015**, *2015* (7), 1226–1232.

(183) Schäfer, S.; Kickelbick, G. *Polymer.* **2015**, *69*, 357–368.

(184) Zhao, J.; Xu, R.; Luo, G.; Wu, J.; Xia, H. *J. Mater. Chem. B* **2016**, *4*, 982–989.

(185) Mcelhanon, J. R.; Russick, E. M.; Wheeler, D. R.; Loy, D. A.; Aubert, J. H. *J. Appl. Polym. Sci.* **2002**, *85* (7), 1496–1502.

(186) Zhang, Y.; Broekhuis, A. A.; Picchioni, F. *Macromolecules* **2009**, *42* (6), 1906–1912.

(187) Trovatti, E.; Lacerda, T. M.; Carvalho, A. J. F.; Gandini, A. *Adv. Mater.* **2015**, *27* (13), 2242–2245.

(188) Polgar, L. M.; Van Duin, M.; Broekhuis, A. A.; Picchioni, F. *Macromolecules* **2015**, *48* (19), 7096–7105.

(189) Engel, T.; Kickelbick, G. In *Self-Healing Polymers*; Wiley-VCH Verlag GmbH & Co. KGaA: Weinheim, Germany, 2013; pp 153–171.

(190) Froimowicz, P.; Frey, H.; Landfester, K. *Macromol. Rapid Commun.* **2011**, *32* (5), 468–473.

(191) Ling, J.; Rong, M. Z.; Zhang, M. Q. *Polymer.* **2012**, *53* (13), 2691–2698.

(192) Chung, C. M.; Roh, Y. S.; Cho, S. Y.; Kim, J. G. *Chem. Mater.* **2004**, *16* (21), 3982–3984.

(193) Hoffmann, R.; Woodward, R. B. *Angew. Chemie Int. Ed.* **1969**, *8* (11), 781–932.

(194) Klukovich, H. M.; Kean, Z. S.; Iacono, S. T.; Craig, S. L. *J. Am. Chem. Soc.* **2011**, *133* (44), 17882–17888.

(195) Beyer, M. K. *J. Chem. Phys.* **2000**, *112* (17), 7307–7312.

(196) Cleland, W. W. *Biochemistry* **1964**, *3* (4), 480–482.

(197) Tobolsky, A. V; MacKnight, W. J.; Takahashi, M. *J. Phys. Chem.* **1964**, *68* (4), 787–790.

(198) Martin, R.; Rekondo, A.; de Luzuriaga, A. R.; Casuso, P.; Dupin, D.; Cabañero, G.; Grande, H. J.; Odriozola, I. *Smart Mater. Struct.* **2016**, *25* (8), 84017.

(199) Amamoto, Y.; Kamada, J.; Otsuka, H.; Takahara, A.; Matyjaszewski, K. *Angew. Chemie Int. Ed.* **2011**, *50* (7), 1660–1663.

(200) Higaki, Y.; Otsuka, H.; Takahara, A. *Macromolecules* **2004**, *37* (5), 1696–1701.

(201) Otsuka, H.; Aotani, K.; Higaki, Y.; Amamoto, Y.; Takahara, A. *Macromolecules* **2007**, *40* (5), 1429–1434.

(202) Yuan, C.; Rong, M. Z.; Zhang, M. Q. *Polym. (United Kingdom)* **2014**, *55* (7), 1782–1791.

(203) Higaki, Y.; Otsuka, H.; Takahara, A. *Macromolecules* **2006**, *39* (6), 2121–2125.

(204) Yang, Y.; Urban, M. W. *Chem. Soc. Rev.* **2013**, *42* (17), 7446–7467.

(205) Canadell, J.; Goossens, H.; Klumperman, B. *Macromolecules* **2011**, *44* (8), 2536–2541.

(206) Yoon, J. A.; Kamada, J.; Koynov, K.; Mohin, J.; Nicolaÿ, R.; Zhang, Y.; Balazs, A. C.; Kowalewski, T.; Matyjaszewski, K. *Macromolecules* **2012**, *45* (1), 142–149.

(207) Liu, F.; Li, F.; Deng, G.; Chen, Y.; Zhang, B.; Zhang, J.; Liu, C.-Y. *Macromolecules* **2012**, *45* (3), 1636–1645.

(208) Deng, G.; Tang, C.; Li, F.; Jiang, H.; Chen, Y. *Macromolecules* **2010**, *43* (3), 1191–1194.

(209) Jay, J. I.; Langheinrich, K.; Hanson, M. C.; Mahalingam, A.; Kiser, P. F. *Soft Matter* **2011**, *7* (12), 5826.

(210) Cambre, J. N.; Sumerlin, B. S. *Polymer.* **2011**, *52* (21), 4631–4643.

(211) He, L.; Fullenkamp, D. E.; Rivera, J. G.; Messersmith, P. B. *Chem. Commun.* **2011**, *47* (26), 7497.

(212) Arora, K.; Program, B.; Arbor, A. **2015**, 165–187.

(213) Ying, H.; Cheng, J. *J. Am. Chem. Soc.* **2014**, *136* (49), 16974–16977.

(214) Hager, M. D.; Greil, P.; Leyens, C.; van der Zwaag, S.; Schubert, U. S. *Adv. Mater.* **2010**, *22* (47), 5424–5430.

(215) Lafont, U.; van Zeijl, H.; van der Zwaag, S. *ACS Appl. Mater. Interfaces* **2012**, *4* (11), 6280–6288.

(216) Michael, P.; Döhler, D.; Binder, W. H. *Polymer.* **2015**, *69*, 216–227.

(217) Diels, O.; Alder, K. *Justus Liebig's Ann. der Chemie* **1928**, *460* (1), 98–122.

(218) Sanyal, A. *Macromol. Chem. Phys.* **2010**, *211* (13), 1417–1425.

(219) Froidevaux, V.; Borne, M.; Laborbe, E.; Auvergne, R.; Gandini, A.; Boutevin, B. *RSC Adv.* **2015**, *5* (47), 37742–37754.

(220) Yoshie, N. In *Encyclopedia of Polymer Science and Technology*; John Wiley & Sons, Inc.: Hoboken, NJ, USA, 2013.

(221) Barner-Kowollik, C.; Du Prez, F. E.; Espeel, P.; Hawker, C. J.; Junkers, T.; Schlaad, H.; Van Camp, W. *Angew. Chemie - Int. Ed.* **2011**, *50* (1), 60–62.

(222) Gandini, A. *Macromolecules* **2008**, *41* (24), 9491–9504.

(223) Gandini, A. *Polym. Chem.* **2010**, *1* (3), 245–251.

(224) Gandini, A. *Prog. Polym. Sci.* **1997**, *22* (6), 1203–1379.

(225) Moreau, C.; Belgacem, M. N.; Gandini, A. *Top. Catal.* **2004**, *27* (1–4), 11–30.

(226) Fukui, K.; Yonezawa, T.; Shingu, H. *J. Chem. Phys.* **1952**, *20* (4), 722–725.

(227) Kumar, S.; Kumar, V.; Singh, S. P. *Pericyclic Reactions. A Mechanistic and Problem-Solving Approach.*, 1st ed.; Academic Press, 2015.

(228) Kahn, S. D.; Pau, C. F.; Overman, L. E.; Hehre, W. J. *J. Am. Chem. Soc.* **1986**, *108* (23), 7381–7396.

(229) Liu, Y.-L.; Chuo, T.-W. *Polym. Chem.* **2013**, *4* (7), 2194.

(230) Reaction, D. A. In *Self-Healing Polymers and Polymer Composites*; John Wiley & Sons, Inc.: Hoboken, NJ, USA, 2011; pp 329–378.

(231) Gevrek, T. N.; Arslan, M.; Sanyal, A. In *Functional Polymers by Post-Polymerization Modification*; Wiley-VCH Verlag GmbH & Co. KGaA: Weinheim, Germany, 2013; pp 119–151.

(232) Zeng, C.; Seino, H.; Ren, J.; Hatanaka, K.; Yoshie, N. *Macromolecules* **2013**, *46* (5), 1794–1802.

(233) Chen, X.; Ruckenstein, E. *J. Polym. Sci. Part A Polym. Chem.* **1999**, *37* (23), 4390–4401.

(234) Chen, X.; Ruckenstein, E. *J. Polym. Sci. Part A Polym. Chem.* **2000**, *38* (9), 1662–1672.

(235) Murphy, E. B.; Bolanos, E.; Schaffner-Hamann, C.; Wudl, F.; Nutt, S. R.; Auad, M. L. *Macromolecules* **2008**, *41* (14), 5203–5209.

(236) Glassner, M.; Blinco, J. P.; Barner-Kowollik, C. *Polym. Chem.* **2011**, *2* (1), 83–87.

(237) Inglis, A. J.; Barner-Kowollik, C. *Polym. Chem.* **2011**, *2* (1), 126.

(238) Inglis, A. J.; Sinnwell, S.; Stenzel, M. H.; Barner-Kowollik, C. *Angew. Chemie Int. Ed.* **2009**, *48* (13), 2411–2414.

(239) Inglis, A. J.; Stenzel, M. H.; Barner-Kowollik, C. *Macromol. Rapid Commun.* **2009**, *30* (21), 1792–1798.

(240) Sinnwell, S.; Synatschke, C. V.; Junkers, T.; Stenzel, M. H.; Barner-Kowollik, C. *Macromolecules* **2008**, *41* (21), 7904–7912.

(241) Zhou, J.; Guimard, N. K.; Inglis, A. J.; Namazian, M.; Lin, C. Y.; Coote, M. L.; Spyrou, E.; Hilf, S.; Schmidt, F. G.; Barner-Kowollik, C. *Polym. Chem.* **2012**, *3* (3), 628–639.

(242) Oehlenschlaeger, K. K.; Guimard, N. K.; Brandt, J.; Mueller, J. O.; Lin, C. Y.; Hilf, S.; Lederer, A.; Coote, M. L.; Schmidt, F. G.; Barner-Kowollik, C. *Polym. Chem.* **2013**, *4* (16), 4348.

(243) Aubert, J. H. *J. Adhes.* **2003**, *79* (6), 609–616.

(244) Boutelle, R. C.; Northrop, B. H. *J. Org. Chem* **2011**, *76*, 7994–8002.

(245) Canadell, J.; Fischer, H.; De With, G.; van Benthem, R. A. T. M. *J. Polym. Sci. Part A Polym. Chem.* **2010**, *48* (15), 3456–3467.

(246) Gheneim, R.; Perez-Berumen, C.; Gandini, A. *Macromolecules* **2002**, *35* (19), 7246–7253.

(247) Nasresfahani, A.; Zelisko, P. M. *Polym. Chem.* **2017**, *8* (19), 2942–2952.

(248) Jia, X.-Y.; Mei, J.-F.; Lai, J.-C.; Li, C.-H.; You, X.-Z. *Chem. Commun.* **2015**, *51* (43), 8928–8930.

(249) Jia, X.; Mei, J.; Lai, J.; Li, C.; You, X. *Macromol. Rapid Commun.* **2016**, *37* (12), 952–956.

(250) Yu, S.; Zhang, R.; Wu, Q.; Chen, T.; Sun, P. *Adv. Mater.* **2013**, *25* (35), 4912–4917.

(251) Goiti, E.; Huglin, M. B.; Rego, J. M. *Macromol. Rapid Commun.* **2003**, *24* (11), 692–696.

(252) Araya-Hermosilla, R.; Fortunato, G.; Pucci, A.; Raffa, P.; Polgar, L.; Broekhuis, A. A.; Pourhossein, P.; Lima, G. M. R.; Beljaars, M.; Picchioni, F. *Eur. Polym. J.* **2016**, *74*, 229–240.

(253) Engel, T.; Kickelbick, G. *Chem. Mater.* **2013**, *25* (2), 149–157.

(254) Zeng, C.; Seino, H.; Ren, J.; Hatanaka, K.; Yoshie, N. *Polymer.* **2013**, *54* (20), 5351–5357.

(255) Heo, Y.; Sodano, H. A. *Adv. Funct. Mater.* **2014**, *24* (33), 5261–5268.

(256) Goiti, E.; Huglin, M. B.; Rego, J. M. *Polymer.* **2001**, *42* (26), 10187–10193.

(257) Roos, K.; Dolci, E.; Carlotti, S.; Caillol, S. *Polym. Chem.* **2016**, *7* (8), 1612–1622.

(258) Chou, C.-I.; Liu, Y.-L. *J. Polym. Sci. Part A Polym. Chem.* **2008**, *46* (19), 6509–6517.

(259) Imai, Y.; Itoh, H.; Naka, K.; Chujo, Y. *Macromolecules* **2000**, *33* (12), 4343–4346.

(260) Vilela, C.; Cruciani, L.; Silvestre, A. J. D.; Gandini, A. *RSC Adv.* **2012**, *2* (7), 2966.

(261) Cho, S. H.; Andersson, H. M.; White, S. R.; Sottos, N. R.; Braun, P. V. *Adv. Mater.* **2006**, *18* (8), 997–1000.

(262) Xu, Z.; Zhao, Y.; Wang, X.; Lin, T. *Chem. Commun.* **2013**, *49* (60), 6755.

(263) Paul, D. R.; Mark, J. E. *Prog. Polym. Sci.* **2010**, *35* (7), 893–901.

(264) Swanson, J. P.; Rozvadovsky, S.; Seppala, J. E.; Mackay, M. E.; Jensen, R. E.; Costanzo, P. J. *Macromolecules* **2010**, *43* (14), 6135–6141.

(265) Laita, H.; Boufi, S.; Gandini, a. *Eur. Polym. J.* **1997**, *33* (8), 1203–1211.

(266) Canary, S. A.; Stevens, M. P. *J. Polym. Sci. Part A Polym. Chem.* **1992**, *30* (8), 1755–1760.

(267) Gandini, A.; Coelho, D.; Silvestre, A. J. D. *Eur. Polym. J.* **2008**, *44* (12), 4029–4036.

(268) Gaina, C.; Ursache, O.; Gaina, V. *Polym. Plast. Technol. Eng.* **2011**, *50* (7), 712–718.

(269) Goussé, C.; Gandini, A. *Polym. Int.* **1999**, *48* (8), 723–731.

(270) Murphy, E. B.; Bolanos, E.; Schaffner-Hamann, C.; Wudl, F.; Nutt, S. R.; Auad, M. L. *Macromolecules* **2008**, *41* (14), 5203–5209.

(271) Adzima, B. J.; Kloxin, C. J.; Bowman, C. N. *Adv. Mater.* **2010**, *22* (25), 2784–2787.

(272) Yuan, C.; Rong, M. Z.; Zhang, M. Q.; Zhang, Z. P.; Yuan, Y. C. *Chem. Mater.* **2011**, *23* (22), 5076–5081.

(273) Tian, Q.; Rong, M. Z.; Zhang, M. Q.; Yuan, Y. C. *Polym. Int.* **2010**, *59* (10), 1339–1345.

(274) Chen, X. *Science (80-.).* **2002**, *295* (5560), 1698–1702.

(275) Wouters, M.; Craenmehr, E.; Tempelaars, K.; Fischer, H.; Stroeks, N.; van Zanten, J. *Prog. Org. Coatings* **2009**, *64* (2–3), 156–162.

(276) Zhang, Y.; Broekhuis, A. A.; Picchioni, F. *Macromolecules* **2009**, *42* (6), 1906–1912.

(277) Toncelli, C.; De Reus, D. C.; Picchioni, F.; Broekhuis, A. A. *Macromol. Chem. Phys.* **2012**, *213* (2), 157–165.

(278) Watanabe, M.; Yoshie, N. *Polymer.* **2006**, *47* (14), 4946–4952.

(279) Magana, S.; Zerroukhi, A.; Jegat, C.; Mignard, N. *React. Funct. Polym.* **2010**, *70* (7), 442–448.

(280) Liu, Y.-L.; Chen, Y.-W. *Macromol. Chem. Phys.* **2007**, *208* (2), 224–232.

(281) Liu, Y.-L.; Hsieh, C.-Y.; Chen, Y.-W. *Polymer.* **2006**, *47* (8), 2581–2586.

(282) Matsumura, S.; Hlil, A. R.; Lepiller, C.; Gaudet, J.; Guay, D.; Shi, Z.; Holdcroft, S.; Hay, A. S. *Am. Chem. Soc. Polym. Prepr. Div. Polym. Chem.* **2008**, *49* (1), 511–512.

(283) Yoshie, N.; Saito, S.; Oya, N. *Polymer.* **2011**, *52* (26), 6074–6079.

(284) Syrett, J. A.; Mantovani, G.; Barton, W. R. S.; Price, D.; Haddleton, D. M. *Polym. Chem.* **2010**, *1* (1), 102.

(285) Peterson, A. M.; Jensen, R. E.; Palmese, G. R. *ACS Appl. Mater. Interfaces* **2010**, *2* (4), 1141–1149.

(286) Scheltjens, G.; Brancart, J.; De Graeve, I.; Van Mele, B.; Terryn, H.; Van Assche, G. *J. Therm. Anal. Calorim.* **2011**, *105* (3), 805–809.

(287) Tian, Q.; Yuan, Y. C.; Rong, M. Z.; Zhang, M. Q. *J. Mater. Chem.* **2009**, *19* (9), 1289.

(288) Liu, Y.-L.; Hsieh, C.-Y. *J. Polym. Sci. Part A Polym. Chem.* **2006**, *44* (2), 905–913.

(289) Peterson, A. M.; Jensen, R. E.; Palmese, G. R. *ACS Appl. Mater. Interfaces* **2009**, *1* (5), 992–995.

(290) Ghosh, B.; Chellappan, K. V.; Urban, M. W. *J. Mater. Chem.* **2011**, *21* (38), 14473.

(291) Ghosh, B.; Chellappan, K. V.; Urban, M. W. *J. Mater. Chem.* **2011**, *21* (38), 14473.

(292) Park, J. O.; Jang, S. H. *J. Polym. Sci. Part A Polym. Chem.* **1992**, *30* (5), 723–729.

(293) Patel, C. B.; Malek, N. I.; Oswal, S. L. *J. Macromol. Sci. Part A* **2006**, *43* (2), 289–303.

(294) Kaxiras, E.; Callister, W. D.; Rethwisch, D. G. *Materials Science*; 2014; Vol. 3.

(295) Wang, Z.; Fan, W.; Tong, R.; Lu, X.; Xia, H. *RSC Adv.* **2014**, *4* (49), 25486.

(296) Chen, X. *Science (80-.).* **2002**, *295* (5560), 1698–1702.